2016-01-01

Investigation of Lunar Subsurface Cavities using Thermal Inertia and Temperature Maximum to Minimum Ratios

Rachel Ann Slank
University of Texas at El Paso, rslank9@gmail.com

INVESTIGATION OF LUNAR SUBSURFACE CAVITIES USING THERMAL INERTIA AND TEMPERATURE MAXIMUM TO MINIMUM RATIOS

RACHEL ANN SLANK

Master's Program in Geological Sciences

APPROVED:

José M. Hurtado, Jr., Ph.D., Chair

Thomas E. Gill , Ph.D.

Evgeny Shafirovich, Ph.D.

Charles Ambler, Ph.D.
Dean of the Graduate School

Dedication

I would like to dedicate this thesis to my mother and father, Laura and Joel Slank. Thank you for supporting me as I pursue my dream. Most parents would have assumed my dream to become an astronaut was just a phase and left it at that. Instead you always encouraged me to follow that dream; from taking me to the Neil Armstrong museum countless times to playing spaceman, to buying me every book you could find about space to enduring cold late nights and mornings staring up at the Moon and stars with me. Thank you for driving me to and from space camp (even if we never made it to Coon dog cemetery), sending me to college, and traveling with me as I drove to my internship at NASA Langley. I appreciate all the little things you have ever done for me. I love you Mom and Dad to the Moon and back!

INVESTIGATION OF LUNAR SUBSURFACE CAVITIES USING THERMAL INERTIA AND TEMPERATURE MAXIMUM TO MINIMUM RATIOS

by

RACHEL ANN SLANK, B.S.

THESIS

Presented to the Faculty of the Graduate School of

The University of Texas at El Paso

in Partial Fulfillment

of the Requirements

for the Degree of

MASTER OF SCIENCE

Department of Geological Sciences

THE UNIVERSITY OF TEXAS AT EL PASO

May 2016

Acknowledgements

There is a plethora of people I would like to thank for helping me succeed on my Master's degree. First and foremost, I would like to thank my amazing fiancé Austin for everything you have done. From giving up weekends, to feeding me at 11 at night, from proofing my writing to always being there to give me a hug, I cannot thank you enough. I would like to thank all of my friends for their support and love, but especially I would like to thank Claire Bailey and Elizabeth Heness for always being by my side, offering a listening ear, and for not allowing me to eat every piece of junk food I could get my hands on. I would like to thank Michael Shook and Rene Ganoe for all of their patience as they taught me how to code, and what coding even is. This thesis would not exist without you two. I would like to give a huge shout out to Dr. Gail Arnold, who always provided me with hot cider and sometimes fancy chocolates when I looked like a needed it. Also thank you for all the times I crashed in your office when I needed to get away. Thank you to all of my family who offered support, even with some of them being all the way across the country. Last, but definitely not least, I would like to thank my advisor Dr. Jose Hurtado. Thank you for all that you have done for me. Without you, this work would not have happened and I would not be graduating. Thank you again!

Abstract

Previous studies have revealed a small number of subsurface cavities, including lava tubes, lava flow pits, and impact melt pits on the Moon. The interiors of such cavities would have been protected from micrometeorite bombardment, solar radiation, space weathering, and extreme diurnal temperature swings over long periods of geologic time. As a result, these subsurface features can provide access to pristine crustal samples and stratigraphy. These cavities would also provide protection of important volatiles, such as water ice, that would enable future exploration missions by relieving many operational constraints, including the supply of propellants and life support. In addition, subsurface cavities could serve as the sites of protective habitats for future lunar explorers.

The goal of this research was to establish a methodology using thermal inertia and temperature maximum and minimum ratios to detect and characterize lava tubes and other subsurface cavities in the lunar subsurface. Using data from the Lunar Reconnaissance Orbiter (LRO), thermal inertia and temperature maximum to minimum ratio maps were created and analyzed. Out of five potential locations for subsurface cavities, four had subsurface cavities present. Out of these four locations one had a circular cavity present below a skylight while the other three had at least one lava tube per site present.

Table of Contents

Acknowledgements v

Abstract vi

Table of Contents vii

List of Tables ix

List of Figures x

1. Introduction 1

2. Background 3

2.1. Formation Mechanisms for Subsurface Cavites 3

2.1.1. Lava Tubes 3

2.1.2. Lava Pits 6

2.2. Previous Strategies for Subsurface Cavity Mappying 8

2.3. Investigating the Thermal Signatures of Subsurface Cavities 9

3. Methods 13

3.1. Data 13

3.2. Study Areas 14

3.3. Data Preprocessing 15

3.4. Thermal Inertia and Temperature Maximum to Minimum Ratio 17

4. Results 19

4.1. Mare Tranquilitatis 19

4.2. Highland 1 19

4.3. Highland 2 21

4.4. Rima Sharp 21

4.5. Lacus Mortis 22

5. Discussion 23

5.1. Mare Tranquilitatis 23

5.2. Highland 1 23

5.3. Highland 2 24

5.4. Rima Sharp 25

5.5. Lacus Mortis 25

5.6 Issue with the Thermal Inertia Technique 26
6. Conclusions 28
References 29
Appendix 1 59
Appendix 2 62
Appendix 3 74
Appendix 4 121
Vita 124

List of Tables

Table 1. Impact Lava Pits 34
Table 2. Lava Flow Pits 35
Table 3. Downloaded Data 36
Table 4. Tile Information 37
Table 5. Potential Site Location Data Check 38
Table 6. Variables 39

List of Figures

Figure 1. Lava tube formation by the growth of rooted crust 40
Figure 2. Lava tube formation by aggregation of floating crustal rafts 41
Figure 3. Lava tube formation by accretion of levees 42
Figure 4. Lava tube formation by extension of pahoehoe lobes 43
Figure 5. Generic cross-section of a lunar pit 44
Figure 6. LOLA DEM with sites of interest 45
Figure 7. Thermal inertia map of Mare Tranquilitatis 46
Figure 8. T_{max} to T_{min} ratio map of Mare Tranquilitatis 47
Figure 9. Thermal inertia map of Highland 1 48
Figure 10. T_{max} to T_{min} ratio map of Highland 1 49
Figure 11. Thermal inertia map of Highland 2 50
Figure 12. T_{max} to T_{min} ratio map of Highland 2 51
Figure 13. An overlay on LOLA DEM 52
Figure 14. Thermal inertia map of Rima Sharp 53
Figure 15. Thermal inertia map of Rima Sharp 54
Figure 16. T_{max} to T_{min} ratio map of Rima Sharp 55
Figure 17. T_{max} to T_{min} ratio map of Rima Sharp 56
Figure 18. Thermal inertia map of Lacus Mortis 57
Figure 19. T_{max} to T_{min} ratio map of Lacus Mortis 58

1. Introduction

Science fiction fans have always envisioned a future where humans would live and thrive on the Moon. This fantasy became more realistic when it was suggested to use lava tubes as potential habitats in the lunar subsurface (Horz, 1985). Since the early 1970s, it has been thought that lava tubes, and other subsurface cavities, are present in the lunar subsurface (Greeley, 1971; Cruikshank et al., 1972). It is now known that there are least 11 lava tubes (Coombs et al., 1992; Daga, 2006; Cushing, 2007; Ximenes et al., 2010; Ashley et al., 2011; Meyer, 2012; Chappaz et al., 2014) and 228 lava pits (Wagner and Robinson, 2014) on the Moon. Many more subsurface cavities, and of other types, may yet to be discovered.

Subsurface cavities such as lava tubes could offer astronauts protection from solar radiation, from bombardment by micrometeoroids, and from drastic diurnal temperature changes (Horz, 1985), and they could also offer valuable access to explore the lunar subsurface (Daga, 2006). Subsurface cavities on the Moon would have been protected from surface processes such as space weathering, solar wind bombardment, and impacts over long periods of time (Daga, 2006). This would allow the preservation of pristine geologic and other materials. Subsurface cavities would also provide access to vertical exposures of the stratigraphy of the upper lunar crust. These characteristics make subsurface cavities potentially important science exploration targets as well as potential sites for human habitation.

Because the interiors of subsurface cavities would be protected from surface processes, there is the potential for volatiles, including water ice, to have been sequestered there (Wynne, 1985). It is believed that, just like caves on Earth, subsurface cavities on the Moon would have low and stable internal temperatures (Wynne, 1985). Combined with the protection they offer from direct solar insolation, the thermal environment in lunar subsurface cavities could produce

cold traps for volatiles such as water ice. In fact, subsurface lunar cavities may have temperatures similar to those in the permanently shadowed craters near the poles (60 K) (Paige et al., 2010), where cold-trapped volatiles have been found (Paige et al., 2010; Mitrofanov et al., 2010). If volatiles could be found within subsurface cavities on the Moon, and in large enough amounts that are easily accessible and extractable, they would enable future exploration missions by relieving many operational constraints, including the supply of propellants and life support (Horz, 1985; Ashley et al., 2011).

Unfortunately, it is difficult to determine where subsurface cavities are located because, unless a "skylight" (a collapsed section of the roof) is present (e.g. Ashley et al., 2011), they are not visible on the surface. Meyer (2012) approached this problem by using thermal infrared data to find temperature signatures of lava tubes in the lunar subsurface. Chappaz et al. (2014) have proposed a different method for finding lava tubes using free air and Bouguer gravity anomalies. In the research performed here, I will expand on the work of Meyer (2012) to locate even more subsurface cavities.

2. Background

2.1 Formation Mechanisms for Subsurface Cavities

Volcanism can create several different types of subsurface features, including lava tubes and lava pits. This section summarizes what these features are and how they form.

2.1.1 Lava Tubes

A lava tube is a roofed channel formed of solidified lava, on or within a lava flow, through which lava flows to an advancing flow front (Neuendorf et al., 2005). Before a lava tube can begin to form, lava has to be flowing in a channel for hours to days, allowing ample time for the lava tube to form (Peterson et al., 1994). On the Moon, lava can flow greater distances, and for longer duration, than on Earth since there is less gravity and no atmosphere (Greeley, 1971; Peterson et al., 1994). Because of this, lava channels, and the resulting tubes, that form on the Moon can have much greater lengths and widths than those on Earth (Peterson et al., 1994), with diameters potentially in excess of 1.6 km (Blair et al., 2015). Based on studies of terrestrial basalt lava flows, there are at least four processes that can form a lava tube (Peterson et al., 1994): growth of a rooted crust; aggregation of floating crustal rafts; accretion to levees; and progressive extension of pahoehoe lobes.

Once a channelized lava flow is established, one mechanism for the formation of a lava tube is the growth of rooted crust (Peterson et al. 1994). In this model (Figure 1), lava begins to solidify on the banks and edges of the lava channel, forming a thin crust. As the process continues, more lava solidifies onto the hardened crust causing it to grow across the lava flow. Eventually the two sides will meet in the middle to form a roof. Once the channelized flow is

completely roofed over, more lava will stick to the underside of the roof, strengthening it and allowing the lava tube to build further down the channel. In order for a lava tube to form by this mechanism, the flux of lava has to be fairly constant, with little turbulence. If the flux diminishes, and the lava level drops too rapidly, the thin crust of a newly forming roof will collapse, causing the lava tube to be destroyed entirely (Peterson et al., 1994). If, instead, the flux increases, the lava level may rise quickly, breaking apart a newly forming roof and carrying away solidified material before it can reform into a roof.

A second mechanism for the formation of lava tubes is aggregation of floating crustal rafts (Peterson et al., 1994). In this scenario (Figure 2), the lava flows in a turbulent manner, but the lava level is constant. Parts of the lava surface will solidify, but, due to the turbulent flow, the solidified crust cannot remain connected to the banks. Instead, solidified fragments float down the channel until they are trapped by a narrowing of the channel, a tight bend, or a similar obstruction. Eventually, a logjam of these fragments will form, and the lava flowing below will help to consolidate them into a single, large raft which becomes a roof over the channel. The roof can then thicken, while the lava still flows beneath it. Eventually, the lava will stop flowing and if the lava drains out a tube will be left.

A third mechanism for the formation of lava tubes is accretion to levees (Peterson et al., 1994). In contrast with the rooted crust and rafting processes, in this formation mechanism it is critical that the level of the channelized lava flow changes so that levees will form and build an arch (Figure 3). As the lava level rises, levees form when lava splashes or floods over the channel bank. The levees then solidify as the lava levels lower, building up the outer banks. This process occurs again and again, causing the levees to grow in size and to curve slightly towards the center of the channel. Eventually a strong surge of lava will occur, causing lava to

go over the growing levees, closing the lava tube. From then on, additional lava will splash around the interior of the tube and will thicken and strengthen the roof.

A fourth mechanism for the formation of lava tubes is progressive extension of pahoehoe lobes (Peterson et al., 1994). In this process, the constant lava supply needs to be low to moderate with unchannelized flow over a low topographic gradient. As the unchannelized lava flows out laterally, it forms small lobes that may either flow independently or coalesce (Deschamps et al., 2014). As the flux of lava increases, new lava is injected beneath the cooled upper crust of existing flow lobes, causing them to inflate to many times their original volume. As the lava lobes inflate, the surface of the flow will begin to rise, spreading further out. The more the surface rises as the lava flow inflates, the greater the surface area of the flow will be, allowing the length to increase (Deschamps et al., 2014). Eventually, the lava will stop flowing and the lava tubes can empty, leaving the empty cavities.

The factors that determine which of these formation process occurs include whether or not the lava is channelized, if the lava level is constant, and if the flow of lava is laminar or turbulent. For example, if the lava level constantly changes, lava tubes may form by accretion of levees, regardless of whether the lava flow is turbulent or laminar. If, instead, the lava level remains constant, and if the flow is laminar, lava tubes may form by growth of rooted crust. However, if the lava level is constant but with turbulent flow, lava tube formation will occur by the aggregation of floating crustal rafts.

If the roof of a lava tube has not had time reach a sustainable thickness, the roof of the tube could collapse. This can result in a “skylight”, or a hole where the roof caved in (Peterson et al., 1994). Skylights are of interest to scientists because it is a way to detect possible subsurface cavities from observing the lunar surface (Ashley et al., 2011; Wagner and Robinson,

2014). Most of the areas of interest in this study involve skylights, and will be used as a way to help locate potential subsurface cavities.

2.1.2 Lava Pits

Lava tubes are not the only type of subsurface cavity that can form in a volcanic terrane. Lava pits are also common (Wagner and Robinson, 2014). A lava pit is a void space, usually a vertical shaft, located in lava flows. Lunar lava pits can be found in two settings: pits formed in flows or sheets of impact melt ("impact melt pits") and pits formed in conventional volcanic lava flows ("lava flow pits").

Lava flow pits can form as a result of lava flow inflation (Deschamps et al., 2014). The difference between this process and the formation of lava tubes by the progressive extension of pahoehoe lobes lies in what occurs when lava flow ceases. If the inflated lava flow cannot support its own weight, or if there are too many fractures, it will collapse, potentially creating a lava flow pit (Deschamps et al., 2014). Lava flow pits can also form when lava breaks out of a channel, causing a sudden drop in the lava volume and a subsequent collapse (Deschamps et al. 2014). A collapse resulting in a lava flow pit can also be caused by a rapid decrease in flux into the lava flow from the vent feeding it (Deschamps et al., 2014).

On the Moon, lava pits can also form in impact melts, creating impact melt pits (Wagner and Robinson, 2014). Because impact melt ponds on the Moon are basically pooled lava flows where the melt is generated by an impact event rather than a volcanic source, pits in impact melts can form via the same inflation mechanisms as pits formed in volcanic lava flows (Wagner and Robinson, 2014). This is important for locating lava pits. Since impact melt pits are not

restricted to conventional lava flows, this type of pit can be located anywhere on the Moon and not just the expansive mare basalts on the lunar nearside.

The structure of both lava flow pits and impact melt pits consists of a funnel, the walls, and the floor (Figure 5) (Wagner and Robinson, 2014). The funnel slopes in from the top of the pit and then transitions to vertical walls. The floor is either flat or slightly concave with some rubble at the bottom. There may be a possible connection to a more extensive tunnel leading out of the pit, if the lava completely drained out. If the lava did not drain out, there would just be lava pit surround by solid basalt. This makes the interpretation of the surface expression of a pit ambiguous: is it just a vertical shaft unconnected to any subsurface cavity or is it a skylight through the roof of a lava tube (or other cavity) with significant lateral extent?

Recently, 228 previously unknown pits were discovered on the Moon (Wagner and Robinson, 2014). These features have diameters ranging from 5 m to 900 m (Wagner and Robinson, 2014). Of the newly discovered lunar pits, only 7 were not found in impact melts. Both impact lava pits (Table 1) and lava flow pits (Table 2) were originally considered in this study for potential subsurface cavity locations. However locating an impact lava pit is not feasible with the relatively coarse spatial resolution of the available thermal infrared data (236.9 m/pixel; see Section 3.1). All of the known impact lava pits (Table 1) have diameters smaller than this, most with diameters in the tens of meters (Wagner and Robinson, 2014). The result is that the thermal anomaly due to an impact melt pit is not likely to be visible, assuming it extends no more than 1-10 diameters from the pit itself. Of the two types of lava pits, this study will only focus on the lava flow pits.

2.2 Previous Strategies for Subsurface Cavity Mapping

Early investigators (e.g. Horz, 1985; Coombs et al., 1992) focused on cataloging possible lunar lava tube candidates as well as developing methods for categorizing the lava tubes using estimated roof thickness, calculated using the equation (Coombs et al., 1992):

$$t = 0.5\, d \qquad (1),$$

where d is the maximum skylight diameter and t is minimum roof thickness. Coombs et al. (1992) suspected that un-collapsed lava tubes might exist in between skylights in areas of past volcanism. Coombs et al. (1992) cataloged 90 of these potential lava tubes using images from the Apollo missions, and, with that data, they measured lava tube lengths and estimated widths and roof thicknesses.

In recent years, new methods for locating subsurface cavities have been tested. Meyer (2012) developed a method using thermal infrared images, visible wavelength images, and topographic data from the Lunar Reconnaissance Orbiter (LRO) to locate apparent thermal inertia anomalies and surface topographic expressions consistent with the presence of subsurface cavities. With this approach, Meyer (2012) was able to locate a lava tube at Ingenii Hole. Meyer (2012) also used this approach to argue that the skylights at Marius Hills Hole and Tranquilitatis Hole found by Ashley et al. (2011) may not be lava tubes, but may instead be other types of subsurface cavities.

Chappaz et al. (2014) have also recently presented a novel approach for detecting subsurface cavities. They examined free-air and Bouguer gravity anomalies using gradiometry and cross correlation to locate subsurface cavities. Chappaz et al. (2014) used their methodology to investigate a known lava rille in Schroeder's Valley and a potential lava tube at Rima Sharp.

Although the Chappaz et al. (2014) efforts were successful, there is still much more testing to be done of their methods since they only applied their method to one lava tube

2.3 Investigating the Thermal Signatures of Subsurface Cavities

Thermal inertia (*P*) describes the resistance of a material to changes in temperature (Scheidt et al., 2010). It is defined as:

$$P = \sqrt{K\rho c} \qquad (2),$$

where *K* is thermal conductivity, ρ is density, and *c* is specific heat. Unfortunately, these parameters cannot be directly measured using remote sensing techniques, so thermal inertia either must be estimated from other directly measured data or it must be modeled. One way to estimate thermal inertia is by calculating apparent thermal inertia (*ATI*), which is defined as (Scheidt et al., 2010):

$$ATI = \frac{1-a}{\Delta T} \qquad (3),$$

where *a* is albedo and ΔT is the temperature range over a diurnal cycle. Albedo is the ratio of the amount of solar radiant energy reflected by a surface to the amount incident upon it (Neuendorf et al., 2005).

In order to calculate ΔT, the temperatures at two times of day are required. Although it is best to use the hottest and coolest temperatures experienced during the diurnal cycle to determine ΔT, they are not always obtainable with satellite data. The maximum (T_{max}) and minimum (T_{min}) temperatures can, however, be estimated given temperatures obtained from other parts of the diurnal cycle using (Scheidt et al., 2010):

$$T_{max} = T_1 + \frac{(T_1 - T_2)[\cos(\omega t_{max}) - \cos(\omega t_1)]}{\cos(\omega t_1) - \cos(\omega t_2)} \qquad (4),$$

$$T_{min} = T_2 + \frac{(T_1 - T_2)[\cos(\omega t_{min}) - \cos(\omega t_2)]}{\cos(\omega t_1) - cos(\omega t_2)} \quad (5),$$

where ω is the rotational angular frequency of the planet (the Moon in this case), t_1 is day satellite overpass time, t_2 is night satellite overpass time, T_1 is temperature at time t_1, and T_2 is temperature at time t_2. With T_{max} to $T_{min,}$ one can determine ΔT and then compute *ATI* using Equation (3).

Although *ATI* is a relative approximation to thermal inertia, it is possible to use *ATI* to make a quantitative absolute estimate of thermal inertia. Xue and Cracknell (1995) presented an equation to calculate thermal inertia (*P*) from *ATI*:

$$P = ATI\left(\frac{S_0 C_t}{\sqrt{\omega}}\right)\left\{\frac{A_1[\cos(\omega t_2 - \delta_1) - \cos(\omega t_1 - \delta_1)]}{\sqrt{1 + \frac{1}{b} + \frac{1}{2b^2}}} + \frac{A_2[\cos(\omega t_2 - \delta_2) - \cos(\omega t_1 - \delta_2)]}{\sqrt{2 + \frac{\sqrt{2}}{b} + \frac{1}{2b^2}}}\right\} \quad (6),$$

where S_0 is the solar constant (1,366 W/m^2 for the Moon; Johnson, 1954), C_t is the atmospheric transmittance (1 for the Moon), δ_1 is solar declination at time t_1, δ_2 is solar declination at time t_2, A_1 and A_2 are Fourier coefficients, and b is a parameter dependent on the time when T_{max} is attained. The Fourier coefficients A_1 and A_2 are given by (Maltese et al., 2012):

$$A_1 = \frac{2}{\pi} sin\delta sin\phi + \frac{1}{2\pi} cos\delta cos\phi[\sin(2\xi) + 2\xi] \quad (7),$$

$$A_2 = \frac{2sin\delta sin\phi}{2\pi}\sin(2\xi) + \frac{2cos\sigma cos\phi}{\pi(2^2 - 1)}[2\sin(2\xi)\cos(\xi) - \cos(2\xi)\sin(\xi)] \quad (8),$$

where ϕ is latitude and:

$$\xi = \arccos[\tan(\delta)\tan(\phi)] \quad (9).$$

The parameter b is determined using the formula (Xue and Cracknell, 1995):

$$b = \frac{\tan(\omega t_{max})}{1 - \tan(\omega t_{max})} \quad (10).$$

The ground surface above the roof of a subsurface cavity should appear to have lower thermal inertia than the surrounding surface. The roof of a cavity would get warmer in a shorter

amount of time during the day than the surrounding area because the roof has less volume, and therefore smaller thermal mass, than the surrounding area. Conversely, the roof of a cavity would get cooler in a shorter amount of time at night than the surrounding area because it has a smaller thermal mass. In addition, the roof can radiate heat into the subsurface cavity below, as well as back into space. By comparison, the surrounding area can only radiate heat back into space and would also receive conductive heating from below. For these reasons, the ground above the roofed section of a cavity would experience a larger day-to-night temperature variation, and, therefore, exhibit lower thermal inertia, than the surrounding area.

As with impact craters (Bandfield et al., 2011), skylights and pits should have higher thermal inertia than their surroundings. One reason for this is because there is likely to be more exposed rock and less regolith inside these features, and regolith has a lower thermal inertia than rocky outcrops (Bandfield et al., 2011). In addition, at various times during the day, an opening such as a skylight or pit would be in shadow, resulting in less radiative heating and, therefore, cooler surface temperatures than the surroundings. At night, the skylight would be expected to have a low temperature similar to that of the surroundings. The result is a smaller day-to-night temperature variation for the ground surface at and around a skylight or pit, and, therefore, a higher thermal inertia for these features than their surroundings.

ATI and thermal inertia are both inversely proportional to the temperature difference over a diurnal cycle. Therefore it makes sense to consider T_{max} to T_{min} as an alternative to locate subsurface cavities. The ground surface above the roof of a subsurface cavity should have a larger T_{max} to T_{min} ratio than the surrounding area. A roofed section of a subsurface cavity would be warmer than the surrounding area during the day and cooler than the surrounding area during the night. Therefore, the temperature variation experienced by the ground surface above the roof

of a subsurface cavity would be greater than that of than the surrounding area. This would also result in a larger T_{max} to T_{min} ratio for the ground surface above the subsurface cavity compared to the surrounding area. A skylight, pit, or other penetration into a cavity should have a T_{max} to T_{min} ratio close to one. During the day, a skylight would be cooler than the surrounding area and at night the skylight would be roughly the same temperature as the surrounding area.

3. Methods

3.1 Data

The Lunar Reconnaissance Orbiter (LRO) was launched in June 2009 and so far has returned more data about the Moon than all other missions combined (Prado, 2013). This study uses data from two instruments on board LRO: Diviner Lunar Radiometer Experiment (DLRE) and Lunar Orbiter Laser Altimeter (LOLA).

The Diviner Lunar Radiometer Experiment (DLRE) is a nine-channel infrared solar reflectance radiometer (Paige et al., 2009). DLRE uses filters to measure radiance at the following wavelengths (and corresponding brightness temperatures): 13-23 μm (>178 K), 25-41 μm (69-178 K), 50-100 μm (43-69 K), and 100-400 μm (<43K). These bands encompass the diurnal variation of temperature at the lunar surface, which ranges from 130-380 K (Paige et al, 2009). The global data products available from DLRE include measurements of diurnal temperature from which surface temperature maps of the Moon can be created. Also available are global measurements of solar wavelength albedo. DLRE channel 1 and 2 measure reflected solar radiation at 0.35-2.8 μm (Paige et al., 2009). The distinction between the two channels is the solar sensitivity, with channel 2 having reduced sensitivity (Paige et al., 2009).

DLRE global daytime and nighttime GDR level 3 bolometric temperature maps (Table 3) with 128 pixels/degree spatial resolution were used to calculate maximum and minimum global temperature maps. These temperature maps were then used to calculate *ATI* and thermal inertia. DRLE global daytime and nighttime GDR level 2 ancillary data for the temperature maps were also obtained at 128 pixels/degree spatial resolution. These data (Table 3) include the local time and Julian date of the DLRE surface temperature observations used. These data were used to

calculate T_{max}, T_{min}, A_1, A_2, ϕ, and thermal inertia. In addition, the higher-sensitivity channel 1 global visual brightness map from the DRLE GDR level 2 dataset at 128 pixels/degree spatial resolution (Table 3) was used for albedo in the *ATI* calculation.

The Lunar Orbiter Laser Altimeter (LOLA) measures lunar topography using time-of-flight and pulse-spread measurement of five laser beams emitted from the instrument and reflected by the lunar surface (Neumann et al., 2009). The data have been used by the LRO team to create digital elevation models (DEMs) with <128 pixels/degree resolution that can be used for visualization and terrain analysis. I used the LOLA Gridded Data Record Shape Map (GRDDEM) at 128 pixels/degree spatial resolution to apply a cosine correction to the albedo map to remove the effects of topography. I also used the DEM as a context map to verify the correct location of the subsurface cavities, lunar pits, and skylights.

All the global data were obtained from the NASA Planetary Data System (PDS) using the Lunar Orbiter Data Explorer (http://ode.rsl.wustl.edu/moon/index.aspx/) tool. For the bolometric temperature maps, I used the DLRE level 3 Gridded Data Record (GDR) dataset LRO-L_DLRE-5-GDR-V1.0. For the albedo, Julian date, and local time maps, I used the DLRE level 2 GDR dataset LRO-L_DLRE-5-GDR-V1.0. The LOLA DEM was obtained from GDR dataset LRO-L-LOLA-4-GDR-V1.0. By design, the DLRE global maps available on the PDS were produced so that they are geographically registered to the LOLA data at the same spatial resolution.

3.2 Study Areas

There were originally 18 areas of interest (Figure 4). All of the areas are either a known lava tube, subsurface cavity, or skylight. Twelve are located in the Northern Hemisphere and 6 are located in the Southern Hemisphere. Because thermal inertia is dependent on temperature

change between the lunar night and lunar day, I wanted consecutive day and night diurnal data in order to calculate thermal inertia. Of the 18 areas of interest the Rima Sharp lava tube was the only location that had data coverage for two diurnal cycles. The other four areas of interest, for which there was data for one diurnal cycle, are known skylight localities (Wagner and Robinson, 2014). One of these areas, Mare Tranquilitatis, was analyzed by Meyer (2012) using *ATI*. No search for subsurface cavities has previously been done for the Highland 1, Highland 2, and Lacus Mortis locations.

3.3 Data Preprocessing

Several preprocessing steps were required to be applied to the data before they were used to compute thermal signatures. Each original, full sized bolometric temperature, local time, Julian Date, visual brightness, and the LOLA DEM map was 46,080 columns by 23,040 rows in extent and 2,073.6 MB in size. The LOLA-derived slope map was 46,080 columns by 23,040 rows in extent and 4,147.2 MB in size. To make data processing more computationally efficient, all of the global maps were first split into ten tiles, each 9,216 columns and 11,520 rows in extent (Table 4). The tiling was necessary because the available computing resources could not efficiently handle the data files at their full extent. By splitting these maps into tiles, the file size was reduced to 207.36 MB for the bolometric temperature, local time, Julian date, visual brightness, and the LOLA DEM maps. The slope map was reduced in size to 414.72 MB.

Second, a topographic slope map was generated from the LOLA DEM using ENVI software. This slope map was then used in the cosine correction to eliminate measurement errors that may have occurred because of terrain. Lambert's cosine law states that radiant intensity of a surface is directly proportional to the cosine of the angle between the incoming light and the

normal of the surface (Teillet et al., 1982). The cosine correction is calculated using the equation (Teillet et al., 1982):

$$a_h = a_t \frac{\cos Z}{cos I} \qquad (12),$$

where a_h is the corrected albedo, a_t is the raw albedo, Z is the solar zenith and I is the incidence angle. I was determined using the equation (Teillet et al., 1982):

$$I = Z - s \qquad (13),$$

where s is slope. Z was determined using the equation (Teillet et al., 1982):

$$Z = \arccos[(\sin(\phi)\sin(\delta)) + (\cos(\phi)\cos(\delta)\cos(h))] \qquad (14),$$

where h is the hour angle, in local time, determined using the formula:

$$h = s_r(t_1 - 12) \qquad (15),$$

where s_r is the rate at which the sun traverses across the sky (180° in 12 local hours, from sunrise to sunset).

The third preprocessing step was to determine the data coverage for the areas of interest. DLRE global maps have extensive gaps in coverage, particularly at low latitudes. This makes locating areas of interest difficult. In addition there is a large volume of diurnal data available dating back to 2009. A way was needed to efficiently search the catalog for consecutive day and night bolometric temperature measurements for the areas of interest. To this end I wrote a MATLAB code (Appendix 1) that searches downloaded bolometric temperature maps to determine if there is data at an area of interest. The results of this search are summarized in Table 5, from which the diurnal cycles with the most coverage for the areas of interest were selected. Two diurnal lunar cycles were selected for analysis: 04/18/2012 (day) and 05/02/2012 (night); 07/23/2012 (day) and 08/06/2012 (night). The 04/18/2012 to 05/02/2012 bolometric temperature maps include data for Mare Tranquilitatis, Highland 1, Highland 2 and Rima Sharp.

The 07/23/2012 to 08/06/2012 bolometric temperature maps include data for Rima Sharp and Lacus Mortis. None of the other diurnal cycles searched had coverage for more than two sites of interest (Table 5).

3.4. Thermal Inertia and Temperature Maximum to Minimum Ratio Calculations

I wrote a MATLAB code (Appendix 2) to calculate *ATI* and thermal inertia. The code first defines the parameters needed for the T_{max}, T_{min}, and thermal inertia calculations: lunar day length (27.321582 Earth days), ω ($2.662*10^{-6}$ radians/second), t_{min} ($6.609637*10^{5}$ s), t_{max} ($1.227504*10^{6}$ s), S ($1.366*10^{3}$ W/m^2), Ct (1), and axial tilt (5.145°) (Table 6). The code then loads the bolometric temperature, local time, Julian date, and visual brightness maps for a given tile. Next it changes all the missing data gap values, set in the PDS to be -32768, to "not a number" (NaN) values. This is to help with statistical analysis, contrast stretching, and to not skew the final results because the missing data value is so small. Then calibration coefficients were applied to the different maps based on their DLRE label files (Appendix 3). After that, the code converted t_1 and t_2 from lunar hours to Earth seconds, to match the units for t_{max}, t_{min}, and ω. To do this, the conversion

$$t_1 = \left[\left(\frac{t_{1l}}{24}\right) d_l(24)(60)(60)\right] \qquad (16),$$

was used, where t_1 is time of day, t_{1l} is day local time, and d_l is lunar day length. This conversion was used on t_1, t_2, ω, t_{min}, and t_{max}.

The code than calculates T_{max} to T_{min}. To obtain the best estimate of ΔT, my approach was to obtain temperature maps for times as near as possible to the hottest and coldest parts of the lunar diurnal cycle. Due to the orbit of LRO and rotation of the Moon, however, not all surface temperature measurements are made at the same local time. This is a problem because

the surface temperatures measured may not be the largest or the smallest temperature during the lunar diurnal cycle. To fix this, Equations (4) and (5) were used to calculate T_{max} and T_{min} using the measured surface temperatures measurements obtained from the bolometric temperature data, thus ensuring a more accurate ΔT. After T_{max} and T_{min} are calculated, they are subtracted to calculate ΔT. Another MATLAB code (Appendix 4) was written to calculate the T_{max} to T_{min} ratio. The code calculates the ratio using Equation (12), displays the results, and saves the result in ENVI-compatible format.

The code than calculates *ATI* using Equation (3). Then b, δ_1, δ_2, ϕ , N, δ, ξ, A_1, and A_2 (Table 6) are calculated using Equations (7)-(10). Once these parameters are calculated, thermal inertia is calculated using Equation (6). Finally, the code displayed the results and saved them in ENVI-compatible format.

4. Results

Of the 18 potential subsurface cavity locations investigated, only five had data in sites of interest. The five areas of interest are Mare Tranquilities, Highland 1, Highland 2, Rima Sharp, and Lacus Mortis (Figure 6).

4.1 Mare Tranquilitatis

At Mare Tranquilitatis there is a bright thermal inertia signature surrounding the skylight (Figure 7). At the skylight itself, the average thermal inertia is 31,378 $Jm^{-2}K^{-1}s^{-1/2}$. There are smaller thermal inertia values encircling the skylight, with an average thermal inertia of 30,366 $Jm^{-2}K^{-1}s^{-1/2}$. The skylight has 1,012 $Jm^{-2}K^{-1}s^{-1/2}$ higher thermal inertia than the surrounding area. The diameter of the skylight is 100 m by 88 m (Wagner and Robinson, 2014). The size of the thermal inertia anomaly surrounding the skylight is 1.481 km by 0.773 km.

The Mare Tranquilitatis skylight has a low T_{max} to T_{min} ratio (Figure 8). The skylight itself has an average T_{max} to T_{min} ratio of 1.570. The ratio is slightly higher, with an average of 1.596, in the surrounding area. The T_{max} to T_{min} ratio is smaller at the skylight than in the surrounding area, with a difference of 0.026. The size of the T_{max} to T_{min} ratio anomaly associated with the skylight is 1.836 km by 1.125 km.

4.2 Highland 1

The skylight at Highland 1 is at the edge of an area with no data coverage. Nevertheless there appears to be a bright thermal inertia anomaly, with a thermal inertia average of 24,189 $Jm^{-2}K^{-1}s^{-1/2}$, in close proximity to where the skylight is expected to be (Figure 9). There are smaller thermal inertia values encircling the skylight, with an average thermal inertia of 22,841 $Jm^{-2}K^{-1}s^{-}$

$^{1/2}$. The skylight has a 1,348 $Jm^{-2}K^{-1}s^{-1/2}$ higher thermal inertia than the surrounding area. The thermal inertia anomaly is elliptical in shape with a long axis that trends north-south. It is roughly 7.699 km by 2.073 km in extent. The diameter of the skylight is 40 m (Wagner and Robinson, 2014).

To the northwest of the skylight are two linear thermal inertia features that intersect (Figure 10). One trends north-south, with an average thermal inertia of 22,777 $Jm^{-2}K^{-1}s^{-1/2}$. It may turn to the east to converge with the location of the skylight. The average thermal inertia of the surface surrounding this linear feature is 23,970 $Jm^{-2}K^{-1}s^{-1/2}$. This linear signature is approximately 13.703 km by 3.586 km. The second, better defined linear feature trends northeast-southwest, with a thermal inertia average of 22,377 $Jm^{-2}K^{-1}s^{-1/2}$. The average thermal inertia of the surface surrounding this linear feature is 23,436 $Jm^{-2}K^{-1}s^{-1/2}$. This linear feature is approximately 12.247 km by 3.057 km in extent.

There appears to be a low T_{max} to T_{min} ratio anomaly visible near the skylight (Figure 10) with an average value of 1.561. The ratio is slightly larger, with an average of 1.600, in the surrounding area. The size of the T_{max} to T_{min} ratio anomaly is roughly 7.288 km by 1.363 km. To the northwest of the skylight are two linear T_{max} to T_{min} ratio features that intersect. They appear to be the same ones detected in the thermal inertia results. One trends north-south, with a T_{max} to T_{min} ratio average of 1.605. The ratio is slightly smaller, with an average of 1.594, in the surrounding area. This linear signature is approximately 16.448 km by 3.279 km in extent. The better defined linear feature also appears to be the same one detected in the thermal inertia results. It has a T_{max} to T_{min} ratio average of 1.613. The ratio is slightly smaller, with an average of 1.594, in the surrounding area. This linear feature is approximately 12.218 km by 3.678 km in extent.

4.3 Highland 2

The skylight at Highland 2 is at the edge of an area with no data coverage. However, to the west of where the skylight is expected to be there is a bright thermal inertia feature (Figure 11), with an average thermal inertia of 25,085 $Jm^{-2}K^{-1}s^{-1/2}$. There are smaller thermal inertia values encircling the skylight, with an average thermal inertia of 22,976 $Jm^{-2}K^{-1}s^{-1/2}$. The skylight has 2,109 $Jm^{-2}K^{-1}s^{-1/2}$ larger thermal inertia than the surrounding area. The thermal inertia signature is elongated in shape and measures 10.068 km by 5.035 km. The diameter of the skylight itself is unknown, since it was below the 10 m resolution used (Wagner and Robinson, 2014). To the northwest of the skylight is a long, dark, linear feature that trends northeast-southwest and is approximately 12.679 km by 6.094 km in size. The linear feature has relatively low thermal inertia, with an average thermal inertia of 22,403 $Jm^{-2}K^{-1}s^{-1/2}$. There are larger thermal inertia values surrounding this linear feature, with an average thermal inertia of 24,289 $Jm^{-2}K^{-1}s^{-1/2}$.

To the west of the skylight is a dark T_{max} to T_{min} ratio feature (Figure 12), with an average of 1.588. The ratio is slightly larger, with an average of 1.597, in the surrounding area. The size of this T_{max} to T_{min} ratio feature is 9.833 km by 5.567 km. To the northwest of the skylight is a long, bright, linear feature that trends northeast-southwest and is approximately 12.598 km by 3.271 km in size. The linear feature has an average T_{max} to T_{min} ratio of 1.610. The ratio is slightly smaller, with an average of 1.589, in the surrounding area.

4.4 Rima Sharp

I measured the lava tube suggested by Chappaz et al. (2014) to be approximately 111 km by 22 km. Since the lava tube covers a large area and it does not have a known skylight to help

pinpoint its location, I overlaid the Chappaz et al. (2014) results onto the LOLA DEM to ensure I was looking in the correct area while analyzing the thermal inertia data. (Figure 13). Although this lava tube is quite large, there are no thermal inertia anomalies visible in the area using data from either of the diurnal pairs (Figures 14 and 15). Similarly, there are no T_{max} to T_{min} ratio anomalies visible (Figures 16 and 17). Roughly 50%-70% of the area lies in data gaps.

4.5 Lacus Mortis

The Lacus Mortis skylight is not associated with a curvilinear high thermal inertia signature (Figure 18), but instead has a circular signature with low thermal inertia. The skylight itself has a thermal inertia value of 38,952 $Jm^{-2}K^{-1}s^{-1/2}$. The surrounding area has a higher thermal inertia, with an average of 39,731 $Jm^{-2}K^{-1}s^{-1/2}$. The diameter of the skylight is 140 m by 110 m (Wagner and Robinson, 2014), and the thermal inertia signature surrounding the skylight is 1.481 km by 0.890 km. There is a faint dark linear feature, with a thermal inertia average of 39,020 $Jm^{-2}K^{-1}s^{-1/2}$, trending southeast of the skylight. There are larger thermal inertia values surrounding this linear feature, with an average thermal inertia of 39,472 $Jm^{-2}K^{-1}s^{-1/2}$. The linear feature is approximately 5.160 km by 2.382 km in extent.

The Lacus Mortis skylight is in an area of large T_{max} to T_{min} ratios (Figure 19), with a T_{max} to T_{min} ratio average of 1.493. The ratio is slightly smaller, with an average of 1.492, in the surrounding area. The size of this T_{max} to T_{min} ratio feature is 9.833 km by 5.567 km. The T_{max} to T_{min} ratio signature of the skylight is 1.686 km by 1.482 km in extent. Connected to the skylight, and trending northwest-southeast, is a bright linear feature with an average T_{max} to T_{min} ratio value of 1.494. The ratio is slightly smaller, with an average of 1.490, in the surrounding area. The linear feature is approximately 6.747 km by 2.491 km in size.

5. Discussion

5.1. Mare Tranquilitatis

The Mare Tranquilitatis skylight has larger a thermal inertia than the surrounding area, which is expected for the signature caused by a skylight. There is a smaller thermal inertia area haloing the skylight, averaging 30,366 $Jm^{-2}K^{-1}s^{-1/}2$, which could be interpreted as the surface expression of a subsurface cavity. Similarly, the Mare Tranquilitatis skylight has a smaller T_{max} to T_{min} ratio than the surrounding area, which is also consistent with the presence of a subsurface cavity. However neither the thermal inertia signature nor the T_{max} to T_{min} ratio signature are linear, suggesting that the cavity may not be a lava tube. Instead, the cavity may be some sort of isolated, near-circular chamber, and the skylight may actually be a pit. This is consistent with the result of Meyer (2012) who suggested that a large circular chamber exists beneath the Mare Tranquilitatis skylight.

5.2 Highland 1

A large thermal inertia signature and small T_{max} to T_{min} ratio signature are associated with the Highland 1 skylight, and are consistent with the T_{max} to T_{min} ratio and thermal signature caused by a skylight. I believe the linear feature that trends north-south is a lava tube. This is because the ground surface above the intact roof of the lava tube has a lower thermal inertia (22,777 $Jm^{-2}K^{-1}s^{-1/2}$) than the surrounding area (23,970 $Jm^{-2}K^{-1}s^{-1/2}$). It also has a higher T_{max} to T_{min} ratio (1.605) than the surrounding area (1.594). The anomaly is curvilinear in shape, and connects with a skylight. Although the linear feature that trends northeast-southwest does not connect with the skylight, I believe it is also a lava tube. The ground surface above the intact

roof of this lava tube has a lower thermal inertia (22,377 $Jm^{-2}K^{-1}s^{-1/2}$) than the surrounding area (23,436 $Jm^{-2}K^{-1}s^{-1/2}$). It also has a higher T_{max} to T_{min} ratio (1.613) than the surrounding area (1.594). The anomaly is linear in shape. There are three explanations for this anomaly. The lava tube could have formed in a different channel, but came from the same source and the same time period as the first lava tube. The lava tube, being in a different channel, came from a different direction and intersected the first lava tube. Alternatively, this second lava tube could have formed from an entirely different volcanic source, potentially at a different time period. The third explanation for the anomaly is it is not a lava tube.

5.3 Highland 2

To the west of the skylight is a large thermal inertia feature and a small T_{max} to T_{min} ratio feature. However, I do not believe this feature is caused by the skylight. The skylight is far enough away from the feature that the visible feature is not caused by the skylight. Also, the feature is not a solid feature, but more like a half ring surrounding an area of small thermal inertia values and large T_{max} to T_{min} ratio values. The linear feature to the northwest of the skylight has a lower thermal inertia (22,403 $Jm^{-2}K^{-1}s^{-1/2}$) than the surrounding area (24,289 $Jm^{-2}K^{-1}s^{-1/2}$). It also has a higher T_{max} to T_{min} ratio (1.610) than the surrounding area (1.589), and the anomaly is linear in shape. I believe this thermal inertia and T_{max} to T_{min} ratio anomaly is associated with a lava tube in the subsurface. However, this lava tube does not appear to connect to the known skylight. However, the lava tube may turn southward, which is not visible due to the lack of data coverage gap around the skylight. There is no way, currently, of knowing if the lava tube connects to the skylight due to the missing data.

5.4 Rima Sharp

Both the thermal inertia and the T_{max} to T_{min} ratio techniques failed to highlight any linear features consistent with the surface expression of an underground lava tube or any other cavity at Rima Sharp. There are several possible reasons for this. One possibility is that thermal inertia may not always detect subsurface cavities, particularly if the temperature difference of the ground surface above the roof of the lava tube is the same as in the surrounding area (see Section 5.6). A second possibility to why thermal inertia and the T_{max} to T_{min} ratio did not detect the lava tube is that the sparse data coverage is masking the presence of a cavity. Roughly 50 to 70% of the data is missing, and it is entirely possible that the thermal anomaly associated with the Rima Sharp lava is in one of these gaps. A third possibility is the lava tube is too deep for thermal methods to detect it. The fourth possibility is that a lava tube (or any other cavity) does not exist at Rima Sharp and Chappaz et al. (2014) detected something else in the gravity data that was not a subsurface cavity.

5.5 Lacus Mortis

The Lacus Mortis skylight is associated with neither the large thermal inertia nor the small T_{max} to T_{min} ratio anomalies expected for a skylight. Instead, the values for the skylight (38,952 $Jm^{-2}K^{-1}s^{-1/2}$ and 1.493) and the surrounding area (39,731 $Jm^{-2}K^{-1}s^{-1/2}$ and 1.492) are not significantly different to one another.

Although a linear feature was difficult to see in the thermal inertia data, the linear feature became apparent in the T_{max} to T_{min} ratio data. I believe a lava tube may be present in the subsurface. The ground surface above the intact roof of the lava tube has a lower thermal inertia (39,020 $Jm^{-2}K^{-1}s^{-1/2}$) than the surrounding area (39,472 $Jm^{-2}K^{-1}s^{-1/2}$). It also had a higher T_{max} to

T_{min} ratio (1.494) than the surrounding area (1.490). In addition, the anomaly is linear in shape, and connects perfectly to the skylight.

5.6 Issue with the Thermal Inertia Technique

I believe there is a flaw in the thermal inertia technique. *ATI* and thermal inertia are inversely proportional to temperature difference (Equations 3 and 6). It is possible to have the same temperature difference at the surface above a subsurface cavity and in the surrounding area. For example, say T_{max} at the surface above a lava tube is 390 K and T_{min} is 159 K. The temperature difference in this case would be 231 K. Nearby, at the ground surface above where a lava tube is not present, T_{max} may be 395 K and T_{min} may be 164 K. The temperature difference in this case is also 231 K. In this example, even though a lava tube is present and has the expected effects on the surface temperature, it would not be detected using either *ATI* or thermal inertia because the temperature difference is, coincidentally, the same in both locations. I must consider this as a possibility to explain the observations at localities such as Rima Sharp.

I believe the T_{max} to T_{min} ratio technique would more accurately detect a lava tube than the thermal inertia technique. Even if the temperature differences are the same in an area above a roofed lava tube and solid rock, the T_{max} to T_{min} ratio would not be. In the hypothetical example, the temperature difference was 231 K for both the ground surface above an intact roof of a lava tube and in the surrounding area. However the T_{max} to T_{min} ratio for the ground surface above the lava tube in this case would be 2.453, while the T_{max} to T_{min} ratio for the surrounding area would be 2.409. The ground surface above a roofed lava tube has a larger T_{max} to T_{min} ratio than the surrounding area. The T_{max} to T_{min} ratio technique may be able to detect the ground surface

anomaly of a subsurface lava tube when thermal inertia cannot. Since both techniques did not detect an anomaly of a subsurface cavity, I do not believe this flaw is to blame.

6. Conclusions

Using both the thermal inertia and T_{max} to T_{min} ratio techniques four of the five sites of interest had subsurface cavities present. Mare Tranquilitatis has a circular cavity located below the skylight. Highland 2 and Lacus Mortis have a lava tube present near or connecting to the known skylights, and Highland 1 has two lava tubes present, with one potentially connecting to the skylight. Although it had been suspected that lava tubes may be present at Highland 1, Highland 2, and Lacus Mortis, it has not been explored until now. Both thermal methods did not detect a lava tube at Rima Sharp.

These large areas have been protected from surface processes and may contain pristine geologic and other materials. These lava tubes present great potential for vertical exposures of the stratigraphy of the upper lunar crust, for exploration and discovery. In addition, these are subsurface cavities would provide protection for future explorers as they conduct research on Moon.

References

Ashley, J.W., Boyd, A.K., Hiesinger, H., Robinson, M.S., Tran, T., Van Der Bogert, C.H., Wagner, R.V., and the LROC Science Team, 2011, Lunar Pits: Sublunarean Voids and the Nature of Mare Emplacement: *Proceedings of the 42nd Lunar and Planetary Science Conference*, abstract 2,771.

Bandfield, J.L., Ghent, R.R., Vasavada, A.R., Paige, D.A., Lawrence, S.J., and Robinson, M.S., 2011, Lunar surface rock abundance and regolith fines temperatures derived from LRO Diviner radiometer data: *Journal of Geophysical Research*, vol. 116, doi:10.1029/2011JE003866.

Blair, D.M., Chappaz, L., Sood, R., Millbury, C., Melosh, H.J., Howell, K.C., and Freed, A.M., 2015, Determining the Structural Stability of Lunar Lava: *Proceedings of the 46rd Lunar and Planetary Science Conference*, abstract 2,174.

Chappaz, L., Melosh, H.J., Howell, K.C., and the GRAIL mission team, 2014, Surface and Buried Lava Tube Detection with GRAIL Data: *Proceedings of the 45rd Lunar and Planetary Science Conference*, abstract 2,019.

Coombs, C.R. and Hawke, B.R., 1992, A search for intact lava tubes on the moon: Possible lunar base habitats: *Proceedings of the Second Conference on Lunar Bases and Space Activities of the 21st Century* (NASA Conference CP-3166), vol. 1, p. 219-229.

Cruikshank, D.P. and Wood, C.A., 1972, Lunar rilles and Hawaiian volcanic features: Possible analogies: *Moon*, vol. 3, p. 412-447.

Cushing, G.E., Titus, T.N., and Wynne, J.J., 2007, THEMIS observes possible cave skylights on Mars: *Proceedings of the 38th Lunar and Planetary Science Conference*, abstract 1,371.

Deschamps, A., Grigne, C., Le Saout, M., Soule, S.A., Allemand, P., Lanoe, B.V.V., and Floc'h, F., 2014, Morphology and dynamics of inflated subaqueous basaltic lava flows: *Geochemistry, Geophysics, Geosystems* (G^3), vol. 15, p. 2,128-2,150.

Greeley, R., 1971, Lava tubes and channels in the lunar Marius Hills: *Moon*, vol. 3, p. 289-314.

Horz, F., 1985, Lava tubes: Potential shelters for habitats*: Proceedings of the Lunar Bases and Space Activities of the 21st Century* (NASA Conference CP-3166), vol. 1, p. 405-412.

Johnson, F.S., 1954, The Solar Constant: *Journal of the Atmospheric Sciences*, vol. 11, p. 431-439.

Maltese, A., Bates, P.D., Capodici, F., Cannarozzo, M., Ciralo.G. and La Loggia, G., 2013, Critical analysis of thermal inertia approaches for surface soil water content retrieval: *Hydrological Sciences Journal*, vol. 58, p. 1144-1161.

Meyer, J.A., 2012, *New Methods for the Discovery and Characterization of Lunar Lava Tubes Using Lunar Reconnaissance Orbiter Data* (M.S. Thesis): The University of Texas at El Paso, 87 p.

Mitrofanov, I.G., Sanin, A.B., Boynton, W.V., Chin, G., Garvin, J.B., Golovin, D., Evans, L.G., Harshman, K., Kozyrev, A.S., Litvak, M.L., Malakhov, A., Mazarico, E., McClanahan, T., Milikh, G., Mokrousov, M., Nandikotkur, G., Neumann, G.A., Nuzhdin, I., Sagdeev, R., Shevchenko, V., Shvetsov, V., Smith, D.E., Starr, R., Tretyakov, V.I., Trombka, J., Usikov, D., Varenikov, A., Vostukhin, A., and Zuber, M.T., 2010, Hydrogen mapping of the lunar South Pole using the LRO neutron detector experiment LEND: *Science*, vol. 330, p. 483-486.

Neuendorf, K.K.E., Mehl Jr., J.P., and Jackson, J.A., 2005, *Glossary of Geology* (5th edition): American Geological Institute (Alexandria, VA), 779 p.

Neumann, G., Riris, H., and Cavanaugh, J., 2009, *Calibration Document for the Lunar Orbiter Laser Altimeter (LOLA) Instrument* (Revision 2): Goddard Space Flight Center LRO Database, 65 p: http://lunarngin.gsfc.nasa.gov.

Paige, D.A., Foote, M.C., Greenhagen, B.T., Schofield, J.T., Calcutt, S., Vasavada, A.R., Preston, D.J., Taylor, F.W., Allen, C.C., Snook, K.J., Jakosky, B.M., Murray, B.C., Soderblom, L.A., Jau, B., Loring, S., Bullharowski, J., Bowles, N.E., Thomas, I.R., Sullivan, M.T., Avis, C., De Jong, E.M., Hartford, W., and McCleese, D.J., 2009, The

Lunar Reconnaissance Orbiter Diviner Lunar Radiometer Experiment: *Space Science Review*, vol. 150, p. 125-160.

Paige, D.A., Siegler, M.A., Zhang, J.A., Hayne, P.O., Foote, E.J., Bennett, K.A., Vasavada, A.R., Greenhagen, B.T., Schofield, J.T., McCleese, D.J., Foote, M.C., DeJong, E., Bills, B.G., Hartford, W., Murray, B.C., Allen, C.C., Snook, K., Soderblom, L.A., Calcutt, S., Taylor, F.W., Bowles, N.E., Bandfield, J.L., Elphic, R., Ghent, R., Glotch, T.D., Wyatt, M.B., and Lucey, P.G., 2010, Diviner lunar radiometer observations of cold traps in the Moon's south pole region: *Science*, vol. 330, p. 479-482

Peterson, D.W., Holcomb, R.T., Tilling, R.I., and Christiansen, R.L., 1994, Development of lava tubes in the light of observations at Mauna Ulu, Kilauea Volcano, Hawaii: *Bulletin of Volcanology*, vol. 56, p. 343-360.

Prado, M., 2013, NASA Lunar Reconnaissance Orbiter (LRO) and LCROSS Polar Crater Impactor: http://www.permanent.com/lunar-reconaissance-orbiter-lro-lcross.html (Accessed April, 2015).

Scheidt, S., Ramsey, M., and Lancaster, N., 2010, Determining soil moisture and sediment availability at White Sands Dune Field, NM from apparent thermal inertia data: *Journal of Geophysical Research*, vol. 115, F02019, doi: 10.1029/2009JF001378.

Teillet, P.M., Guindon, B. and Goodenough, D.G., 1982, On the slope-aspect correction of multispectral scanner data, *Canadian Journal of Remote Sensing*, vol. 8, pp. 1537-1540.

Wagner, R.V. and Robinson, M.S., 2014, Distribution, Formation Mechanisms, and Significance of Lunar Pits: *Icarus*, vol. 237, p. 52-60.

Williams, J.P., Paige, D.A., Sefton-Nash, E., Greenhagen, B.T., 2015, Global surface temperatures of the Moon: *2015 AGU Fall Meeting*, abstract 2110.

Wynne, J.J. Titus, T.N., and Diaz, G.C., 2008, On developing thermal cave detection techniques for Earth, the Moon and Mars: *Earth and Planetary Science Letters*, vol. 272, p. 240-250.

Ximenes, S.W., Mardon, A.A., Baiden, G., Osinski, G.R., Ghafoor, N., Gurtuna, O., Prevot, A., and Daly, M.G., 2010, Lava tubes analog mission for lunar science and human performance studies: *Proceedings of the 41st Lunar and Planetary Science Conference*, abstract 2,575.

Xue, Y. and A.P. Cracknell, 1995, Advanced thermal inertia modeling: *International Journal of Remote Sensing*, vol. 3, p. 431-446.

Table 1: Impact Lava Pits

Crater Name	Latitude	Longitude	Crater diameter (km)	Approximate % searched	# Pits >5m wide	Biggest pit size (m)	Median depth (m)	Median diameter (m)
King	6.50 N	119.8 E	76	100	51	57 x 24 x 13	6	11
Tycho	-43.30 S	348.8 W	85	40	31	85 x 60 x 17	12	34
Copernicus	9.60 N	339.9 W	96	75	17	100 x 40 x 25	11	14
Lalande	-4.40 S	351.4 W	23	95	19	25 x 10 x 11	5	10
Stevinus	-32.50 S	54.1 E	71	90	16	55 x 30 x 20	4	7
Aristarchus	23.70 N	312.5 W	40	25	13	25 x 8 x 14	7	13
Crookes	-10.40 S	194.9 W	48	25	11	70 x 30 x 17	17	19
Jackson	22.00 N	196.7 W	71	15	7	25 x 14 x 22	17	10
Das	-26.60 S	223.2 W	36	100	6	30 x 12 x 14	5	13
Aristillus	33.90 N	1.2 E	54	20	4	28 x 27 x 20	11	17
Kepler	8.10 N	322 W	29	35	4	50 x 25 x 18	8	11
Klute W	38.00 N	216.7 W	31	20	4	20 x 10 x 8	6	11
Adams B	-31.40 S	65.7 E	31 x 25	20	3	17 x 12 x 6	5	11
Dollond E	-10.30 S	15.7 E	5	100	2	35 x 20 x >35	N/A *	24
Messier A	-2.00 S	46.9 E	11	90	2	7 x 4 x 6	7	5
Near Wood S	43.90 N	235.7 W	11	100	2	40 x 25 x 6	7	19
Ohm	18.30 N	246.2 W	62	15	2	19 x 12 x ~18	16	16
Proclus	16.10 N	46.9 E	27	20	2	40 x 25 x 8	7	29
Stefan L	44.40 N	251.9 W	26	25	2	34 x 33 x 10	10	28
Guthnick	-47.80 S	266 W	37	60	1	6 x 5 x 3	3	6
Harriot	33.30 N	114.4 E	38	15	1	30 x 20 x 12	12	25
Hayn	64.60 N	83.9 E	86	1	1	20 x 15 x ~6	6	17
Milichius A	9.30 N	327.9 W	8	100	1	13 x 10 x >17	N/A *	12
Near Virtanen	15.80 N	177.3 E	11	100	1	28 x 14 x 17	17	21
Palitzsch B	-26.30 S	68.2 E	38	20	1	15 x 10 x 10	10	13
Picard	14.60 N	54.7 E	22	25	1	15 x 12 x 6	6	14
Rutherfurd	-61.10 S	347.8 W	50	10	1	23 x 20 x 4	4	21
Sharonov	12.40 N	173.1 E	75	60	1	5 x 5 x 6	6	5
Wiener F	41.20 N	150 E	31	35	1	70 x 70 x 20	20	70

* indicates pit does not have a measured median depth. Table after Wagner and Robinson (2014).

Table 2: Lava Flow Pits

Location	Latitude	Longitude	Central pit size (m)	Central pit depth (m)	Outer funnel (approx.) size (m)	Outer funnel (approx.) depth (m)
Lacus Mortis	44.962 N	45.61 W	140 x 110	80	280 x 210	35
Central Mare Fecunditatis	-0.917 S	48.66 W	130 x 110	~30	190 x 160	~15
Mare Tranquilitatis	8.335 N	33.111 W	100 x 88	105	170 x 150	~5-9
Mare Ingenii	-35.948 N	166.053 W	100 x 68	45-65	160 x 130	15-20
Southwest Mare Fecunditatis	-6.752 S	42.759 W	16 x 14	~35	60 x 55	~40
Marius Hills	14.091 N	303.23 E	58 x 49	40	70 x 80	~4-10
Schluter Crater	-5.839 S	276.95 E	40 x 20	~45	65 x 50	~15
Highland 1	43.966 N	23.083 W	40 x 40	25	55 x 55	not measured*
Highland 2	41.156 N	18.819 W	not measured*	28	40 x 35	not measured*
Runge Crater	-2.702 S	86.78 W	17 x 13	5	N/A *	N/A *

* indicates an area where a measurement was not taken because the size was below resolution.
Table after Wagner and Robinson (2014).

Table 3: Downloaded Data

Data Type	Bolometric Temperature	Local Time	Julian Date	Visual Brightness	LOLA DEM
Abbreviation	tbol	ltim	jd	vb1	ldem
Resolution (pixels/degree)	5/7/1900	128	128	128	128
04/18/2012 data names	dgdr_tbol_cyl_20120418d_jp2.jp2	dgdr_ltim_cyl_20120418d_jp2.jp2	dgdr_jd_cyl_20120418d_jp2.jp2	dgdr_vb1_cyl_20120418d_jp2.jp2	
05/02/2012 data names	dgdr_tbol_cyl_201200502n_jp2.jp2	dgdr_ltim_cyl_201200502n_jp2.jp2	dgdr_jd_cyl_201200502n_jp2.jp2	dgdr_vb1_cyl_201200502n_jp2.jp2	
07/23/2012 data names	dgdr_tbol_cyl_201207/23d_jp2.jp2	dgdr_ltim_cyl_201207/23d_jp2.jp2	dgdr_jd_cyl_201207/23d_jp2.jp2	dgdr_vb1_cyl_201207/23d_jp2.jp2	
08/06/2012 data names	dgdr_tbol_cyl_20120806n_jp2.jp2	dgdr_ltim_cyl_20120806n_jp2.jp2	dgdr_jd_cyl_20120806n_jp2.jp2	dgdr_vb1_cyl_20120806n_jp2.jp2	
data name for LOLA DEM					ldem_12_jp2.jp2

Note: This table dislays the downloaded data from the Planetary Data System. The abbreviations are used in the label files (Appendix 3). The data names are the actual files downloaded for the PDS.

Table 4: Tile Information

Tile Number	Northern Row	Southern Row	Northern Latitude	Southern Latitude	Western Column	Eastern Column	Western Longitude	Eastern Longitude
1	1	11,520	90	0	1	9,216	-180	-108
2	1	11,520	90	0	9,217	18,432	-108	-36
3	1	11,520	90	0	18,433	27,648	-36	36
4	1	11,520	90	0	27,649	36,864	36	108
5	1	11,520	90	0	36,865	46,080	108	180
6	11,521	23,040	0	-90	1	9,216	-180	-108
7	11,521	23,040	0	-90	9,217	18,432	-108	-36
8	11,521	23,040	0	-90	18,433	27,648	-36	36
9	11,521	23,040	0	-90	27,649	36,864	36	108
10	11,521	23,040	0	-90	36,865	46,080	108	180

Note: This tables shows how each of the original data maps was broken down into 10 equal tiles. Each tile has 9,216 columns and 11,520 rows.

Table 5: Potential Site Location Data Check

Location	Latitude	Longitude	Row	Column	Tile	12/31/2011	1/14/2012	1/28/2012	2/10/2012	3/23/2012	4/5/2012	4/18/2012	5/2/2012	5/16/2012	7/23/2012	8/6/2012	8/19/2012
Mare Ingenii	-35.95	166.06	16122	44296	10				X		X			X			
Mare Tranquilitatis	8.34	33.22	10452	27292	3		X			X		X	X				
Rima Sharp begin	36	-48	6912	16896	2			X			X				X	X	X
Rima Sharp end	36	-44	6912	17408	2		X			X		X	X				
Location C	35	-43	7040	17536	2		X			X		X	X				
Ina Crater	18.66	5.3	9132	23718	3					X							X
Rima Hadley- crater	25.3	2.55	8282	23366	3			X					X			X	
Rima Hadley- flat	26.25	2.48	8160	23357	3			X					X				
Lacus Mortis	44.962	25.61	5765	26318	3			X	X	X					X		X
Central Mare Fecunditatis	-0.917	48.66	11637	29268	9						X						
Mare Tranquillitatis	8.335	33.22	10453	27292	3		X			X		X	X				
Mare Ingenii	-35.948	166.053	16121	44295	10				X		X			X			
Sothwest Mare Fecunditatis	-6.752	42.759	12384	28513	9	X											X
Marius Hills	14.091	-56.77	9716	155773	2				X			X		X			
Schluter Crater	-5.839	-83.05	11267	12410	7											X	
Highland 1	43.966	23.083	5892	25995	3					X	X	X					X
Highland 2	41.156	18.819	6252	25449	3					X			X				
Runge Crater	-2.702	86.78	11866	34148	9										X		X

Note: This data displays dates checked to determine if a potential site of interest has usable data. For tiling information see table 5. The dates in the black boxes are night dates and the dates in the white boxes are day dates. The "X"s represent data.

Table 6: Variables

Variable	Variable Meaning	Value	Units
lunardaylength	length of the lunar day	27.322	Earth days
ω	angular frequency	2.66E-06	radians/s
t_{max}	time maximum	1.23E+06	s
t_{min}	time minimum	6.61E+05	s
S	solar constant	1.37E+03	W/m^2
Ct	atmospheric transmittance	1.00	*
a	albedo		%
Tday	daytime temperature		K
t_1	daytime time		s
Tnight	nighttime temperature		K
t_2	nighttime time		s
JDday	Julian date day		day
JDnight	Julian date night		day
T1	daytime temperature		K
T2	nighttime temperature		K
T_{max}	temperature maximum		K
T_{min}	temperature minimum		K
ΔT	temperature difference		K
ATI	apparent thermal inertia		*
δ_1	solar declination at time 1		radians
δ_2	solar declination at time 2		radians
ϕ	latitude		degrees
N	converted Julian Date		day
δ	solar declination		degrees
s_r	rate sun traverses the sky		degrees/hr
h	hour angle		degrees
z	solar zenith		degrees
I	incidence angle		degrees
s	slope		*
ξ	xi- see Equation 9		degrees
A_1	Fourier coefficient		degrees
A_2	Fourier coefficient		degrees
P	thermal inertia		$Jm^{-2}K^{-1}s^{-1/2}$

Note: Table lists all variables used in both the paper and codes.
* indicates unitless variables. Blank cells indicate the value varies.

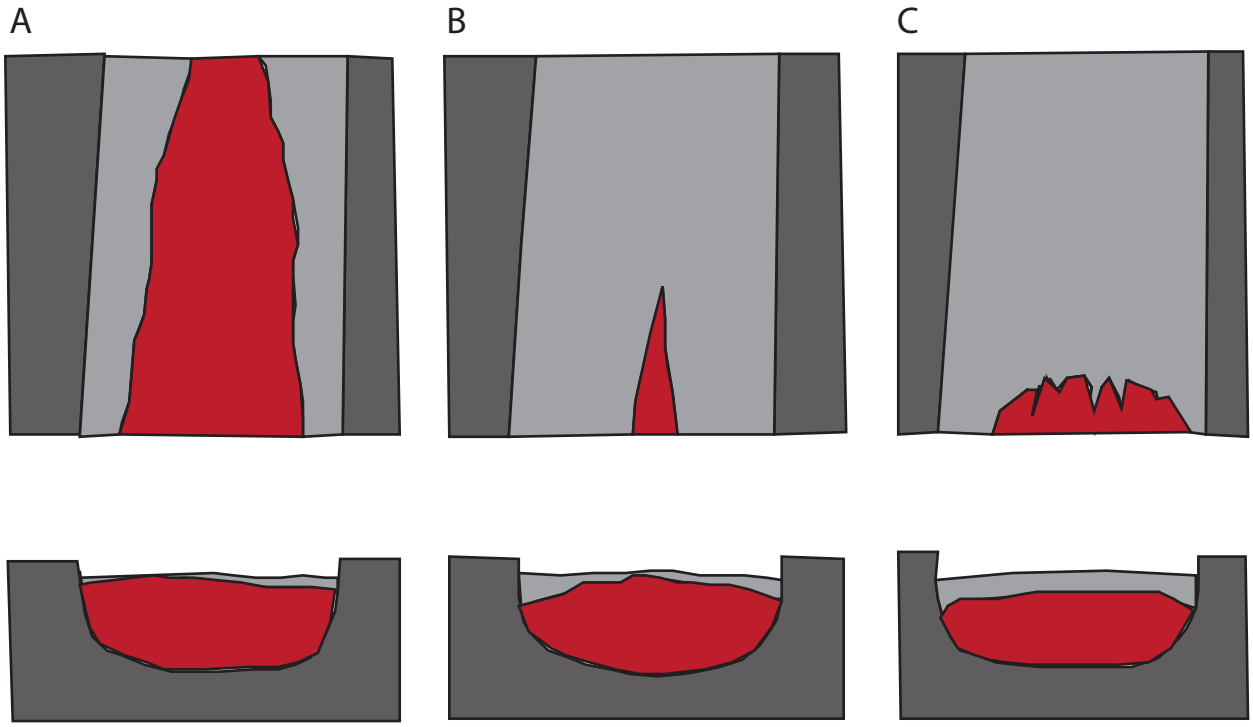

Figure 1: Lava tube formation by the growth of rooted crust (from Peterson et al. 1994). The series of events goes from left (a) to right (d). The top row illustrates the process in map view and the bottom rows illustrate the process in cross-sectional views perpendicular to the direction of flow. In this scenario, as the lava flows down the channel at a constant level and in laminar flow, the lava surface will solidify. This starts at the banks and continues towards the middle of the channel where the two sides become one solid roof. The roof can then thicken, while the lava still flows beneath it. Eventually, the lava will stop flowing, and, if the lava drains out, a tube will remain.

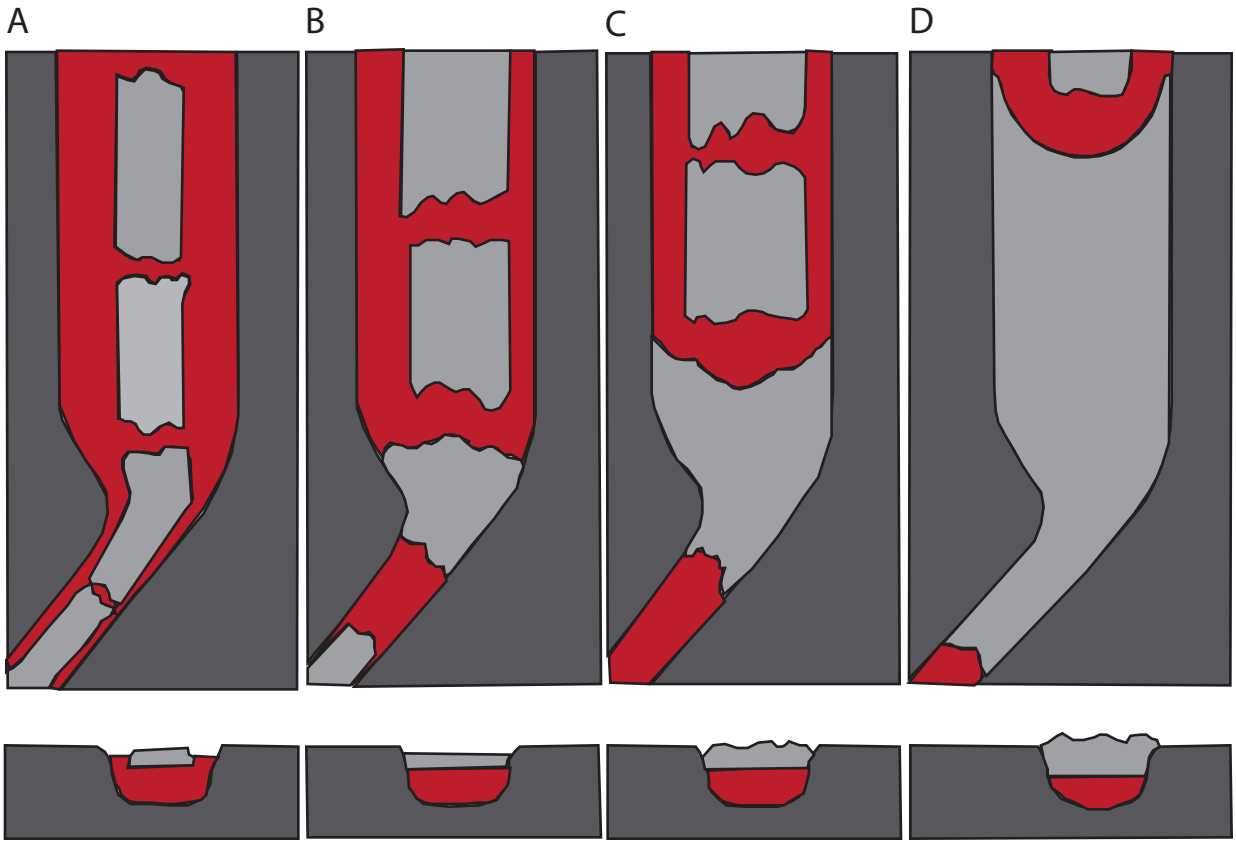

Figure 2: Lava tube formation by aggregation of floating crustal rafts (from Peterson et al., 1994). The series of events goes from left (a) to right (d). The top row shows the process in map view and bottom row shows the process in cross-sectional views perpendicular to the direction of flow. In this scenario, the lava flows in a turbulent manner, but the lava level is constant. Parts of the lava surface will solidify, but, due to the turbulent flow, the solidified crust cannot remain connected to the banks. Instead, solidified fragments float down the channel until they are trapped by a narrowing of the channel, a tight bend, or a similar obstruction. Eventually, a logjam of these fragments will form, and the lava flowing below will help to consolidate them into a single, large raft which becomes a roof over the channel. The roof can then thicken, while the lava still flows beneath it. Eventually, the lava will stop flowing, and, if the lava drains out, a tube will remain.

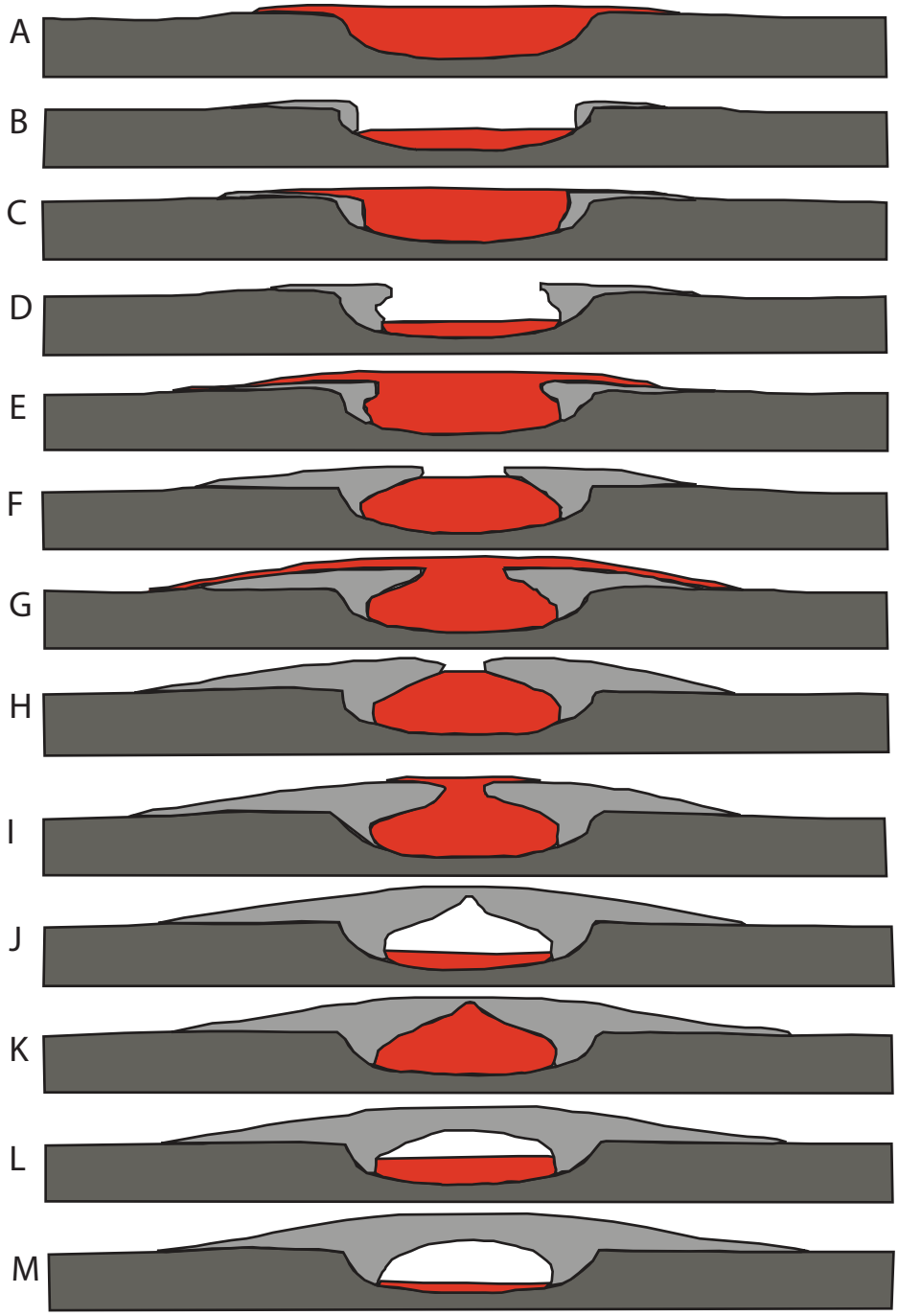

Figure 3: Lava tube formation by accretion of levees (from Peterson et al. 1994). The series of events starts at (a), and it proceeds vertically down, ending at (m). In this scenario, as the lava flows down the channel, the lava level constantly changes, at times overtopping the banks. As the channel undergoes multiple cycles of flooding, levees start to form from the solidified lava. These levees take on an arch shape. Eventually the levees will join together to form an arched roof over the lava channel. The roof can then thicken, while the lava still flows beneath it. Eventually, the lava will stop flowing, and, if the lava drains out, a tube will remain.

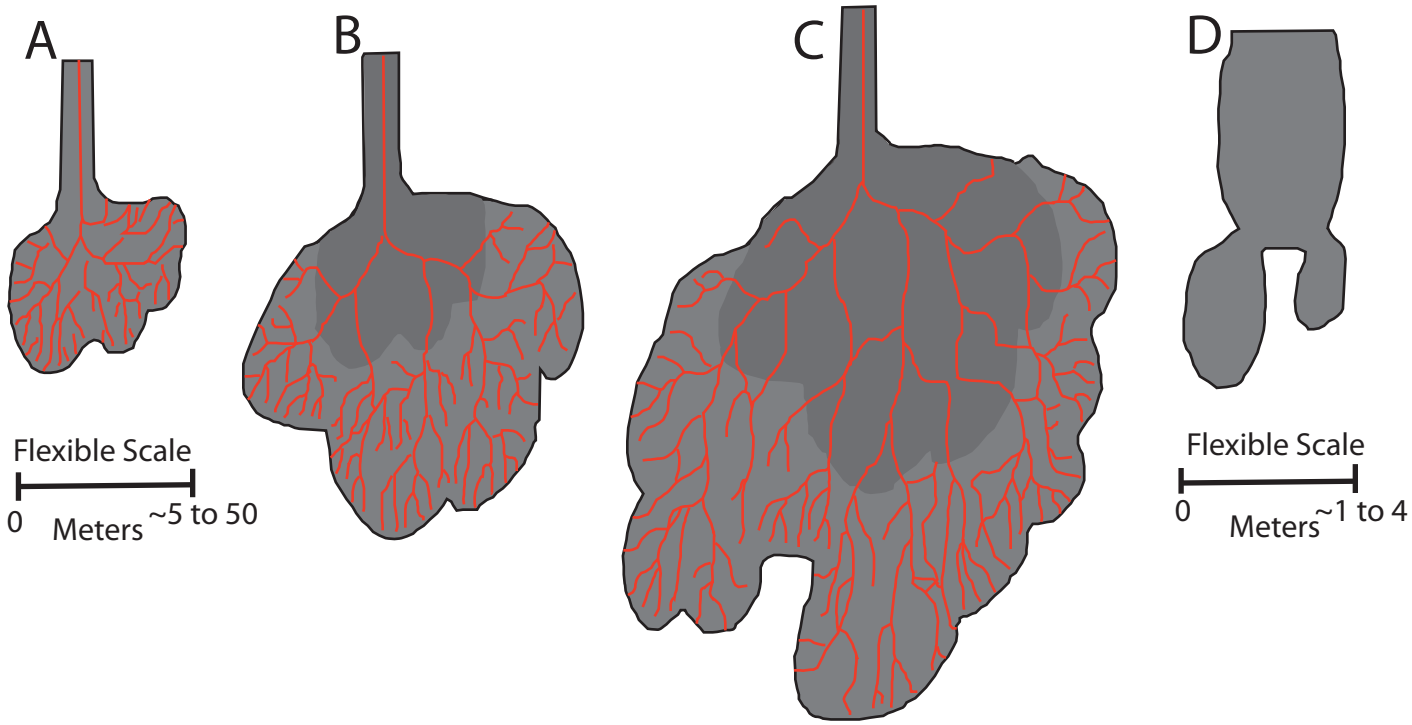

Figure 4: Lava tube formation by extension of pahoehoe lobes (from Peterson et al., 1994). (a)-(c) Progressive extension of the pahoehoe lobes over time. (d) A zoomed-in illustration of one of the flow lobes. In this scenario, the lava is not flowing in a channel, but instead on a low topographic gradient. As the lava stalls, it starts to inflate, or build, upon itself. This process continues as the lobes spread further out, inflating on themselves, and then spreading farther. Eventually, the lava will stop flowing, and, if the lava drains out, a tube will remain.

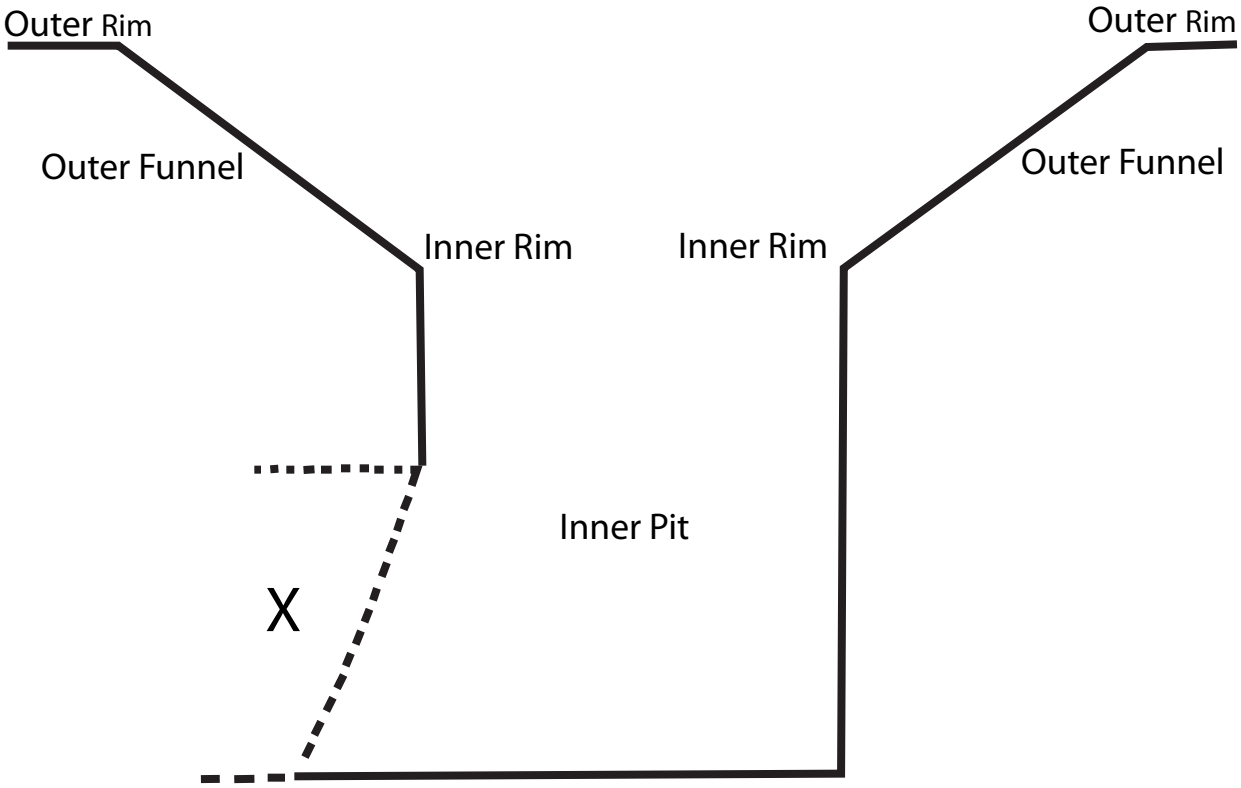

Figure 5: Generic cross-section of a lunar pit (from Wagner and Robinson, 2014). The "X" denotes a possible connection to a more extensive tunnel. The lava may not have drained out, leaving that section solid basalt.

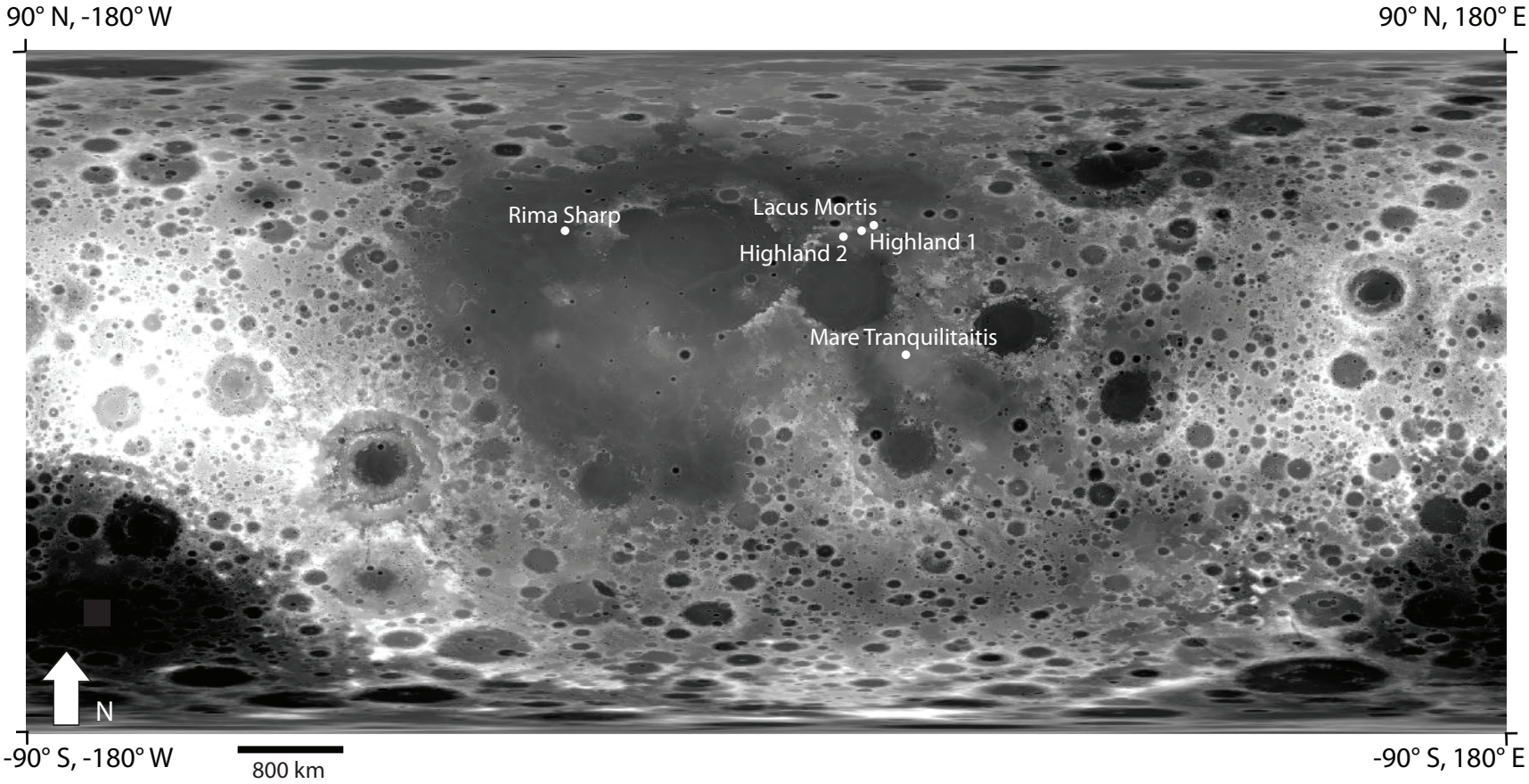

Figure 6: LOLA DEM with sites of interest. The five potential subsurface cavites locations are marked with the white circles.

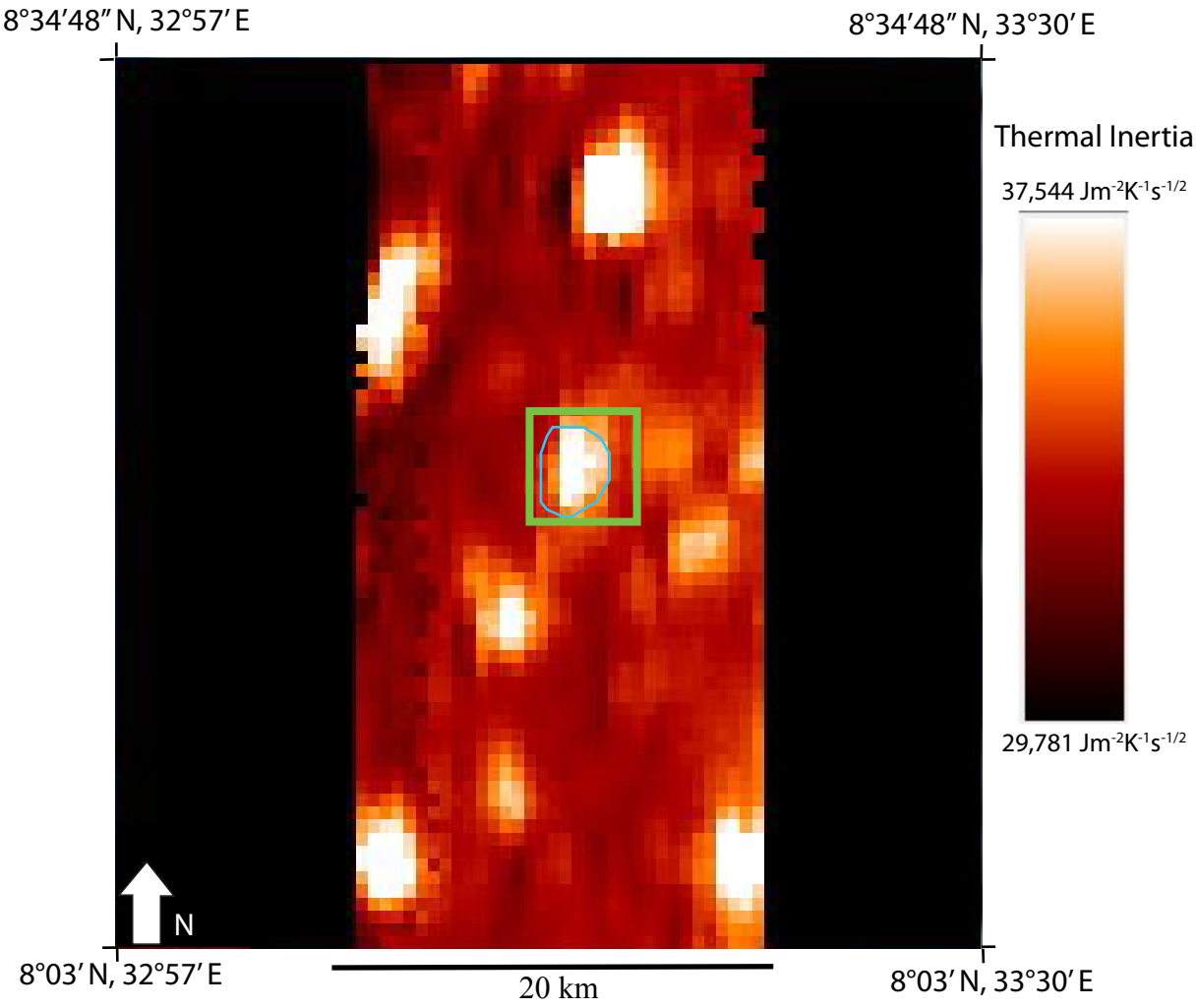

Figure 7: Thermal inertia map of Mare Tranquilitatis generated using data from the 04/18/2012 to 05/02/2012 lunar diurnal cycle. In the middle of the green box is the center point of the potential skylight location (Meyer, 2012; Wagner and Robinson, 2014). The brighter colors denote larger thermal inertia values while the darker colors are smaller thermal inertia values. Black indicates areas of missing data or very low thermal inertia. If a lava tube was present, there should be darker colors along a linear feature. However, in this case, the thermal inertia signature is a bright circular feature around the skylight (outlined in blue), hence it may not be a lava tube. Instead, it may be a circular cavity of some other type.

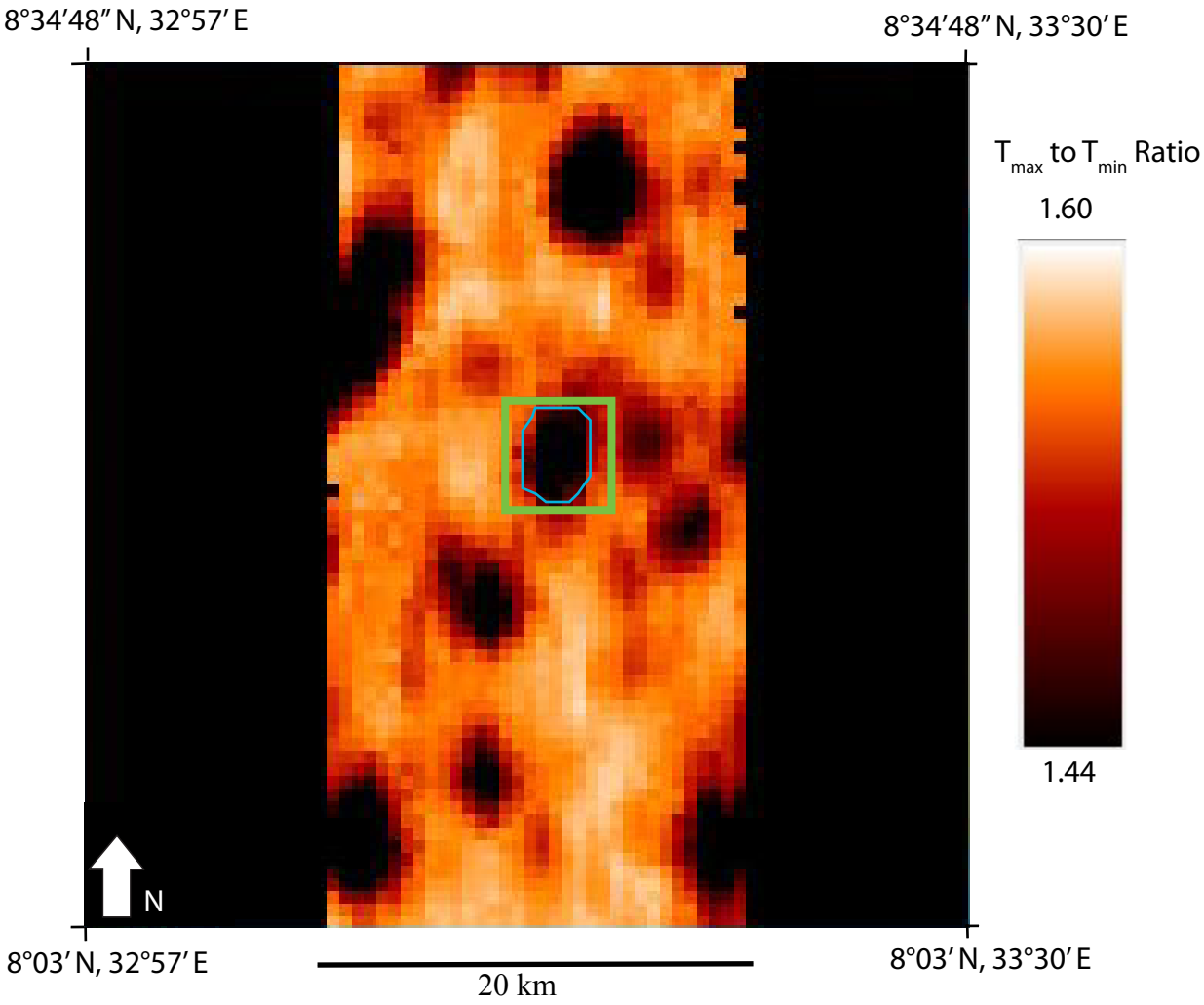

Figure 8: Tmax to Tmin ratio map of Mare Tranquilitatis generated using data from the 04/18/2012 to 05/02/2012 lunar diurnal cycle. The area in the middle of the green box is the center point for the potential skylight location (Wagner and Robinson, 2014; Meyer, 2012). The brighter colors denote larger ratios while the darker colors are smaller ratios. Black indicates areas of missing data or very small ratio values. If a lava tube was present, there should be brighter colors along a linear feature. However, in this case, the ratio signature is a dark circular feature (outlined in blue) around the skylight, hence it may not be a lava tube. Instead, it may be a circular cavity of some other type.

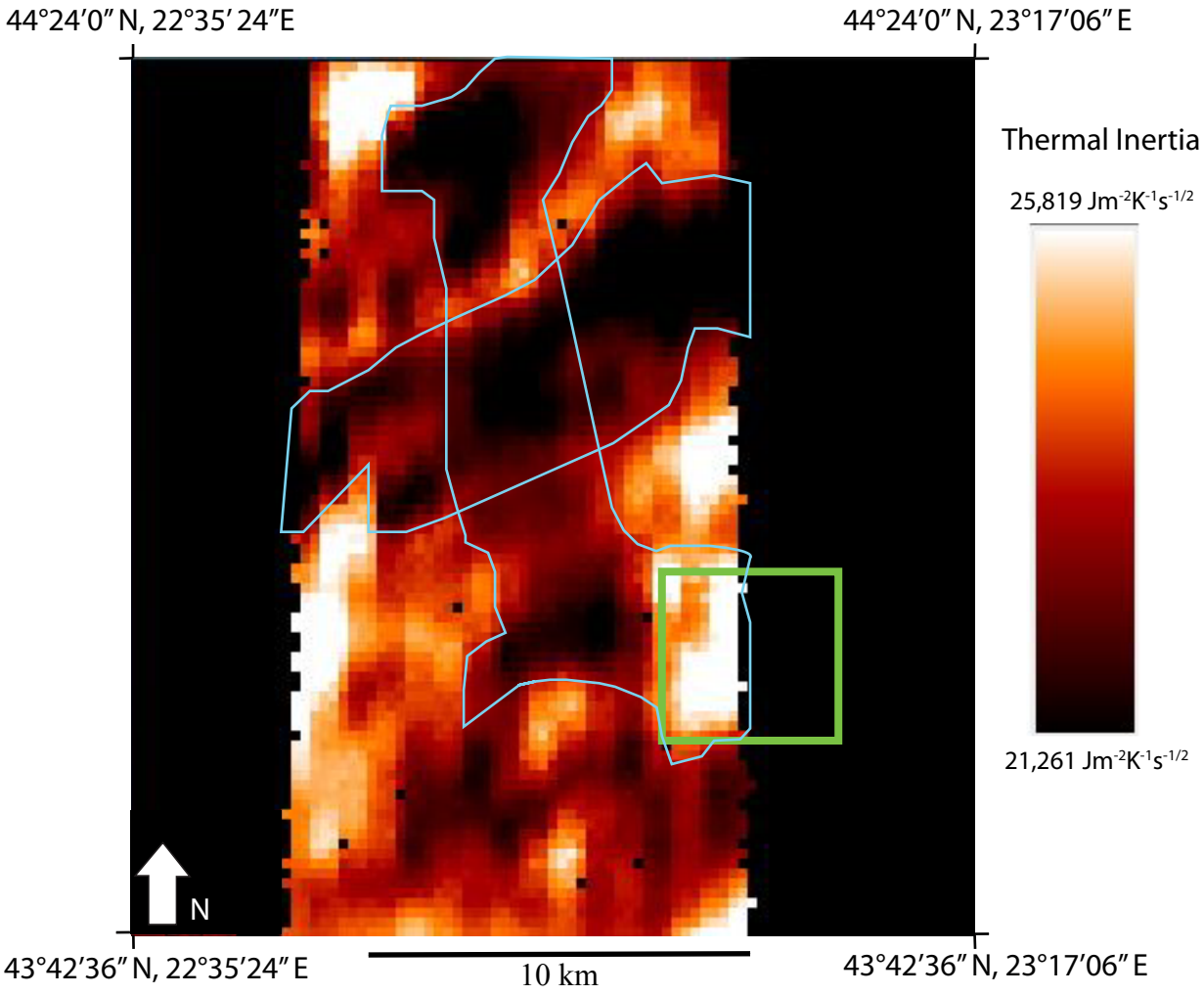

Figure 9: Thermal inertia map of Highland 1 generated using data from the 04/18/2012 to 05/02/2012 lunar diurnal cycle. The area in the middle of the green box is the center point for the potential skylight location (Wagner and Robinson, 2014). The brighter colors denote larger thermal inertia values while the darker colors are smaller thermal inertia values. Black indicates areas of missing data or very low thermal inertia values. If a lava tube was present there should be darker colors along linear feature. There are two dark linear features present (outlined in blue). One trends roughly north south and turns connect to the skylight (the bright circular feature) and the other one trends northeast south-west. As explained in the text, I believe these two features are lava tubes.

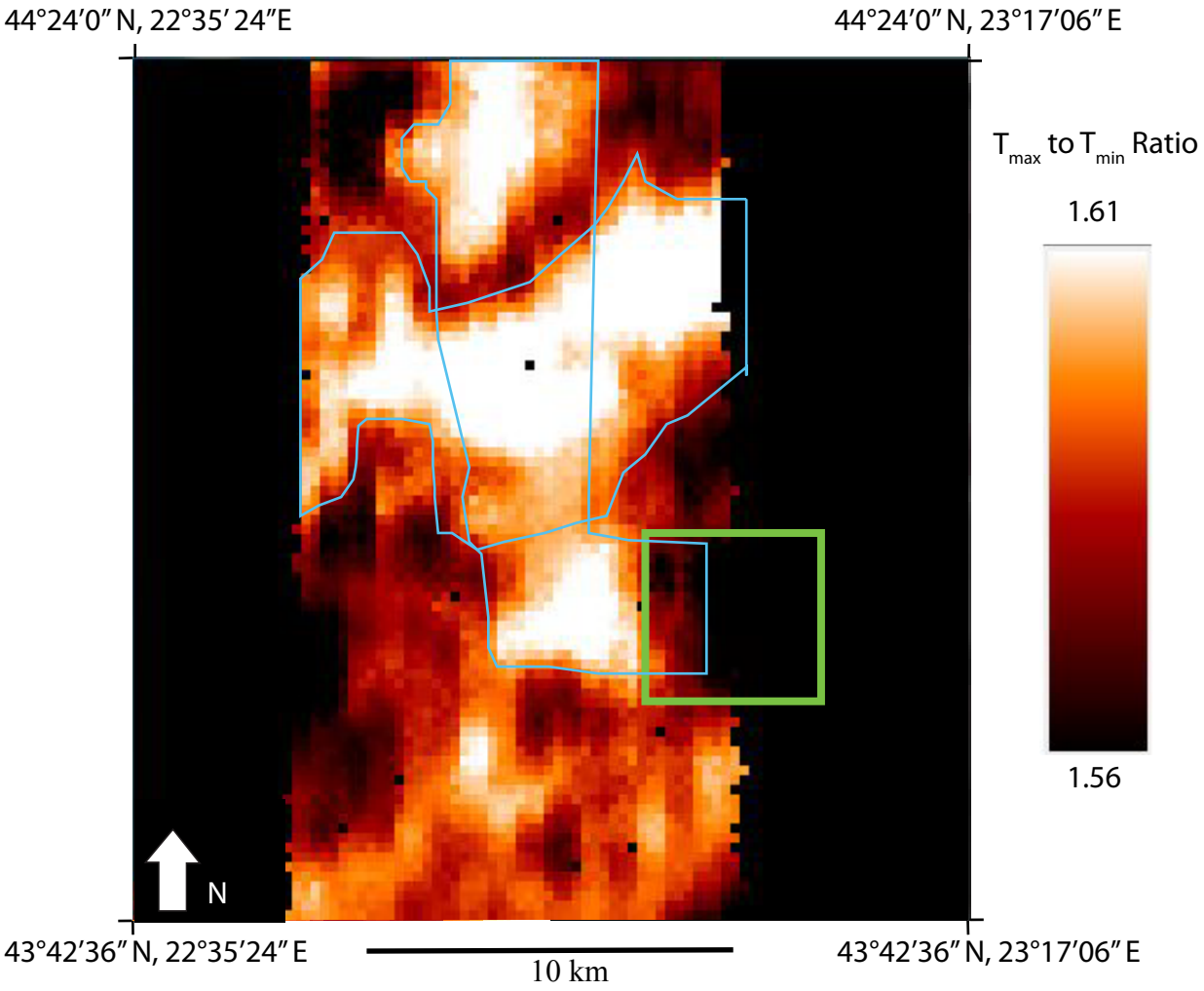

Figure 10: Tmax to Tmin ratio map of Highland 1 generated using data from the 04/18/2012 to 05/02/2012 lunar diurnal cycle. The area in the middle of the green box is the center point for the potential skylight location (Wagner and Robinson, 2014). The brighter colors denote larger ratios while the darker colors are smaller ratios. Black indicates areas of missing data or very small ratio values. If a lava tube was present there should be brighter colors along a linear feature. There are two bright linear features present (outlined in blue). One trends roughly north south and turns to connect to the skylight (the dark circular feature) and the other one trends northeast southwest. I believe these two features are lava tubes.

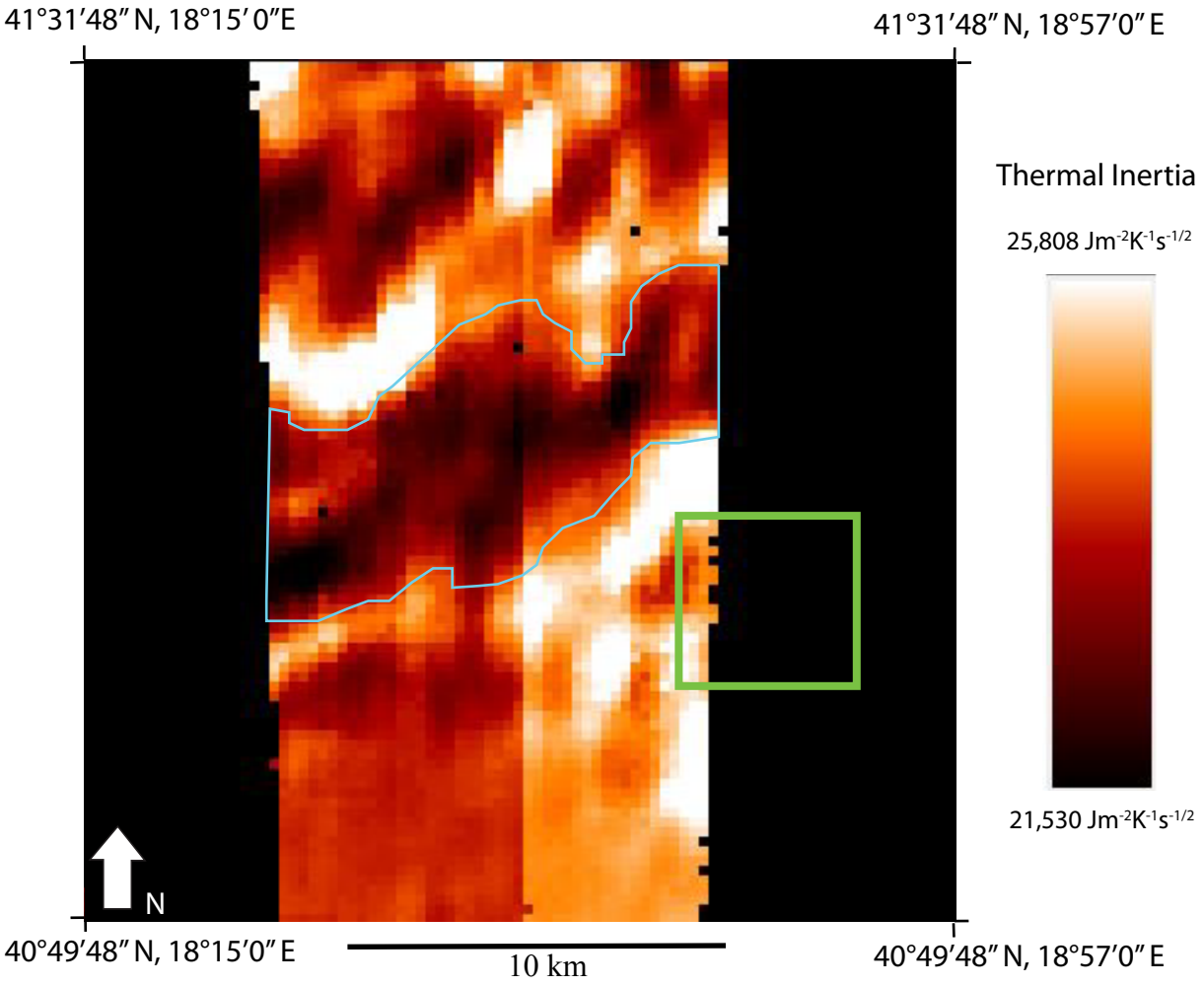

Figure 11: Thermal inertia map of Highland 2 generated using data from the 04/18/2012 to 05/02/2012 lunar diurnal cycle. The area in the middle of the green box is the center point for the potential skylight location (Wagner and Robinson, 2014). The brighter colors denote larger thermal inertia values while the darker colors are smaller thermal inertia values. Black indicates areas of missing data or very low thermal inertia values. If a lava tube was present, there should be darker colors along a linear feature. There is a dark linear feature north of the skylight, that trends northeast southwest (outlined in blue). I believe this feature is a lava tube. The skylight is in a data gap, so there is no way to know for sure if the lava tube connects to the skylight.

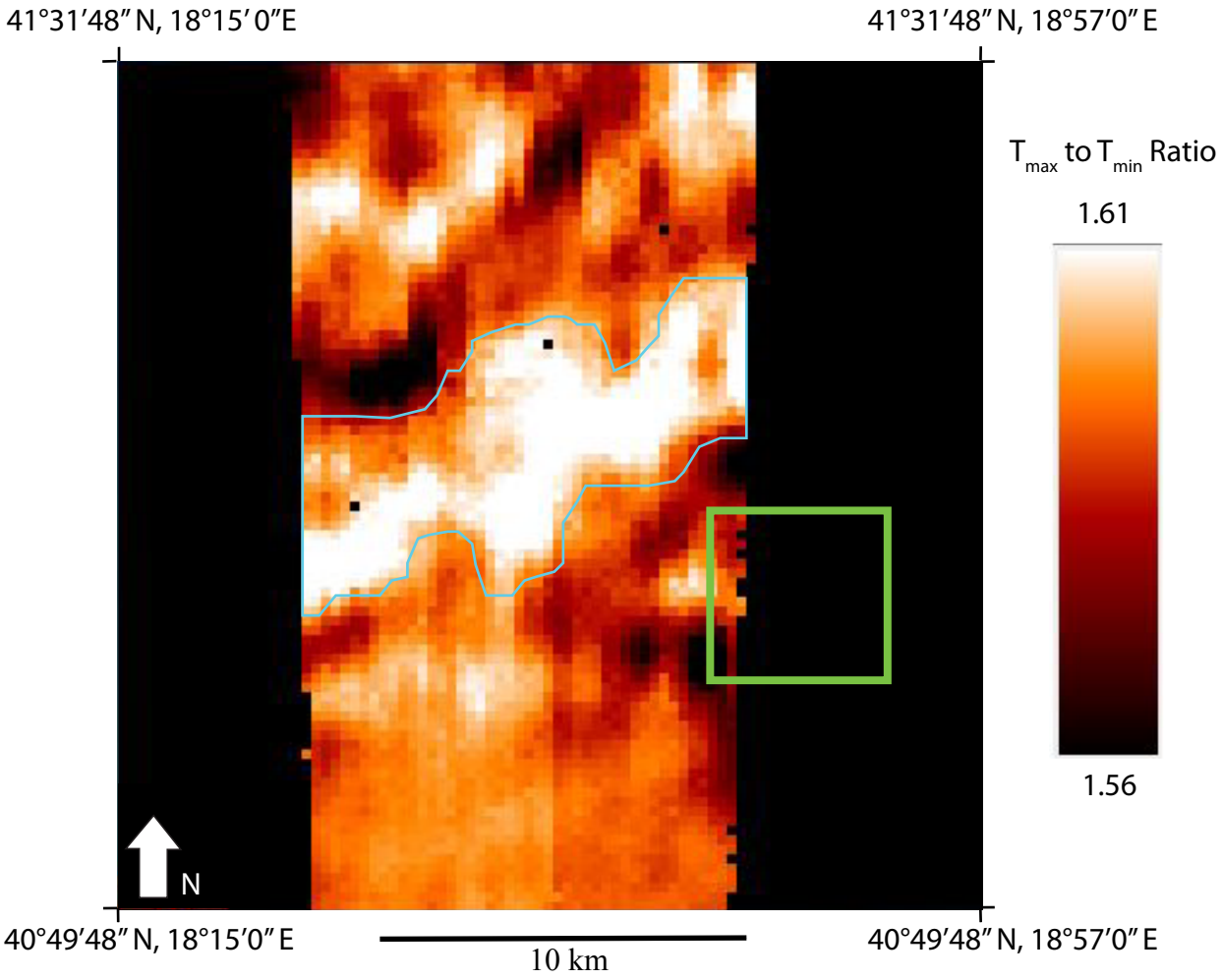

Figure 12: Tmax to Tmin ratio map of Highland 2 generated using data from the 04/18/2012 to 05/02/2012 lunar diurnal cycle. The area in the middle of the green box is the center point for the potential skylight location (Wagner and Robinson, 2014). The brighter colors denote larger ratios while the darker colors are smaller ratios. Black indicates areas of missing data or small low ratio values. If a lava tube was present, there should be brighter colors along a linear feature. There is a bright linear feature north of the skylight, that trends northeast southwest (outlined in blue). I believe this feature is a lava tube. The skylight is in a data gap, so there is no way to know for sure if the lava tube connects to the skylight.

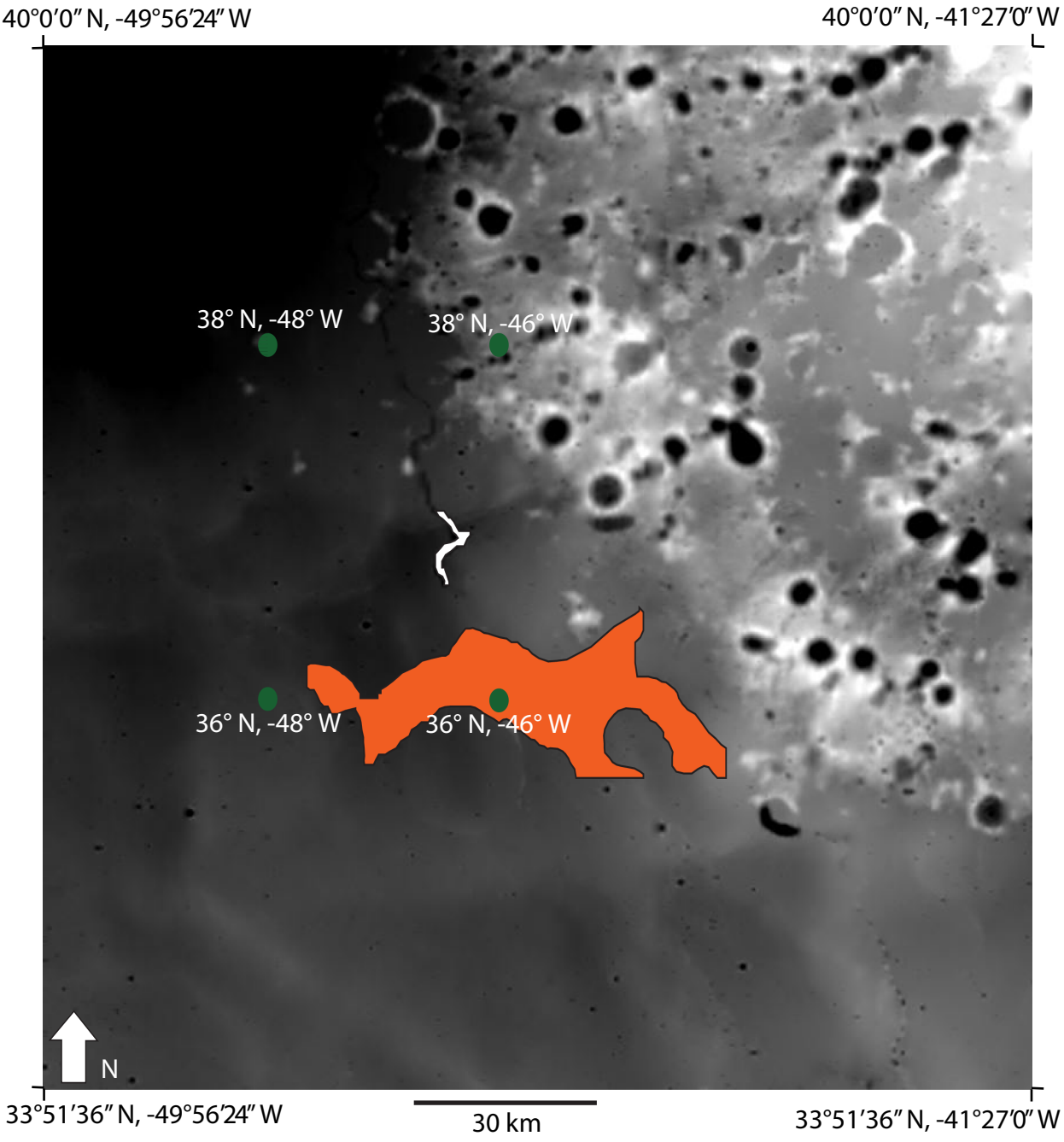

Figure 13: An overlay of part of the gradiometery image analyzed by Chappaz et al. (2014) onto the LOLA DEM. The orange polygon shows the presumed location of the Rima Sharp lava tube (Chappaz et al., 2014). The white polygon outlines a prominent bend in the Rima Sharp rille, and the green dots are ground control points with known coordinates. These features were used to co-register the thermal inertia data presented in this work with the Chappaz et al. (2014) results.

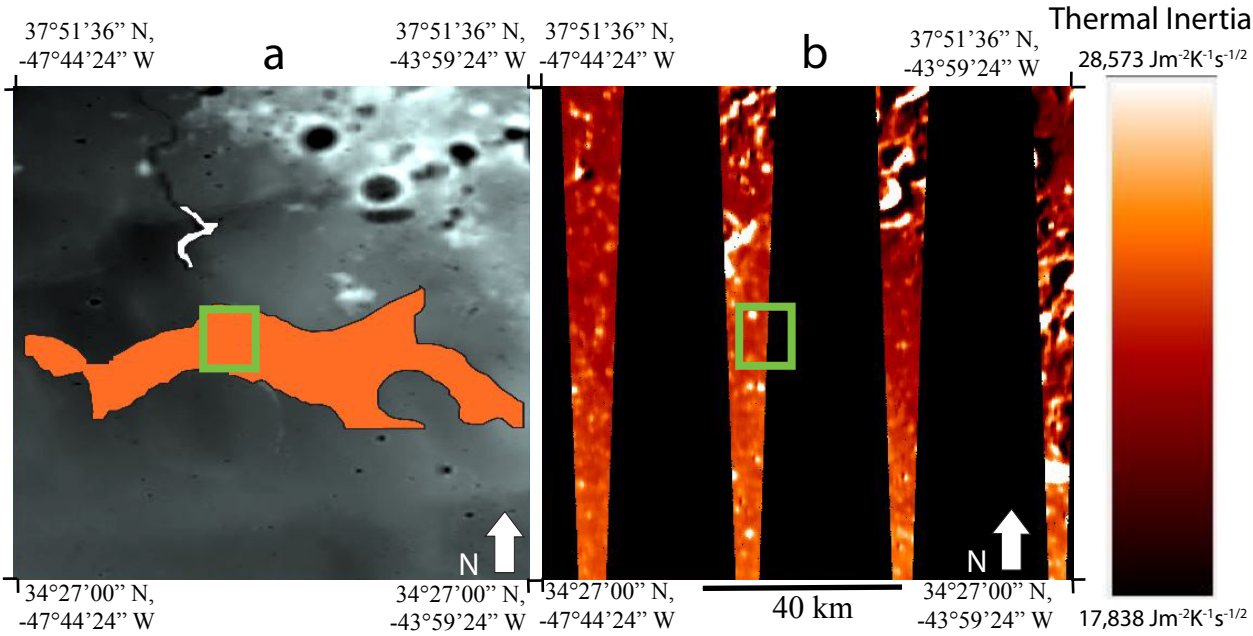

Figure 14: Thermal inertia map of Rima Sharp generated using data from the 04/18/2012 to 05/02/2012 lunar diurnal cycle. The green boxes in both (a) and (b) correspond to the Rima Sharp lava tube (Chappaz et al., 2014). The brighter colors denote larger thermal inertia values while the darker colors are smaller thermal inertia values. Black indicates areas of missing data or very low thermal inertia values. If a lava tube was present, there should be darker colors along a linear feature. However, no such linear feature is present.

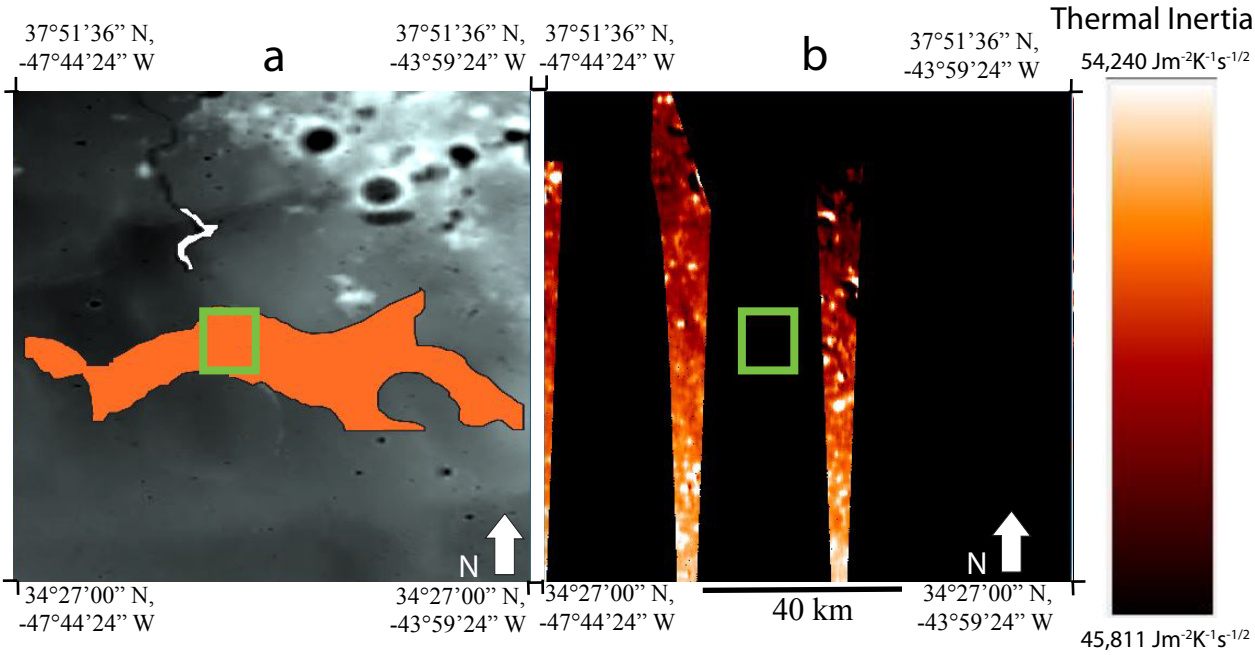

Figure 15: Thermal inertia map of Rima Sharp generated using data from the 07/23/2012 to 08/06/2012 lunar diurnal cycle. The green boxes in both (a) and (b) correspond to the Rima Sharp lava tube (Chappaz et al., 2014). The brighter colors denote larger thermal inertia values while the darker colors are smaller thermal inertia values. Black indicates areas of missing data or very low thermal inertia values. If a lava tube was present, there should be brighter colors along a linear feature. However, no such linear feature is present.

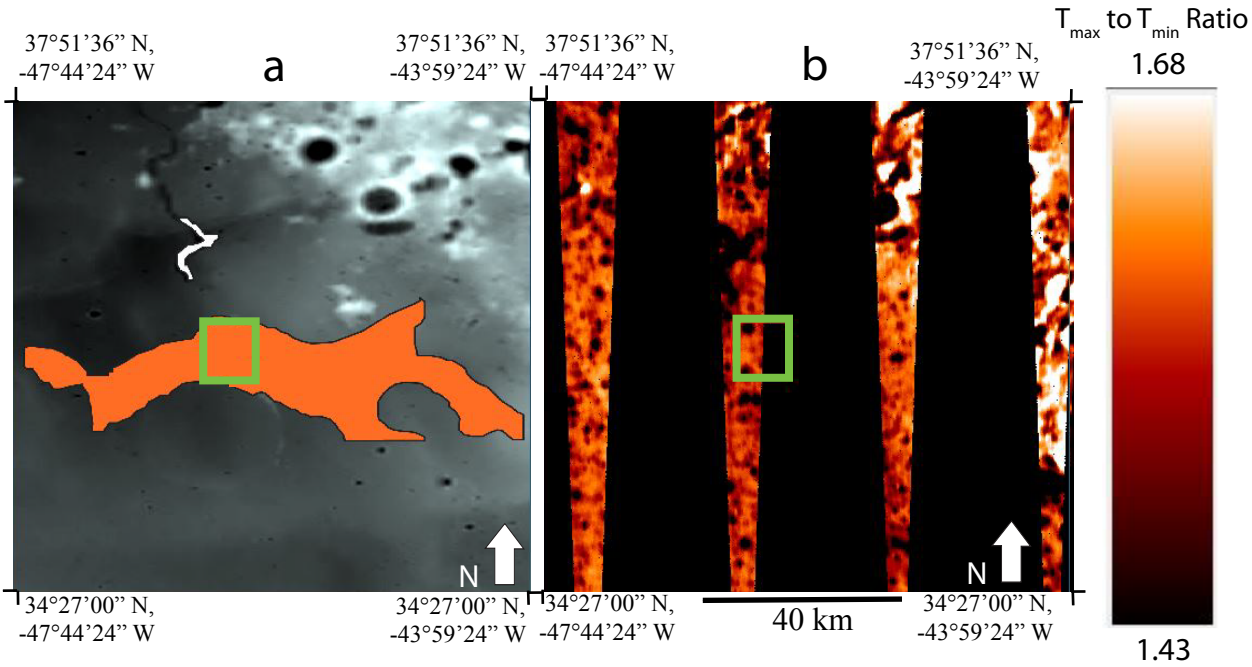

Figure 16: Tmax to Tmin ratio map of Rima Sharp generated using data from the 04/18/2012 to 05/02/2012 lunar diurnal cycle. The green boxes in both (a) and (b) correspond to the same location in the Rima Sharp lava tube suggested by Chappaz et al. (2014). The brighter colors denote larger ratios while the darker colors are smaller ratios. Black indicates areas of missing data or very small ratios. If a lava tube was present, there should be brighter colors along a linear feature. However, no linear feature present.

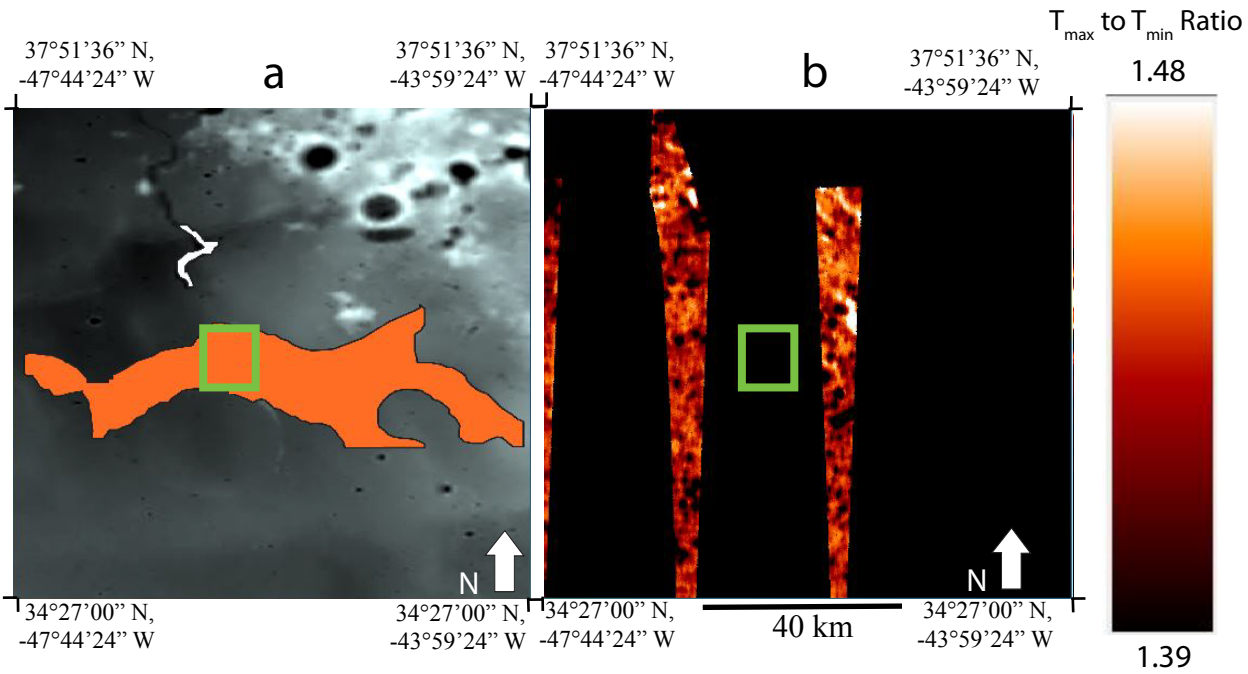

Figure 17: Tmax to Tmin ratio map of Rima Sharp generated using data from the 07/23/2012 to 08/06/2012 lunar diurnal cycle. The green boxes in both (a) and (b) correspond to the same location in the Rima Sharp lava tube suggested by Chappaz et al. (2014). The brighter colors denote larger ratios while the darker colors are smaller ratios. Black indicates areas of missing data or very small ratios. If a lava tube was present, there should be brighter colors along a linear feature. However, no linear feature present.

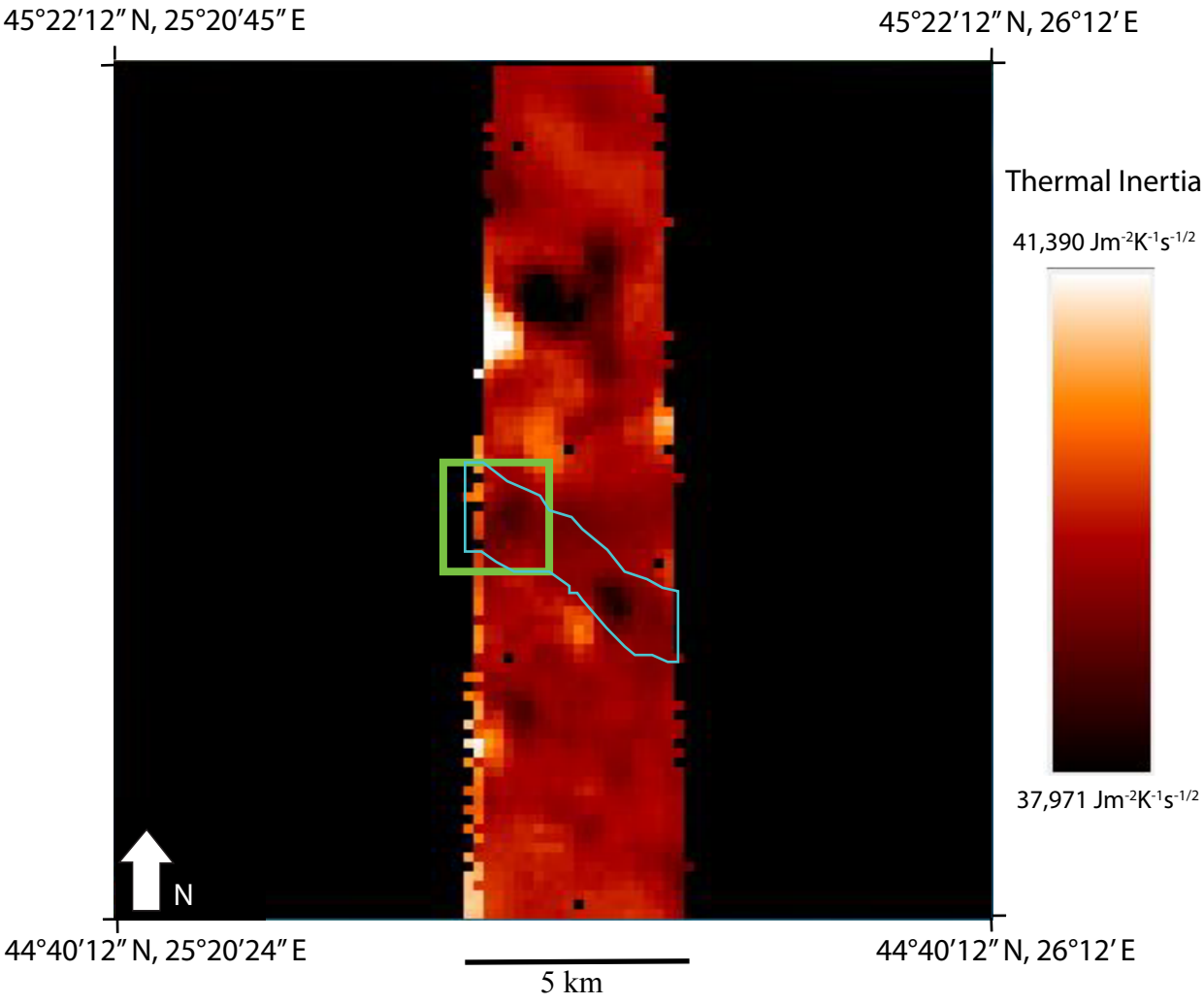

Figure 18: Thermal inertia map of Lacus Mortis generated using data from the 07/23/2012 to 08/06/2012 lunar diurnal cycle. The area in the middle of the green box is the center point for the potential skylight location (Wagner and Robinson, 2014). The brighter colors denote larger thermal inertia values while the darker colors are smaller thermal inertia values. Black indicates areas of missing data or very low thermal inertia. If a lava tube was present, there should be brighter colors along a linear feature. There is a slightly dark linear feature that trends northwest southeast (outlined in blue). As explained in the text, I believe this feature is a lava tube.

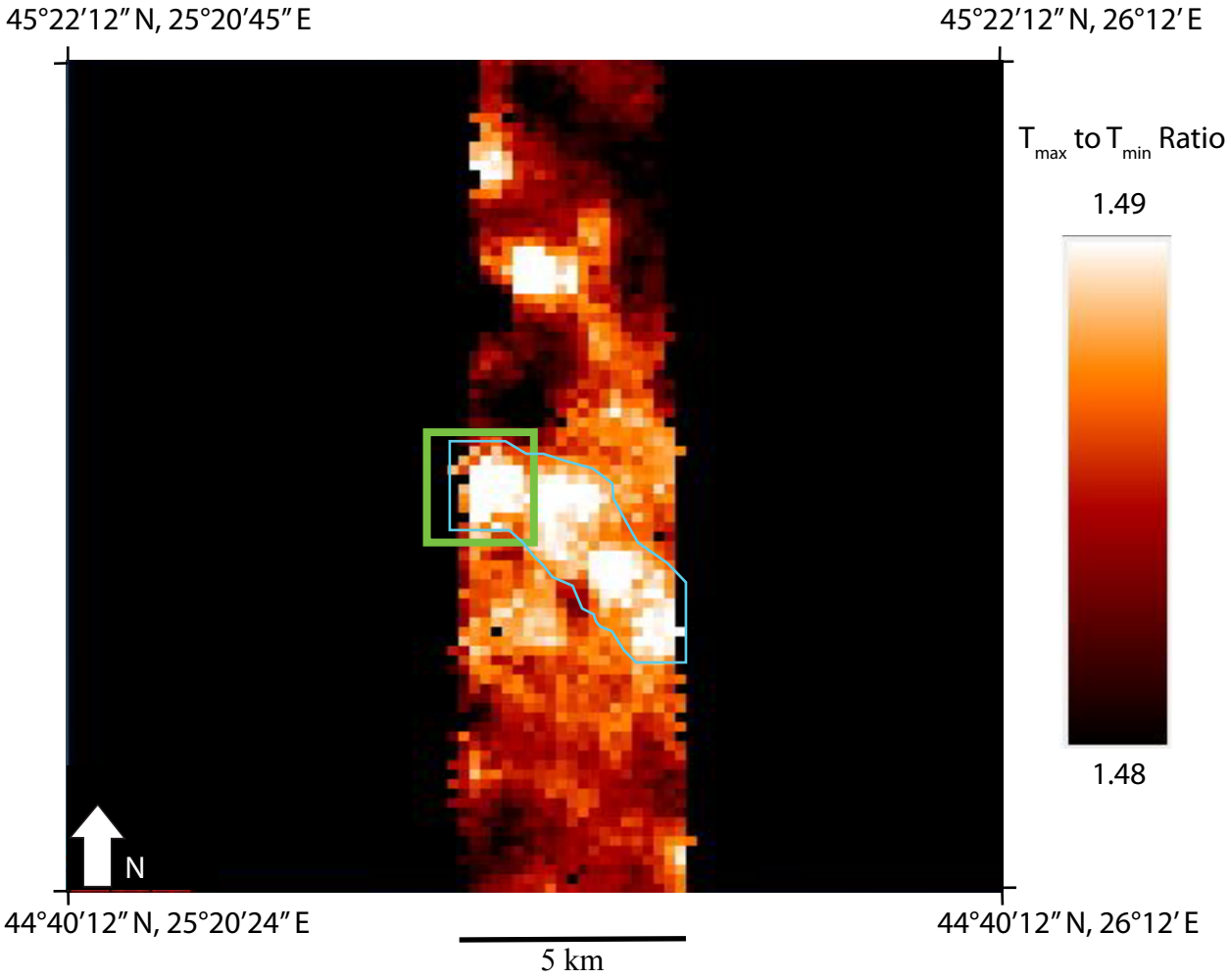

Figure 19: Tmax to Tmin ratios map of Lacus Mortis generated using data from the 07/23/2012 to 08/06/2012 lunar diurnal cycle. The area in the middle of the green box is the center point for the potential skylight location. The brighter colors demote larger ratios while the darker colors are smaller ratios. Black indicates areas of missing data and very small temperature ratios. If a lava tube was present, there should be brighter colors along a linear feature. There is a bright linear feature that trends northwest southeast (outlined in blue). The linear feature connects with the skylight. I believe the feature is a lava tube.

Appendix 1: Location Data Check

This MATLAB code (`datacheck.m`) reads in a global map of day or night bolometric temperature in JPEG 2000 format. It then checks to see if that data is available at the sites of interest (Table 5). The code returns to the command line the day or night bolometric temperature value recorded for all of the sites of interest. If the code outputs a data value of -32,768, the site does not have a temperature reading and therefore lies in a "data gap". The code was written in MATLAB version R2012. To run the code, make sure it is in the same folder as the data file you wish to analyze. The code is available upon e-mail request to rslank9@gmail.com or jhurtado@utep.edu.

```
% Code for seeing if certain areas on the Lunar Global Map have data
% 04162016 RAS

clear
clc

%read in data
A = imread('dgdr_tbol_avg_cyl_20120819d_128_jp2.jp2') ;
%load( 'imagedata.mat')

rows = 23040 ;
cols = 46080 ;
baddatavalue = -32768 ;

% Look at sites
%Mare Ingenii
A(16122,44296)

%Mare Tranquilitatis
A(10452,27292)

%Rima Sharp begin
A(6912,16896)

%Rima Sharp end
A(6912,17408)

%Location C
A(7040,17536)

%Lacus Mortis
A(5765,26318)

%Central Mare Fec
A(11637,29268)

%Mare Tranquilitatis
A(10453,27292)

%Mare Ingenii
A(16121,44295)

%Southwest Mare Fec
A(12384,28513)

%Marius Hills
A(9716,15773)

%Schluter Crater
A(12267,12410)

%Highland 1
A(5892,25995)
```

```
%Highland 2
A(6252,25449)

%Runge Crater
A(11866,34148)

%Ina Crater
A(9131,23718)

%Rima Hadley- crater
A(8282,23366)

%Rima Hadley- flat
A(8160,23357)
```

Appendix 2: Thermal Inertia Calculation

This MATLAB code (`TI2.m`) computes thermal inertia on the lunar surface using DLRE datasets. The inputs for this code are ENVI standard files for bolometric temperature, local time, Julian data, visual brightness, and slope for a particular tile, and it outputs ENVI-compatible file (with no `.hdr` files) for Tday, Tnight, T_{max}, T_{min}, days elapsed between when the day and night temperatures were measured, ATI, log(ATI), cosine-corrected albedo, and thermal inertia, log(thermal inertia). It also outputs a MATLAB binary file (`outputfile.mat`) containing all these variables. The code was written in MATLAB version R2012. To run the code, make sure it is in the same folder as the data file you wish to analyze. The code is available upon e-mail request to rslank9@gmail.com or jhurtado@utep.edu.

```
%Code for computing thermal inertia of the lunar surface using Diviner
datasets
%This version (v2) does a cosine correction to the albedo

% 021516 -rs, jmh
%THIS IS THE CURRENT VERSION OF TICODE2.M!!!

clear
clc

%DEFINE PARAMETERS

lunardaylength = 27.321582 ; % in Earth days, the length of the
sideral lunar day (29.5 for synodic lunar day)

%omega = 2.662e-6 ; % angular frequency of Moon's rotation (radians/s)
/ 27.321582 days = period  omega = 2pi/period
omega = ( 2 .* pi ) ./ ( lunardaylength .* 24 .* 60 .* 60 ) ; %
angular frequency of Moon's rotation (radians/s) / 27.321582 days =
period  omega = 2pi/period

%tmax = 368.16 .* 60 .* 60 ; % time of maximum diurnal temperature (s)
(~.52 Lunar Days in Earth hours; wattsupwiththat.com/2012/01/08/the-
moon-is-a-cold-mistress/)
tmax = 0.52 .* lunardaylength .* 24 .* 60 .* 60 ;

%tmin = 198.24 .* 60 .* 60 ; % time of minimum diurnal temperature (s)
(~.28 Lunar Days in Earth hours; wattsupwiththat.com/2012/01/08/the-
moon-is-a-cold-mistress/)
tmin = 0.28 .* lunardaylength .* 24 .* 60 .* 60 ;

S = 1.366e3 ; % solar constant; W/m^2 (Johnshon, 1954)

Ct = 1 ; % atmospheric transmittance (unitless) (Scheidt et al. p. 41
use 0.75 for Earth; Price p. 60 (V))

axialtilt = 5.145 ; % axial tilt (degrees)
https://en.wikipedia.org/wiki/Moon

%% READ IN DATA

%size of the tile (segment of complete map) being used for this run
columns = 9216 ;
rows = 11520 ;
startrow = 1 ;
endrow = 11520 ;
%layers = 5 ;
resolution = 128 ; % pixels per degree
totalrows = 23040 ; %total number of rows in the complete map

%NOTE CALIBRATION CONSTANTS FOR DATA FILES ARE HARDWIRED INTO THE CODE
BELOW!
```

```
%fileid = fopen('datastack.hdr');
%datastack = multibandread( 'datastack.hdr' , [ columns , rows ,
layers ] , 'double' , 0 , 'bsq' , 'ieee-be' ) ;

%albedo map (VB1AVG in DLRE Level 2 GDR)
%albedo = datastack( : , : , 1 ) ;
fid = fopen( 'albedo' , 'r' , 'l' ) ;
albedo = fread( fid , [ columns , rows ] , 'int16' ) ;
fclose( fid ) ;
albedo = albedo' ;

%emissivity map (where will we get this?  i dunno)
%emiss =  ;

%daytime temperature map (TBOLAV in DLRE Level 3 GDR)
%Tday = datastack( : , : , 2 ) ;
fid = fopen( 'Tday' , 'r' , 'l' ) ;
Tday = fread( fid , [ columns , rows ] , 'int16' ) ;
fclose( fid ) ;
Tday = Tday' ;

%daytime time map (LTIM in DLRE Level 2 GDR)
%t1 = datastack( : , : , 4 ) ;
fid = fopen( 't1' , 'r' , 'l' ) ;
t1 = fread( fid , [ columns , rows ] , 'int16' ) ;
fclose( fid ) ;
t1 = t1' ;

%nighttime temperature map (TBOLAV in DLRE Level 3 GDR)
%Tnight = datastack( : , : , 3 ) ;
fid = fopen( 'Tnight' , 'r' , 'l' ) ;
Tnight = fread( fid , [ columns , rows ] , 'int16' ) ;
fclose( fid ) ;
Tnight = Tnight' ;

%nighttime time map (LTIM in DLRE Level 2 GDR)
%t2 = datastack( : , : , 5 ) ;
fid = fopen( 't2' , 'r' , 'l' ) ;
t2 = fread( fid , [ columns , rows ] , 'int16' ) ;
fclose( fid ) ;
t2 = t2' ;

%julian date information (day)
fid = fopen( 'JDday' , 'r' , 'l' ) ;
JDday = fread( fid , [ columns , rows ] , 'int16' ) ;
fclose( fid ) ;
JDday = JDday' ;

%julian date information (night)
fid = fopen( 'JDnight' , 'r' , 'l' ) ;
JDnight = fread( fid , [ columns , rows ] , 'int16' ) ;
```

```
fclose( fid ) ;
JDnight = JDnight' ;

%get rid of bad data values (i.e. holes in the data)
baddatavalue = -32768 ;
for i = 1 : rows
    for j = 1 : columns
        if albedo( i , j ) == baddatavalue
            albedo( i , j ) = NaN ;
        end

        if Tday( i , j ) == baddatavalue
            Tday( i , j ) = NaN ;
        end

        if t1( i , j ) == baddatavalue
            t1( i , j ) = NaN ;
        end

        if Tnight( i , j ) == baddatavalue
            Tnight( i , j ) = NaN ;
        end

        if t2( i , j ) == baddatavalue
            t2( i , j ) = NaN ;
        end

        if JDday( i , j ) == baddatavalue
            JDday( i , j ) = NaN ;
        end

        if JDnight( i , j ) == baddatavalue
            JDnight( i , j ) = NaN ;
        end

    end
end

%apply calibration coefficients to convert from DN to real values
albedo = 0.0001 .* albedo ; %coverting from dgital number to visual
brightness (albedo) see vb1 day lbl
Tday = 0.02 .* Tday ; %converting from digital number to temperature
in Kelvin see tbol day lbl
t1 = ( ( t1 .* 0.0833333333 ) + 2730.00273000273 ) ; %converting from
digital number to local time in hours see Ltim day lbl
Tnight =  0.02 .* Tnight ; %converting from digital number to
temperature in Kelvin see tbol night lbl
t2 = ( ( t2 .* 0.0833333333 ) + 2730.00273000273 ) ; %converting from
dgital number to local time in hours see Ltim night lbl ;
JDday = ( ( JDday .* 0.011296333 ) + 2455818.0 ) ; %converting from
digital number to Julian date see JD day lbl
```

```
JDnight = ( ( JDnight .* 0.011296333 ) + 2455818.0 ) ; %converting
from digital number to Julian date see JD night lbl

%convert t1 and t2 to same time units as tmin, tmax, and omega
t1local = t1 ;
t1 = ( t1 ./ 24 ) .* lunardaylength .* 24 .* 60 .* 60 ;
t2 = ( t2 ./ 24 ) .* lunardaylength .* 24 .* 60 .* 60 ;

%plot input data files
%comment this all out if you need to (will make code run faster)

% figure( 1 )                % Makes a new figure window.
% hold off               % Allows the figure to be overwritten.
% imagesc( albedo )       % Plots the image.
% colormap( bone )        % Sets the colormap.
% colorbar
% title( ' Albedo ' )     % Sets the title.
% %axis image                % Formats the axes.
% %xlabel( ' column ' )    % Labels the x axis
% %ylabel( ' row ' )       % Labels the y axis
% hold on                  % Prevents the figure from being
overwritten.
%
% figure ( 2 )
% %placeholder for emissivity
%
% figure( 3 )                % Makes a new figure window.
% hold off               % Allows the figure to be overwritten.
% imagesc( Tday )         % Plots the image.
% colormap( hot )         % Sets the colormap.
% colorbar
% title( ' Tday ' )     % Sets the title.
% hold on                    % Prevents the figure from being
overwritten.
%
% figure( 4 )                % Makes a new figure window.
% hold off               % Allows the figure to be overwritten.
% imagesc( t1 )     % Plots the image.
% colormap( bone )        % Sets the colormap.
% colorbar
% title( ' t1 ' )     % Sets the title.
% hold on                    % Prevents the figure from being
overwritten.
%
% figure( 5 )                % Makes a new figure window.
% hold off               % Allows the figure to be overwritten.
% imagesc( Tnight )       % Plots the image.
% colormap( hot )         % Sets the colormap.
% colorbar
% title( ' Tnight ' )     % Sets the title.
% hold on                  % Prevents the figure from being
overwritten.
```

```
%
% figure( 6 )                % Makes a new figure window.
% hold off               % Allows the figure to be overwritten.
% imagesc( t2 )      % Plots the image.
% colormap( bone )         % Sets the colormap.
% colorbar
% title( ' t2 ' )      % Sets the title.
% hold on                    % Prevents the figure from being
overwritten.
%
% figure( 7 )                % Makes a new figure window.
% hold off               % Allows the figure to be overwritten.
% imagesc( JDday )         % Plots the image.
% colormap( bone )         % Sets the colormap.
% colorbar
% title( ' JDday ' )      % Sets the title.
% hold on                    % Prevents the figure from being
overwritten.
%
% figure( 8 )                % Makes a new figure window.
% hold off               % Allows the figure to be overwritten.
% imagesc( JDnight )       % Plots the image.
% colormap( bone )         % Sets the colormap.
% colorbar
% title( ' JDnight ' )      % Sets the title.
% hold on                    % Prevents the figure from being
overwritten.

%CORRECT FOR EMISSIVITY (maybe - need emissivity map first)

%T1 = ( emiss .^ ( 1 ./ 4 ) ) * Tday ;
T1 = Tday ;

%T2 = ( emiss .^ ( 1 ./ 4 ) ) * Tnight ;
T2 = Tnight ;

%FIND WHERE THERE IS EITHER MISSING T1 OR MISSING T2 OR BOTH AND MAKE
THOSE PIXELS NaN
for iii = 1 : rows
    for jjj = 1 : columns
        if isnan( T1( iii , jjj ) ) | isnan( T2( iii , jjj ) )
            T1( iii , jjj ) = NaN ;
            T2( iii , jjj ) = NaN ;
            albedo( iii , jjj ) = NaN ;
            t1( iii , jjj ) = NaN ;
            t2( iii , jjj ) = NaN ;
            JDday( iii , jjj ) = NaN ;
            JDnight( iii , jjj ) = NaN ;
        end
    end
end
```

```
%CALCULATE Tmax AND Tmin

Tmax = T1 + ( ( ( T1 - T2 ) .* ( cos( omega .* tmax ) - cos( omega .*
t1 ) ) ) ./ ( cos( omega .* t1 ) - cos( omega .* t2 ) ) ) ; % Scheidt
et al. equation 12, p. 42

figure( 9 )                 % Makes a new figure window.
hold off                % Allows the figure to be overwritten.
imagesc( Tmax )      % Plots the image.
colormap( hot )      % Sets the colormap.
colorbar
title( ' Tmax ' )     % Sets the title.
hold on                     % Prevents the figure from being
overwritten.

Tmin = T2 + ( ( ( T1 - T2 ) .* ( cos( omega .* tmin ) - cos( omega .*
t2 ) ) ) ./ ( cos( omega .* t1 ) - cos( omega .* t2 ) ) ) ; % Scheidt
et al. equation 12, p. 42

figure( 10 )                % Makes a new figure window.
hold off                % Allows the figure to be overwritten.
imagesc( Tmin )      % Plots the image.
colormap( hot )      % Sets the colormap.
colorbar
title( ' Tmin ' )     % Sets the title.
hold on                     % Prevents the figure from being
overwritten.

%CALCULATE deltaT

deltaT = Tmax - Tmin ;

figure( 11 )                % Makes a new figure window.
hold off                % Allows the figure to be overwritten.
imagesc( deltaT )         % Plots the image.
colormap( colorcube )     % Sets the colormap.
colorbar
title( ' deltaT ' )     % Sets the title.
hold on                     % Prevents the figure from being
overwritten.


%produce a map of time elapsed between "day" and "night" data
timedifference = abs( JDday - JDnight ) ;

figure( 14 )                % Makes a new figure window.
hold off                % Allows the figure to be overwritten.
imagesc( timedifference )      % Plots the image.
colormap( colorcube )     % Sets the colormap.
colorbar
title( ' Days between "day" and "night" temperatures ' )     % Sets
the title.
```

```
hold on                         % Prevents the figure from being
overwritten.

%#######

%DO COSINE CORRECTION TO THE ALBEDO MAP

%load slope map derived from LOLA data
fid = fopen( 'slope' , 'r' , 'l' ) ;
slope = fread( fid , [ columns , rows ] , 'float' ) ;
fclose( fid ) ;
slope = slope' ;

%define constants
localsunrate = 180 ./ 12 ; % in degrees per "local hour"; sun
traverses 180 degrees across sky from sunrise to sunset in ~12 local
hours
localnoon = 12 ; %noon is at 1200 hour local time

%determine hour angle https://en.wikipedia.org/wiki/Hour_angle
h = localsunrate .* ( t1local - localnoon ) ;

%determine solar zenith
https://en.wikipedia.org/wiki/Solar_zenith_angle
solarzenith = acosd( ( sind( phi ) .* sind( delta ) ) + ( cosd( phi )
.* cosd( delta ) .* cosd( h ) ) ) ;

%determine incidence angle
incidence = solarzenith - slope ;

%do the correction
%see, for example, http://www.utsa.edu/lrsg/Teaching/ES6973/topo.pdf
albedo2 = albedo .* ( cosd( solarzenith ) ./ cosd( incidence ) ) ;

%CALCULATE ATI

ATI = ( 1 - albedo2 ) ./ deltaT ;

%find infinities

for ii = 1 : rows
    for jj = 1 : columns
        if isinf( ATI( ii , jj ) )
            ATI( ii , jj ) = NaN ;
        end
    end
end

% %TRY A NORMALIZATION
% albedonorm = nanmean( nanmean( albedo ) ) ;
% deltaTnorm = nanmean( nanmean( deltaT ) ) ;
```

```
% ATInorm = ( 1 - ( albedo - albedonorm ) ) ./ ( deltaT - deltaTnorm )
;

ATI2 = real( log( ATI ) ) ;

figure( 12 )                % Makes a new figure window.
hold off                % Allows the figure to be overwritten.
imagesc( ATI )       % Plots the image.
colormap( colorcube )     % Sets the colormap.
colorbar
title( ' ATI ' )     % Sets the title.
hold on                     % Prevents the figure from being
overwritten.

figure( 13 )                % Makes a new figure window.
hold off                % Allows the figure to be overwritten.
imagesc( ATI2 )      % Plots the image.
colormap( colorcube )     % Sets the colormap.
colorbar
title( ' log (ATI) ' )     % Sets the title.
hold on                     % Prevents the figure from being
overwritten.

figure( 17 )                % Makes a new figure window.
hold off                % Allows the figure to be overwritten.
imagesc( albedo2 )        % Plots the image.
colormap( bone )     % Sets the colormap.
colorbar
title( ' cosine-corrected albedo ' )     % Sets the title.
hold on                     % Prevents the figure from being
overwritten.

%#######

%CALCULATE P

b = tan( omega .* tmax ) ./ ( 1 - tan( omega .* tmax ) ) ; % Scheidt
et al. equation 6, p. 41
delta1 = atan( b ./ ( 1 + b ) ) ; % Scheidt et al. equation 7, p. 41
delta2 = atan( ( b .* sqrt( 2 ) ) ./ ( 1 + ( b .* sqrt( 2 ) ) ) ) ; %
Scheidt et al. equation 8, p. 41

%calculate latitude (in degrees) for each pixel in the map
middle = ( totalrows ./ 2 ) ;
for k = 1 : totalrows
   if k <= middle %north
        latitude( k ) = 90 - ( ( k - 1 ) ./ 128 ) ;
   end
   %if k = middle %equator
    %grid has even number of rows, so there is no equator row
    %NEED TO MODIFY THIS CODE IF A GRID WITH ODD NUMBER OF ROWS IS
USED
```

```
   %else
   if k > middle %south
       latitude( k ) = 90 - ( ( k ) ./ 128 ) ;
   end
end
latitude = latitude( startrow : endrow ) ;
latitude = latitude' ;
phi = ones( rows , columns ) ;
for kk = 1 : columns
    phi( : , kk ) = latitude .* phi( : , kk ) ;
end

N = ( ( JDday - 2451545 ) ) - ( floor( ( ( JDday - 2451545 ) ./ 365.25
) ) .* 365.25 ) ; % day of the year (N = 0 on Jan 1, etc.) derived
from JDday data (converted using JD of 01/01/2000 = 2,451,545 and 1
year = 365.25 days)

%delta = -1 .* asind( ( 0.39779 .* cosd( 0.98565 .* ( N + 10 ) ) ) + (
1.914 .* sind( 0.98565 .* ( N - 2 ) ) ) ) ; % solar declination
(degrees)as computed using formula found at
https://en.wikipedia.org/wiki/Position_of_the_Sun
delta = -1 .* axialtilt .* cosd( ( 360 ./ 365 ) .* ( N + 10 ) ) ; %
solar declination (degrees)as computed using formula found at
https://en.wikipedia.org/wiki/Position_of_the_Sun

delphi = tand( delta ) .* tand( phi ) ;

%find problematic values that would make xi imaginary and set to NaN
for kkk = 1 : rows
    for lll = 1 : columns
        if delphi( kkk , lll ) > 1 | delphi( kkk , lll ) < -1
           delphi( kkk , lll ) = NaN ;
        end
    end
end

xi = acosd( delphi ) ; % in degrees; Scheidt et al. equation 10, p. 41

%note the fourier coefficients A1 and A2 are taken from Maltese et
al.(2013), equation (15)-(17), p. 1151 (see also Scheidt et al.
equation 9, p. 41)
A1 = ( ( 2 ./ pi ) .* sind( delta ) .* sind( phi ) ) + ( ( ( 1 ./ ( 2
.* pi ) ) .* cosd( delta ) .* cosd( phi ) ) .* ( sind( 2 .* xi ) + ( 2
.* xi ) ) ) ;
A2 = ( ( ( 2 .* sind( delta ) .* sind( phi ) ) ./ ( 2 .* pi ) ) .*
sind( 2 .* xi ) ) + ( ( ( 2 .* cosd( delta ) .* cosd( phi ) ) ./ ( pi
.* ( ( 2 .* 2 ) - 1 ) ) ) .* ( ( 2 .* sind( 2 .* xi ) .* cosd( xi ) )
- ( cosd( 2 .* xi ) .* sind( xi ) ) ) ) ;

P = ( ( ( 1 - albedo2 ) .* S .* Ct ) ./ ( deltaT .* sqrt( omega ) ) )
.* ( ( ( A1 .* ( cos( ( omega .* t2 ) - delta1 ) - cos( ( omega .* t1
) - delta1 ) ) ) ./ sqrt( 1 + ( 1 ./ b ) + ( 1 ./ ( 2 .* b .* b ) ) )
```

```
) + ( ( A2 .* ( cos( ( omega .* t2 ) - delta2 ) - cos( ( omega .* t1 )
- delta2 ) ) ) ./ sqrt( 2 + ( sqrt( 2 ) ./ b ) + ( 1 ./ ( 2 .* b .* b
) ) ) ) ) ; % Scheidt et al. equation 5, p. 40

% Pclean = P ;
% %Pclean( find( Pclean < 0 ) ) = NaN ;
% %Pclean( find( Pclean > 5000 ) ) = NaN ;
% for kkkk = 1 : rows
%     for llll = 1 : columns
%         if Pclean( kkkk , llll ) > 10000 | Pclean( kkkk , llll ) < 0
%            Pclean( kkkk , llll ) = NaN ;
%         end
%     end
% end

figure( 15 )                % Makes a new figure window.
hold off                % Allows the figure to be overwritten.
imagesc( P )         % Plots the image.
colormap( colorcube )     % Sets the colormap.
colorbar
title( ' P ' )     % Sets the title.
hold on                     % Prevents the figure from being
overwritten.

P2 = real( log( P ) ) ;

figure( 16 )                % Makes a new figure window.
hold off                % Allows the figure to be overwritten.
imagesc( P2 )        % Plots the image.
colormap( colorcube )     % Sets the colormap.
colorbar
title( ' log (P) ' )     % Sets the title.
hold on                     % Prevents the figure from being
overwritten.

%EXPORT DATA PRODUCTS AS ENVI-COMPATIBLE FILES
%NOTE: THIS DOES NOT OUTPUT FIGURES!  IT OUTPUTS DATA

% T1 = T1' ;
% fid = fopen( 'Temp1' , 'wb' ) ;
% fwrite( fid , T1 , 'float' ) ;
% fclose( fid ) ;
%
% T2 = T2' ;
% fid = fopen( 'Temp2' , 'wb' ) ;
% fwrite( fid , T2 , 'float' ) ;
% fclose( fid ) ;

Tmax = Tmax' ;
fid = fopen( 'Tmax' , 'wb' ) ;
fwrite( fid , Tmax , 'float' ) ;
fclose( fid ) ;
```

```
Tmin = Tmin' ;
fid = fopen( 'Tmin' , 'wb' ) ;
fwrite( fid , Tmin , 'float' ) ;
fclose( fid ) ;

deltaT = deltaT' ;
fid = fopen( 'deltaT' , 'wb' ) ;
fwrite( fid , deltaT , 'float' ) ;
fclose( fid ) ;

albedo2 = albedo2' ;
fid = fopen( 'albedo2' , 'wb' ) ;
fwrite( fid , albedo2 , 'float' ) ;
fclose( fid ) ;

ATI = ATI' ;
fid = fopen( 'ATI' , 'wb' ) ;
fwrite( fid , ATI , 'float' ) ;
fclose( fid ) ;

ATI2 = ATI2' ;
fid = fopen( 'ATI2' , 'wb' ) ;
fwrite( fid , ATI2 , 'float' ) ;
fclose( fid ) ;

timedifference = timedifference' ;
fid = fopen( 'timedifference' , 'wb' ) ;
fwrite( fid , timedifference , 'float' ) ;
fclose( fid ) ;

P = P' ;
fid = fopen( 'P' , 'wb' ) ;
fwrite( fid , P , 'float' ) ;
fclose( fid ) ;

P2 = P2' ;
fid = fopen( 'P2' , 'wb' ) ;
fwrite( fid , P2 , 'float' ) ;
fclose( fid ) ;

% %EXPORT MATLAB VARIABLES TO FILE (RELOAD INTO MATLAB USING "LOAD")
%save( 'outputfile.mat' , T1 , T2 , Tmax , Tmin , deltaT , albedo2 ,
ATI , ATI2 , timedifference , P , P2 )
save( 'outputfile.mat' )
```

Appendix 3: Planetary Data System Label Files

This appendix contains example PDS label files for all of the data used. The label files included are for day bolometric temperature, night bolometric temperature, day local time, night local time, day Julian date, night Julian date, and day visual brightness for both the 04/23/2012 to 05/02/2012 and 07/23/2012 to 08/06/2012 diurnal cycles as well as the LOLA DEM. The label files came with the downloaded PDS data obtained in January and March of 2016. The calibration coefficients are listed in the label files are used in Appendix 2.

```
PDS_VERSION_ID            = "PDS3"

PRODUCT_VERSION_ID        = "V4.1"
DATA_SET_ID               = "LRO-L-DLRE-5-GDR-V1.0"
PRODUCT_ID                = "DGDR_TBOL_AVG_CYL_20120418D_128_JP2.JP2"
SOURCE_PRODUCT_ID         = "DGDR_TBOL_AVG_CYL_20120418D_128_IMG.IMG"
INSTRUMENT_HOST_NAME      = "LUNAR RECONNAISSANCE ORBITER"
INSTRUMENT_HOST_ID        = "LRO"
INSTRUMENT_NAME           = "DIVINER LUNAR RADIOMETER EXPERIMENT"
INSTRUMENT_ID             = "DLRE"
MISSION_PHASE_NAME        = {"NOMINAL MISSION"}
TARGET_NAME               = MOON
START_TIME                = 2012-04-18T23:00:00.000
STOP_TIME                 = 2012-05-16T06:00:00.000
PRODUCT_CREATION_TIME     = 2013-01-06T10:13:32.000
PRODUCER_ID               = LRO_DLRE_TEAM
PRODUCER_FULL_NAME        = "DAVID A. PAIGE"
PRODUCER_INSTITUTION_NAME = "UNIVERSITY OF CALIFORNIA, LOS ANGELES"
LRO:LOLA_DEM_VERS           = "1.0"
LRO:DLRE_GEOM_VERSION_ID    = "1.0"
LRO:CALIBRATION_SOFTWARE_VER_ID = "4.1"
LRO:DLRE_JDATE_MIN          = 2456036.459697
LRO:DLRE_JDATE_MAX          = 2456063.762061
LRO:DLRE_CLOCTIME_MIN       = 6.0000
LRO:DLRE_CLOCTIME_MAX       = 18.0000
MINIMUM_WAVELENGTH          = 0.35 <micron>
MAXIMUM_WAVELENGTH          = 400.0 <micron>


DESCRIPTION               = "

Each sample represents the Visual Brightness (VB) for
Channel 1, scaled by the value of SCALING_FACTOR.
Conversion from Digital Number (DN) to average
is given by the equation:

TB = (DN * SCALING_FACTOR) + OFFSET

Data is derived from Diviner nadir only data. The effective
field of view for each data point is determined with a 2D
Monte Carlo routine that accounts for the in-track and
cross-track instantaneous field of view of the detectors,
as the detector response and the integration time smearing
results from spacecraft motion in the in-track direction.
Bins are then weighted appropriately where there is detector
overlap. Each map cycle start and stop time is selected to
correspond to 180 and -180 degrees longitude. LRO orbits
progress from 180 degrees longitude to -180 degrees longitude
during that time period resulting in a drift in local time
across each map.

"

OBJECT                    = UNCOMPRESSED_FILE
```

```
FILE_NAME                = "DGDR_TBOL_AVG_CYL_20120418D_128_JP2.JP2"
RECORD_TYPE              = FIXED_LENGTH
FILE_RECORDS             = 23040
RECORD_BYTES             = 92160
^IMAGE                   = "DGDR_TBOL_AVG_CYL_20120418D_128_JP2.JP2"


 OBJECT                  = IMAGE
  NAME                   = "BOLOMETRIC TEMPERATURE"
  LINES                  = 23040
  LINE_SAMPLES           = 46080
  SAMPLE_TYPE            = LSB_INTEGER
  SAMPLE_BITS            = 16
  UNIT                   = NORMALIZED_RADIANCE
  SCALING_FACTOR         = 0.02
  OFFSET                 = 0.
  DERIVED_MINIMUM             = 0
  DERIVED_MAXIMUM             = 391.197814941
  MISSING_CONSTANT       = -32768
 END_OBJECT              = IMAGE

END_OBJECT               = UNCOMPRESSED_FILE

OBJECT                   = IMAGE_MAP_PROJECTION
 ^DATA_SET_MAP_PROJECTION     = "DSMAP.CAT"
 MAP_PROJECTION_TYPE          = "SIMPLE CYLINDRICAL"
 KEYWORD_LATITUDE_TYPE        = "PLANETOCENTRIC"
 MAP_RESOLUTION               = 128 <pix/degree>
 A_AXIS_RADIUS                = 1737.4 <km>
 B_AXIS_RADIUS                = 1737.4 <km>
 C_AXIS_RADIUS                = 1737.4 <km>
 FIRST_STANDARD_PARALLEL      = 'N/A'
 SECOND_STANDARD_PARALLEL     = 'N/A'
 POSITIVE_LONGITUDE_DIRECTION = "EAST"
 CENTER_LATITUDE              = 0.0 <deg>
 CENTER_LONGITUDE             = 0.0 <deg>
 REFERENCE_LATITUDE           = 'N/A'
 REFERENCE_LONGITUDE          = 'N/A'
 LINE_FIRST_PIXEL             = 1
 LINE_LAST_PIXEL              = 23040
 SAMPLE_FIRST_PIXEL           = 1
 SAMPLE_LAST_PIXEL            = 46080
 MAP_PROJECTION_ROTATION      = 0.0
 MAP_SCALE                    = 236.901175 <m/pix>
 MAXIMUM_LATITUDE             = 90 <deg>
 MINIMUM_LATITUDE             = -90 <deg>
 WESTERNMOST_LONGITUDE        = -180.0 <deg>
 EASTERNMOST_LONGITUDE        = 180.0 <deg>
 LINE_PROJECTION_OFFSET       = 11519.5 <pixel>
 SAMPLE_PROJECTION_OFFSET     = 23039.5 <pixel>
 COORDINATE_SYSTEM_TYPE       = "BODY-FIXED ROTATING"
 COORDINATE_SYSTEM_NAME       = "MEAN EARTH/POLAR AXIS OF DE421"
END_OBJECT                   = IMAGE_MAP_PROJECTION
```

```
END
```

```
PDS_VERSION_ID            = "PDS3"

PRODUCT_VERSION_ID        = "V4.1"
DATA_SET_ID               = "LRO-L-DLRE-5-GDR-V1.0"
PRODUCT_ID                = "DGDR_TBOL_AVG_CYL_20120502N_128_JP2.JP2"
SOURCE_PRODUCT_ID         = "DGDR_TBOL_AVG_CYL_20120502N_128_IMG.IMG"
INSTRUMENT_HOST_NAME      = "LUNAR RECONNAISSANCE ORBITER"
INSTRUMENT_HOST_ID        = "LRO"
INSTRUMENT_NAME           = "DIVINER LUNAR RADIOMETER EXPERIMENT"
INSTRUMENT_ID             = "DLRE"
MISSION_PHASE_NAME        = {"NOMINAL MISSION"}
TARGET_NAME               = MOON
START_TIME                = 2012-05-02T11:00:00.000
STOP_TIME                 = 2012-05-29T18:00:00.000
PRODUCT_CREATION_TIME     = 2013-01-07T02:14:41.000
PRODUCER_ID               = LRO_DLRE_TEAM
PRODUCER_FULL_NAME        = "DAVID A. PAIGE"
PRODUCER_INSTITUTION_NAME = "UNIVERSITY OF CALIFORNIA, LOS ANGELES"
LRO:LOLA_DEM_VERS           = "1.0"
LRO:DLRE_GEOM_VERSION_ID    = "1.0"
LRO:CALIBRATION_SOFTWARE_VER_ID = "4.1"
LRO:DLRE_JDATE_MIN          = 2456049.988785
LRO:DLRE_JDATE_MAX          = 2456077.291307
LRO:DLRE_CLOCTIME_MIN       = 18.0000
LRO:DLRE_CLOCTIME_MAX       = 6.0000
MINIMUM_WAVELENGTH          = 0.35 <micron>
MAXIMUM_WAVELENGTH          = 400.0 <micron>


DESCRIPTION               = "

Each sample represents the Visual Brightness (VB) for
Channel 1, scaled by the value of SCALING_FACTOR.
Conversion from Digital Number (DN) to average
is given by the equation:

TB = (DN * SCALING_FACTOR) + OFFSET

Data is derived from Diviner nadir only data. The effective
field of view for each data point is determined with a 2D
Monte Carlo routine that accounts for the in-track and
cross-track instantaneous field of view of the detectors,
as the detector response and the integration time smearing
results from spacecraft motion in the in-track direction.
Bins are then weighted appropriately where there is detector
overlap. Each map cycle start and stop time is selected to
correspond to 180 and -180 degrees longitude. LRO orbits
progress from 180 degrees longitude to -180 degrees longitude
during that time period resulting in a drift in local time
across each map.

"

OBJECT                    = UNCOMPRESSED_FILE
```

```
FILE_NAME                = "DGDR_TBOL_AVG_CYL_20120502N_128_JP2.JP2"
RECORD_TYPE              = FIXED_LENGTH
FILE_RECORDS             = 23040
RECORD_BYTES             = 92160
^IMAGE                   = "DGDR_TBOL_AVG_CYL_20120502N_128_JP2.JP2"


 OBJECT                  = IMAGE
  NAME                   = "BOLOMETRIC TEMPERATURE"
  LINES                  = 23040
  LINE_SAMPLES           = 46080
  SAMPLE_TYPE            = LSB_INTEGER
  SAMPLE_BITS            = 16
  UNIT                   = NORMALIZED_RADIANCE
  SCALING_FACTOR         = 0.02
  OFFSET                 = 0.
  DERIVED_MINIMUM             = 0
  DERIVED_MAXIMUM             = 437.851593018
  MISSING_CONSTANT       = -32768
 END_OBJECT              = IMAGE

END_OBJECT               = UNCOMPRESSED_FILE

OBJECT                   = IMAGE_MAP_PROJECTION
 ^DATA_SET_MAP_PROJECTION     = "DSMAP.CAT"
 MAP_PROJECTION_TYPE          = "SIMPLE CYLINDRICAL"
 KEYWORD_LATITUDE_TYPE        = "PLANETOCENTRIC"
 MAP_RESOLUTION               = 128 <pix/degree>
 A_AXIS_RADIUS                = 1737.4 <km>
 B_AXIS_RADIUS                = 1737.4 <km>
 C_AXIS_RADIUS                = 1737.4 <km>
 FIRST_STANDARD_PARALLEL      = 'N/A'
 SECOND_STANDARD_PARALLEL     = 'N/A'
 POSITIVE_LONGITUDE_DIRECTION = "EAST"
 CENTER_LATITUDE              = 0.0 <deg>
 CENTER_LONGITUDE             = 0.0 <deg>
 REFERENCE_LATITUDE           = 'N/A'
 REFERENCE_LONGITUDE          = 'N/A'
 LINE_FIRST_PIXEL             = 1
 LINE_LAST_PIXEL              = 23040
 SAMPLE_FIRST_PIXEL           = 1
 SAMPLE_LAST_PIXEL            = 46080
 MAP_PROJECTION_ROTATION      = 0.0
 MAP_SCALE                    = 236.901175 <m/pix>
 MAXIMUM_LATITUDE             = 90 <deg>
 MINIMUM_LATITUDE             = -90 <deg>
 WESTERNMOST_LONGITUDE        = -180.0 <deg>
 EASTERNMOST_LONGITUDE        = 180.0 <deg>
 LINE_PROJECTION_OFFSET       = 11519.5 <pixel>
 SAMPLE_PROJECTION_OFFSET     = 23039.5 <pixel>
 COORDINATE_SYSTEM_TYPE       = "BODY-FIXED ROTATING"
 COORDINATE_SYSTEM_NAME       = "MEAN EARTH/POLAR AXIS OF DE421"
END_OBJECT                   = IMAGE_MAP_PROJECTION
```

```
END
```

```
PDS_VERSION_ID            = "PDS3"

PRODUCT_VERSION_ID        = "V4.1"
DATA_SET_ID               = "LRO-L-DLRE-5-GDR-V1.0"
PRODUCT_ID                = "DGDR_LTIM_AVG_CYL_20120723D_128_JP2.JP2"
SOURCE_PRODUCT_ID         = "DGDR_LTIM_AVG_CYL_20120723D_128_IMG.IMG"
INSTRUMENT_HOST_NAME      = "LUNAR RECONNAISSANCE ORBITER"
INSTRUMENT_HOST_ID        = "LRO"
INSTRUMENT_NAME           = "DIVINER LUNAR RADIOMETER EXPERIMENT"
INSTRUMENT_ID             = "DLRE"
MISSION_PHASE_NAME        = {"NOMINAL MISSION"}
TARGET_NAME               = MOON
START_TIME                = 2012-07-23T10:00:00.000
STOP_TIME                 = 2012-08-19T15:00:00.000
PRODUCT_CREATION_TIME     = 2013-01-10T19:55:18.000
PRODUCER_ID               = LRO_DLRE_TEAM
PRODUCER_FULL_NAME        = "DAVID A. PAIGE"
PRODUCER_INSTITUTION_NAME = "UNIVERSITY OF CALIFORNIA, LOS ANGELES"
LRO:LOLA_DEM_VERS           = "1.0"
LRO:DLRE_GEOM_VERSION_ID    = "1.0"
LRO:CALIBRATION_SOFTWARE_VER_ID = "4.1"
LRO:DLRE_JDATE_MIN          = 2456131.955511
LRO:DLRE_JDATE_MAX          = 2456159.163566
LRO:DLRE_CLOCTIME_MIN       = 6.0000
LRO:DLRE_CLOCTIME_MAX       = 18.0000
MINIMUM_WAVELENGTH          = 0.35 <micron>
MAXIMUM_WAVELENGTH          = 400.0 <micron>


DESCRIPTION               = "

Each sample represents the average local time for
all channels, scaled by the value of SCALING_FACTOR.
Conversion from Digital Number (DN) to average
is given by the equation:

TB = (DN * SCALING_FACTOR) + OFFSET

Data is derived from Diviner nadir only data. The effective
field of view for each data point is determined with a 2D
Monte Carlo routine that accounts for the in-track and
cross-track instantaneous field of view of the detectors,
as the detector response and the integration time smearing
results from spacecraft motion in the in-track direction.
Bins are then weighted appropriately where there is detector
overlap. Each map cycle start and stop time is selected to
correspond to 180 and -180 degrees longitude. LRO orbits
progress from 180 degrees longitude to -180 degrees longitude
during that time period resulting in a drift in local time
across each map.

"

OBJECT                    = UNCOMPRESSED_FILE
```

```
FILE_NAME                = "DGDR_LTIM_AVG_CYL_20120723D_128_JP2.JP2"
RECORD_TYPE              = FIXED_LENGTH
FILE_RECORDS             = 23040
RECORD_BYTES             = 92160
^IMAGE                   = "DGDR_LTIM_AVG_CYL_20120723D_128_JP2.JP2"


 OBJECT                  = IMAGE
  NAME                   = "LOCAL TIME"
  LINES                  = 23040
  LINE_SAMPLES           = 46080
  SAMPLE_TYPE            = LSB_INTEGER
  SAMPLE_BITS            = 16
  UNIT                   = HOURS
  SCALING_FACTOR         = 0.0833333333
  OFFSET                 = 2730.00273000273
  DERIVED_MINIMUM             = 6.00791501999
  DERIVED_MAXIMUM             = 18
  MISSING_CONSTANT       = -32768
 END_OBJECT              = IMAGE

END_OBJECT               = UNCOMPRESSED_FILE

OBJECT                   = IMAGE_MAP_PROJECTION
 ^DATA_SET_MAP_PROJECTION     = "DSMAP.CAT"
 MAP_PROJECTION_TYPE          = "SIMPLE CYLINDRICAL"
 KEYWORD_LATITUDE_TYPE        = "PLANETOCENTRIC"
 MAP_RESOLUTION               = 128 <pix/degree>
 A_AXIS_RADIUS                = 1737.4 <km>
 B_AXIS_RADIUS                = 1737.4 <km>
 C_AXIS_RADIUS                = 1737.4 <km>
 FIRST_STANDARD_PARALLEL      = 'N/A'
 SECOND_STANDARD_PARALLEL     = 'N/A'
 POSITIVE_LONGITUDE_DIRECTION = "EAST"
 CENTER_LATITUDE              = 0.0 <deg>
 CENTER_LONGITUDE             = 0.0 <deg>
 REFERENCE_LATITUDE           = 'N/A'
 REFERENCE_LONGITUDE          = 'N/A'
 LINE_FIRST_PIXEL             = 1
 LINE_LAST_PIXEL              = 23040
 SAMPLE_FIRST_PIXEL           = 1
 SAMPLE_LAST_PIXEL            = 46080
 MAP_PROJECTION_ROTATION      = 0.0
 MAP_SCALE                    = 236.901175 <m/pix>
 MAXIMUM_LATITUDE             = 90 <deg>
 MINIMUM_LATITUDE             = -90 <deg>
 WESTERNMOST_LONGITUDE        = -180.0 <deg>
 EASTERNMOST_LONGITUDE        = 180.0 <deg>
 LINE_PROJECTION_OFFSET       = 11519.5 <pixel>
 SAMPLE_PROJECTION_OFFSET     = 23039.5 <pixel>
 COORDINATE_SYSTEM_TYPE       = "BODY-FIXED ROTATING"
 COORDINATE_SYSTEM_NAME       = "MEAN EARTH/POLAR AXIS OF DE421"
END_OBJECT                   = IMAGE_MAP_PROJECTION
```

```
END
```

```
PDS_VERSION_ID            = "PDS3"

PRODUCT_VERSION_ID        = "V4.1"
DATA_SET_ID               = "LRO-L-DLRE-5-GDR-V1.0"
PRODUCT_ID                = "DGDR_TBOL_AVG_CYL_20120806N_128_JP2.JP2"
SOURCE_PRODUCT_ID         = "DGDR_TBOL_AVG_CYL_20120806N_128_IMG.IMG"
INSTRUMENT_HOST_NAME      = "LUNAR RECONNAISSANCE ORBITER"
INSTRUMENT_HOST_ID        = "LRO"
INSTRUMENT_NAME           = "DIVINER LUNAR RADIOMETER EXPERIMENT"
INSTRUMENT_ID             = "DLRE"
MISSION_PHASE_NAME        = {"NOMINAL MISSION"}
TARGET_NAME               = MOON
START_TIME                = 2012-08-06T01:00:00.000
STOP_TIME                 = 2012-09-02T08:00:00.000
PRODUCT_CREATION_TIME     = 2013-01-11T11:12:46.000
PRODUCER_ID               = LRO_DLRE_TEAM
PRODUCER_FULL_NAME        = "DAVID A. PAIGE"
PRODUCER_INSTITUTION_NAME = "UNIVERSITY OF CALIFORNIA, LOS ANGELES"
LRO:LOLA_DEM_VERS           = "1.0"
LRO:DLRE_GEOM_VERSION_ID    = "1.0"
LRO:CALIBRATION_SOFTWARE_VER_ID = "4.1"
LRO:DLRE_JDATE_MIN          = 2456145.557515
LRO:DLRE_JDATE_MAX          = 2456172.847033
LRO:DLRE_CLOCTIME_MIN       = 18.0000
LRO:DLRE_CLOCTIME_MAX       = 6.0000
MINIMUM_WAVELENGTH          = 0.35 <micron>
MAXIMUM_WAVELENGTH          = 400.0 <micron>


DESCRIPTION               = "

Each sample represents the Visual Brightness (VB) for
Channel 1, scaled by the value of SCALING_FACTOR.
Conversion from Digital Number (DN) to average
is given by the equation:

TB = (DN * SCALING_FACTOR) + OFFSET

Data is derived from Diviner nadir only data. The effective
field of view for each data point is determined with a 2D
Monte Carlo routine that accounts for the in-track and
cross-track instantaneous field of view of the detectors,
as the detector response and the integration time smearing
results from spacecraft motion in the in-track direction.
Bins are then weighted appropriately where there is detector
overlap. Each map cycle start and stop time is selected to
correspond to 180 and -180 degrees longitude. LRO orbits
progress from 180 degrees longitude to -180 degrees longitude
during that time period resulting in a drift in local time
across each map.

"

OBJECT                    = UNCOMPRESSED_FILE
```

```
FILE_NAME                = "DGDR_TBOL_AVG_CYL_20120806N_128_JP2.JP2"
RECORD_TYPE              = FIXED_LENGTH
FILE_RECORDS             = 23040
RECORD_BYTES             = 92160
^IMAGE                   = "DGDR_TBOL_AVG_CYL_20120806N_128_JP2.JP2"


 OBJECT                  = IMAGE
  NAME                   = "BOLOMETRIC TEMPERATURE"
  LINES                  = 23040
  LINE_SAMPLES           = 46080
  SAMPLE_TYPE            = LSB_INTEGER
  SAMPLE_BITS            = 16
  UNIT                   = NORMALIZED_RADIANCE
  SCALING_FACTOR         = 0.02
  OFFSET                 = 0.
  DERIVED_MINIMUM             = 17.5655994415
  DERIVED_MAXIMUM             = 284.281402588
  MISSING_CONSTANT       = -32768
 END_OBJECT              = IMAGE

END_OBJECT               = UNCOMPRESSED_FILE

OBJECT                   = IMAGE_MAP_PROJECTION
 ^DATA_SET_MAP_PROJECTION     = "DSMAP.CAT"
 MAP_PROJECTION_TYPE          = "SIMPLE CYLINDRICAL"
 KEYWORD_LATITUDE_TYPE        = "PLANETOCENTRIC"
 MAP_RESOLUTION               = 128 <pix/degree>
 A_AXIS_RADIUS                = 1737.4 <km>
 B_AXIS_RADIUS                = 1737.4 <km>
 C_AXIS_RADIUS                = 1737.4 <km>
 FIRST_STANDARD_PARALLEL      = 'N/A'
 SECOND_STANDARD_PARALLEL     = 'N/A'
 POSITIVE_LONGITUDE_DIRECTION = "EAST"
 CENTER_LATITUDE              = 0.0 <deg>
 CENTER_LONGITUDE             = 0.0 <deg>
 REFERENCE_LATITUDE           = 'N/A'
 REFERENCE_LONGITUDE          = 'N/A'
 LINE_FIRST_PIXEL             = 1
 LINE_LAST_PIXEL              = 23040
 SAMPLE_FIRST_PIXEL           = 1
 SAMPLE_LAST_PIXEL            = 46080
 MAP_PROJECTION_ROTATION      = 0.0
 MAP_SCALE                    = 236.901175 <m/pix>
 MAXIMUM_LATITUDE             = 90 <deg>
 MINIMUM_LATITUDE             = -90 <deg>
 WESTERNMOST_LONGITUDE        = -180.0 <deg>
 EASTERNMOST_LONGITUDE        = 180.0 <deg>
 LINE_PROJECTION_OFFSET       = 11519.5 <pixel>
 SAMPLE_PROJECTION_OFFSET     = 23039.5 <pixel>
 COORDINATE_SYSTEM_TYPE       = "BODY-FIXED ROTATING"
 COORDINATE_SYSTEM_NAME       = "MEAN EARTH/POLAR AXIS OF DE421"
END_OBJECT                   = IMAGE_MAP_PROJECTION
```

```
END
```

```
PDS_VERSION_ID            = "PDS3"

PRODUCT_VERSION_ID        = "V4.1"
DATA_SET_ID               = "LRO-L-DLRE-5-GDR-V1.0"
PRODUCT_ID                = "DGDR_LTIM_AVG_CYL_20120418D_128_JP2.JP2"
SOURCE_PRODUCT_ID         = "DGDR_LTIM_AVG_CYL_20120418D_128_IMG.IMG"
INSTRUMENT_HOST_NAME      = "LUNAR RECONNAISSANCE ORBITER"
INSTRUMENT_HOST_ID        = "LRO"
INSTRUMENT_NAME           = "DIVINER LUNAR RADIOMETER EXPERIMENT"
INSTRUMENT_ID             = "DLRE"
MISSION_PHASE_NAME        = {"NOMINAL MISSION"}
TARGET_NAME               = MOON
START_TIME                = 2012-04-18T23:00:00.000
STOP_TIME                 = 2012-05-16T06:00:00.000
PRODUCT_CREATION_TIME     = 2013-01-06T11:43:32.000
PRODUCER_ID               = LRO_DLRE_TEAM
PRODUCER_FULL_NAME        = "DAVID A. PAIGE"
PRODUCER_INSTITUTION_NAME = "UNIVERSITY OF CALIFORNIA, LOS ANGELES"
LRO:LOLA_DEM_VERS           = "1.0"
LRO:DLRE_GEOM_VERSION_ID    = "1.0"
LRO:CALIBRATION_SOFTWARE_VER_ID = "4.1"
LRO:DLRE_JDATE_MIN          = 2456036.459697
LRO:DLRE_JDATE_MAX          = 2456063.762061
LRO:DLRE_CLOCTIME_MIN       = 6.0000
LRO:DLRE_CLOCTIME_MAX       = 18.0000
MINIMUM_WAVELENGTH          = 0.35 <micron>
MAXIMUM_WAVELENGTH          = 400.0 <micron>


DESCRIPTION               = "

Each sample represents the average local time for
all channels, scaled by the value of SCALING_FACTOR.
Conversion from Digital Number (DN) to average
is given by the equation:

TB = (DN * SCALING_FACTOR) + OFFSET

Data is derived from Diviner nadir only data. The effective
field of view for each data point is determined with a 2D
Monte Carlo routine that accounts for the in-track and
cross-track instantaneous field of view of the detectors,
as the detector response and the integration time smearing
results from spacecraft motion in the in-track direction.
Bins are then weighted appropriately where there is detector
overlap. Each map cycle start and stop time is selected to
correspond to 180 and -180 degrees longitude. LRO orbits
progress from 180 degrees longitude to -180 degrees longitude
during that time period resulting in a drift in local time
across each map.

"

OBJECT                    = UNCOMPRESSED_FILE
```

```
FILE_NAME                = "DGDR_LTIM_AVG_CYL_20120418D_128_JP2.JP2"
RECORD_TYPE              = FIXED_LENGTH
FILE_RECORDS             = 23040
RECORD_BYTES             = 92160
^IMAGE                   = "DGDR_LTIM_AVG_CYL_20120418D_128_JP2.JP2"


 OBJECT                  = IMAGE
  NAME                   = "LOCAL TIME"
  LINES                  = 23040
  LINE_SAMPLES           = 46080
  SAMPLE_TYPE            = LSB_INTEGER
  SAMPLE_BITS            = 16
  UNIT                   = HOURS
  SCALING_FACTOR         = 0.0833333333
  OFFSET                 = 2730.00273000273
  DERIVED_MINIMUM             = 6
  DERIVED_MAXIMUM             = 17.9878463745
  MISSING_CONSTANT       = -32768
 END_OBJECT              = IMAGE

END_OBJECT               = UNCOMPRESSED_FILE

OBJECT                   = IMAGE_MAP_PROJECTION
 ^DATA_SET_MAP_PROJECTION     = "DSMAP.CAT"
 MAP_PROJECTION_TYPE          = "SIMPLE CYLINDRICAL"
 KEYWORD_LATITUDE_TYPE        = "PLANETOCENTRIC"
 MAP_RESOLUTION               = 128 <pix/degree>
 A_AXIS_RADIUS                = 1737.4 <km>
 B_AXIS_RADIUS                = 1737.4 <km>
 C_AXIS_RADIUS                = 1737.4 <km>
 FIRST_STANDARD_PARALLEL      = 'N/A'
 SECOND_STANDARD_PARALLEL     = 'N/A'
 POSITIVE_LONGITUDE_DIRECTION = "EAST"
 CENTER_LATITUDE              = 0.0 <deg>
 CENTER_LONGITUDE             = 0.0 <deg>
 REFERENCE_LATITUDE           = 'N/A'
 REFERENCE_LONGITUDE          = 'N/A'
 LINE_FIRST_PIXEL             = 1
 LINE_LAST_PIXEL              = 23040
 SAMPLE_FIRST_PIXEL           = 1
 SAMPLE_LAST_PIXEL            = 46080
 MAP_PROJECTION_ROTATION      = 0.0
 MAP_SCALE                    = 236.901175 <m/pix>
 MAXIMUM_LATITUDE             = 90 <deg>
 MINIMUM_LATITUDE             = -90 <deg>
 WESTERNMOST_LONGITUDE        = -180.0 <deg>
 EASTERNMOST_LONGITUDE        = 180.0 <deg>
 LINE_PROJECTION_OFFSET       = 11519.5 <pixel>
 SAMPLE_PROJECTION_OFFSET     = 23039.5 <pixel>
 COORDINATE_SYSTEM_TYPE       = "BODY-FIXED ROTATING"
 COORDINATE_SYSTEM_NAME       = "MEAN EARTH/POLAR AXIS OF DE421"
END_OBJECT                   = IMAGE_MAP_PROJECTION
```

```
END
```

```
PDS_VERSION_ID            = "PDS3"

PRODUCT_VERSION_ID        = "V4.1"
DATA_SET_ID               = "LRO-L-DLRE-5-GDR-V1.0"
PRODUCT_ID                = "DGDR_LTIM_AVG_CYL_20120502N_128_JP2.JP2"
SOURCE_PRODUCT_ID         = "DGDR_LTIM_AVG_CYL_20120502N_128_IMG.IMG"
INSTRUMENT_HOST_NAME      = "LUNAR RECONNAISSANCE ORBITER"
INSTRUMENT_HOST_ID        = "LRO"
INSTRUMENT_NAME           = "DIVINER LUNAR RADIOMETER EXPERIMENT"
INSTRUMENT_ID             = "DLRE"
MISSION_PHASE_NAME        = {"NOMINAL MISSION"}
TARGET_NAME               = MOON
START_TIME                = 2012-05-02T11:00:00.000
STOP_TIME                 = 2012-05-29T18:00:00.000
PRODUCT_CREATION_TIME     = 2013-01-07T03:44:41.000
PRODUCER_ID               = LRO_DLRE_TEAM
PRODUCER_FULL_NAME        = "DAVID A. PAIGE"
PRODUCER_INSTITUTION_NAME = "UNIVERSITY OF CALIFORNIA, LOS ANGELES"
LRO:LOLA_DEM_VERS           = "1.0"
LRO:DLRE_GEOM_VERSION_ID    = "1.0"
LRO:CALIBRATION_SOFTWARE_VER_ID = "4.1"
LRO:DLRE_JDATE_MIN          = 2456049.988785
LRO:DLRE_JDATE_MAX          = 2456077.291307
LRO:DLRE_CLOCTIME_MIN       = 18.0000
LRO:DLRE_CLOCTIME_MAX       = 6.0000
MINIMUM_WAVELENGTH          = 0.35 <micron>
MAXIMUM_WAVELENGTH          = 400.0 <micron>


DESCRIPTION               = "

Each sample represents the average local time for
all channels, scaled by the value of SCALING_FACTOR.
Conversion from Digital Number (DN) to average
is given by the equation:

TB = (DN * SCALING_FACTOR) + OFFSET

Data is derived from Diviner nadir only data. The effective
field of view for each data point is determined with a 2D
Monte Carlo routine that accounts for the in-track and
cross-track instantaneous field of view of the detectors,
as the detector response and the integration time smearing
results from spacecraft motion in the in-track direction.
Bins are then weighted appropriately where there is detector
overlap. Each map cycle start and stop time is selected to
correspond to 180 and -180 degrees longitude. LRO orbits
progress from 180 degrees longitude to -180 degrees longitude
during that time period resulting in a drift in local time
across each map.

"

OBJECT                    = UNCOMPRESSED_FILE
```

```
FILE_NAME                = "DGDR_LTIM_AVG_CYL_20120502N_128_JP2.JP2"
RECORD_TYPE              = FIXED_LENGTH
FILE_RECORDS             = 23040
RECORD_BYTES             = 92160
^IMAGE                   = "DGDR_LTIM_AVG_CYL_20120502N_128_JP2.JP2"


 OBJECT                  = IMAGE
  NAME                   = "LOCAL TIME"
  LINES                  = 23040
  LINE_SAMPLES           = 46080
  SAMPLE_TYPE            = LSB_INTEGER
  SAMPLE_BITS            = 16
  UNIT                   = HOURS
  SCALING_FACTOR         = 0.0833333333
  OFFSET                 = 2730.00273000273
  DERIVED_MINIMUM             = 2.49999999369e-07
  DERIVED_MAXIMUM             = 24
  MISSING_CONSTANT       = -32768
 END_OBJECT              = IMAGE

END_OBJECT               = UNCOMPRESSED_FILE

OBJECT                   = IMAGE_MAP_PROJECTION
 ^DATA_SET_MAP_PROJECTION     = "DSMAP.CAT"
 MAP_PROJECTION_TYPE          = "SIMPLE CYLINDRICAL"
 KEYWORD_LATITUDE_TYPE        = "PLANETOCENTRIC"
 MAP_RESOLUTION               = 128 <pix/degree>
 A_AXIS_RADIUS                = 1737.4 <km>
 B_AXIS_RADIUS                = 1737.4 <km>
 C_AXIS_RADIUS                = 1737.4 <km>
 FIRST_STANDARD_PARALLEL      = 'N/A'
 SECOND_STANDARD_PARALLEL     = 'N/A'
 POSITIVE_LONGITUDE_DIRECTION = "EAST"
 CENTER_LATITUDE              = 0.0 <deg>
 CENTER_LONGITUDE             = 0.0 <deg>
 REFERENCE_LATITUDE           = 'N/A'
 REFERENCE_LONGITUDE          = 'N/A'
 LINE_FIRST_PIXEL             = 1
 LINE_LAST_PIXEL              = 23040
 SAMPLE_FIRST_PIXEL           = 1
 SAMPLE_LAST_PIXEL            = 46080
 MAP_PROJECTION_ROTATION      = 0.0
 MAP_SCALE                    = 236.901175 <m/pix>
 MAXIMUM_LATITUDE             = 90 <deg>
 MINIMUM_LATITUDE             = -90 <deg>
 WESTERNMOST_LONGITUDE        = -180.0 <deg>
 EASTERNMOST_LONGITUDE        = 180.0 <deg>
 LINE_PROJECTION_OFFSET       = 11519.5 <pixel>
 SAMPLE_PROJECTION_OFFSET     = 23039.5 <pixel>
 COORDINATE_SYSTEM_TYPE       = "BODY-FIXED ROTATING"
 COORDINATE_SYSTEM_NAME       = "MEAN EARTH/POLAR AXIS OF DE421"
END_OBJECT                   = IMAGE_MAP_PROJECTION
```

```
END
```

```
PDS_VERSION_ID            = "PDS3"

PRODUCT_VERSION_ID        = "V4.1"
DATA_SET_ID               = "LRO-L-DLRE-5-GDR-V1.0"
PRODUCT_ID                = "DGDR_LTIM_AVG_CYL_20120723D_128_JP2.JP2"
SOURCE_PRODUCT_ID         = "DGDR_LTIM_AVG_CYL_20120723D_128_IMG.IMG"
INSTRUMENT_HOST_NAME      = "LUNAR RECONNAISSANCE ORBITER"
INSTRUMENT_HOST_ID        = "LRO"
INSTRUMENT_NAME           = "DIVINER LUNAR RADIOMETER EXPERIMENT"
INSTRUMENT_ID             = "DLRE"
MISSION_PHASE_NAME        = {"NOMINAL MISSION"}
TARGET_NAME               = MOON
START_TIME                = 2012-07-23T10:00:00.000
STOP_TIME                 = 2012-08-19T15:00:00.000
PRODUCT_CREATION_TIME     = 2013-01-10T19:55:18.000
PRODUCER_ID               = LRO_DLRE_TEAM
PRODUCER_FULL_NAME        = "DAVID A. PAIGE"
PRODUCER_INSTITUTION_NAME = "UNIVERSITY OF CALIFORNIA, LOS ANGELES"
LRO:LOLA_DEM_VERS           = "1.0"
LRO:DLRE_GEOM_VERSION_ID    = "1.0"
LRO:CALIBRATION_SOFTWARE_VER_ID = "4.1"
LRO:DLRE_JDATE_MIN          = 2456131.955511
LRO:DLRE_JDATE_MAX          = 2456159.163566
LRO:DLRE_CLOCTIME_MIN       = 6.0000
LRO:DLRE_CLOCTIME_MAX       = 18.0000
MINIMUM_WAVELENGTH          = 0.35 <micron>
MAXIMUM_WAVELENGTH          = 400.0 <micron>


DESCRIPTION               = "

Each sample represents the average local time for
all channels, scaled by the value of SCALING_FACTOR.
Conversion from Digital Number (DN) to average
is given by the equation:

TB = (DN * SCALING_FACTOR) + OFFSET

Data is derived from Diviner nadir only data. The effective
field of view for each data point is determined with a 2D
Monte Carlo routine that accounts for the in-track and
cross-track instantaneous field of view of the detectors,
as the detector response and the integration time smearing
results from spacecraft motion in the in-track direction.
Bins are then weighted appropriately where there is detector
overlap. Each map cycle start and stop time is selected to
correspond to 180 and -180 degrees longitude. LRO orbits
progress from 180 degrees longitude to -180 degrees longitude
during that time period resulting in a drift in local time
across each map.

"

OBJECT                    = UNCOMPRESSED_FILE
```

```
FILE_NAME                = "DGDR_LTIM_AVG_CYL_20120723D_128_JP2.JP2"
RECORD_TYPE              = FIXED_LENGTH
FILE_RECORDS             = 23040
RECORD_BYTES             = 92160
^IMAGE                   = "DGDR_LTIM_AVG_CYL_20120723D_128_JP2.JP2"


 OBJECT                  = IMAGE
  NAME                   = "LOCAL TIME"
  LINES                  = 23040
  LINE_SAMPLES           = 46080
  SAMPLE_TYPE            = LSB_INTEGER
  SAMPLE_BITS            = 16
  UNIT                   = HOURS
  SCALING_FACTOR         = 0.0833333333
  OFFSET                 = 2730.00273000273
  DERIVED_MINIMUM             = 6.00791501999
  DERIVED_MAXIMUM             = 18
  MISSING_CONSTANT       = -32768
 END_OBJECT              = IMAGE

END_OBJECT               = UNCOMPRESSED_FILE

OBJECT                   = IMAGE_MAP_PROJECTION
 ^DATA_SET_MAP_PROJECTION     = "DSMAP.CAT"
 MAP_PROJECTION_TYPE          = "SIMPLE CYLINDRICAL"
 KEYWORD_LATITUDE_TYPE        = "PLANETOCENTRIC"
 MAP_RESOLUTION               = 128 <pix/degree>
 A_AXIS_RADIUS                = 1737.4 <km>
 B_AXIS_RADIUS                = 1737.4 <km>
 C_AXIS_RADIUS                = 1737.4 <km>
 FIRST_STANDARD_PARALLEL      = 'N/A'
 SECOND_STANDARD_PARALLEL     = 'N/A'
 POSITIVE_LONGITUDE_DIRECTION = "EAST"
 CENTER_LATITUDE              = 0.0 <deg>
 CENTER_LONGITUDE             = 0.0 <deg>
 REFERENCE_LATITUDE           = 'N/A'
 REFERENCE_LONGITUDE          = 'N/A'
 LINE_FIRST_PIXEL             = 1
 LINE_LAST_PIXEL              = 23040
 SAMPLE_FIRST_PIXEL           = 1
 SAMPLE_LAST_PIXEL            = 46080
 MAP_PROJECTION_ROTATION      = 0.0
 MAP_SCALE                    = 236.901175 <m/pix>
 MAXIMUM_LATITUDE             = 90 <deg>
 MINIMUM_LATITUDE             = -90 <deg>
 WESTERNMOST_LONGITUDE        = -180.0 <deg>
 EASTERNMOST_LONGITUDE        = 180.0 <deg>
 LINE_PROJECTION_OFFSET       = 11519.5 <pixel>
 SAMPLE_PROJECTION_OFFSET     = 23039.5 <pixel>
 COORDINATE_SYSTEM_TYPE       = "BODY-FIXED ROTATING"
 COORDINATE_SYSTEM_NAME       = "MEAN EARTH/POLAR AXIS OF DE421"
END_OBJECT                   = IMAGE_MAP_PROJECTION
```

```
END
```

```
PDS_VERSION_ID            = "PDS3"

PRODUCT_VERSION_ID        = "V4.1"
DATA_SET_ID               = "LRO-L-DLRE-5-GDR-V1.0"
PRODUCT_ID                = "DGDR_LTIM_AVG_CYL_20120806N_128_JP2.JP2"
SOURCE_PRODUCT_ID         = "DGDR_LTIM_AVG_CYL_20120806N_128_IMG.IMG"
INSTRUMENT_HOST_NAME      = "LUNAR RECONNAISSANCE ORBITER"
INSTRUMENT_HOST_ID        = "LRO"
INSTRUMENT_NAME           = "DIVINER LUNAR RADIOMETER EXPERIMENT"
INSTRUMENT_ID             = "DLRE"
MISSION_PHASE_NAME        = {"NOMINAL MISSION"}
TARGET_NAME               = MOON
START_TIME                = 2012-08-06T01:00:00.000
STOP_TIME                 = 2012-09-02T08:00:00.000
PRODUCT_CREATION_TIME     = 2013-01-11T12:42:46.000
PRODUCER_ID               = LRO_DLRE_TEAM
PRODUCER_FULL_NAME        = "DAVID A. PAIGE"
PRODUCER_INSTITUTION_NAME = "UNIVERSITY OF CALIFORNIA, LOS ANGELES"
LRO:LOLA_DEM_VERS           = "1.0"
LRO:DLRE_GEOM_VERSION_ID    = "1.0"
LRO:CALIBRATION_SOFTWARE_VER_ID = "4.1"
LRO:DLRE_JDATE_MIN          = 2456145.557515
LRO:DLRE_JDATE_MAX          = 2456172.847033
LRO:DLRE_CLOCTIME_MIN       = 18.0000
LRO:DLRE_CLOCTIME_MAX       = 6.0000
MINIMUM_WAVELENGTH          = 0.35 <micron>
MAXIMUM_WAVELENGTH          = 400.0 <micron>


DESCRIPTION               = "

Each sample represents the average local time for
all channels, scaled by the value of SCALING_FACTOR.
Conversion from Digital Number (DN) to average
is given by the equation:

TB = (DN * SCALING_FACTOR) + OFFSET

Data is derived from Diviner nadir only data. The effective
field of view for each data point is determined with a 2D
Monte Carlo routine that accounts for the in-track and
cross-track instantaneous field of view of the detectors,
as the detector response and the integration time smearing
results from spacecraft motion in the in-track direction.
Bins are then weighted appropriately where there is detector
overlap. Each map cycle start and stop time is selected to
correspond to 180 and -180 degrees longitude. LRO orbits
progress from 180 degrees longitude to -180 degrees longitude
during that time period resulting in a drift in local time
across each map.

"

OBJECT                    = UNCOMPRESSED_FILE
```

```
FILE_NAME                = "DGDR_LTIM_AVG_CYL_20120806N_128_JP2.JP2"
RECORD_TYPE              = FIXED_LENGTH
FILE_RECORDS             = 23040
RECORD_BYTES             = 92160
^IMAGE                   = "DGDR_LTIM_AVG_CYL_20120806N_128_JP2.JP2"


 OBJECT                  = IMAGE
  NAME                   = "LOCAL TIME"
  LINES                  = 23040
  LINE_SAMPLES           = 46080
  SAMPLE_TYPE            = LSB_INTEGER
  SAMPLE_BITS            = 16
  UNIT                   = HOURS
  SCALING_FACTOR         = 0.0833333333
  OFFSET                 = 2730.00273000273
  DERIVED_MINIMUM             = 0
  DERIVED_MAXIMUM             = 24
  MISSING_CONSTANT       = -32768
 END_OBJECT              = IMAGE

END_OBJECT               = UNCOMPRESSED_FILE

OBJECT                   = IMAGE_MAP_PROJECTION
 ^DATA_SET_MAP_PROJECTION     = "DSMAP.CAT"
 MAP_PROJECTION_TYPE          = "SIMPLE CYLINDRICAL"
 KEYWORD_LATITUDE_TYPE        = "PLANETOCENTRIC"
 MAP_RESOLUTION               = 128 <pix/degree>
 A_AXIS_RADIUS                = 1737.4 <km>
 B_AXIS_RADIUS                = 1737.4 <km>
 C_AXIS_RADIUS                = 1737.4 <km>
 FIRST_STANDARD_PARALLEL      = 'N/A'
 SECOND_STANDARD_PARALLEL     = 'N/A'
 POSITIVE_LONGITUDE_DIRECTION = "EAST"
 CENTER_LATITUDE              = 0.0 <deg>
 CENTER_LONGITUDE             = 0.0 <deg>
 REFERENCE_LATITUDE           = 'N/A'
 REFERENCE_LONGITUDE          = 'N/A'
 LINE_FIRST_PIXEL             = 1
 LINE_LAST_PIXEL              = 23040
 SAMPLE_FIRST_PIXEL           = 1
 SAMPLE_LAST_PIXEL            = 46080
 MAP_PROJECTION_ROTATION      = 0.0
 MAP_SCALE                    = 236.901175 <m/pix>
 MAXIMUM_LATITUDE             = 90 <deg>
 MINIMUM_LATITUDE             = -90 <deg>
 WESTERNMOST_LONGITUDE        = -180.0 <deg>
 EASTERNMOST_LONGITUDE        = 180.0 <deg>
 LINE_PROJECTION_OFFSET       = 11519.5 <pixel>
 SAMPLE_PROJECTION_OFFSET     = 23039.5 <pixel>
 COORDINATE_SYSTEM_TYPE       = "BODY-FIXED ROTATING"
 COORDINATE_SYSTEM_NAME       = "MEAN EARTH/POLAR AXIS OF DE421"
END_OBJECT                   = IMAGE_MAP_PROJECTION
```

```
END
```

```
PDS_VERSION_ID            = "PDS3"

PRODUCT_VERSION_ID        = "V4.1"
DATA_SET_ID               = "LRO-L-DLRE-5-GDR-V1.0"
PRODUCT_ID                = "DGDR_JD_AVG_CYL_20120418D_128_JP2.JP2"
SOURCE_PRODUCT_ID         = "DGDR_JD_AVG_CYL_20120418D_128_IMG.IMG"
INSTRUMENT_HOST_NAME      = "LUNAR RECONNAISSANCE ORBITER"
INSTRUMENT_HOST_ID        = "LRO"
INSTRUMENT_NAME           = "DIVINER LUNAR RADIOMETER EXPERIMENT"
INSTRUMENT_ID             = "DLRE"
MISSION_PHASE_NAME        = {"NOMINAL MISSION"}
TARGET_NAME               = MOON
START_TIME                = 2012-04-18T23:00:00.000
STOP_TIME                 = 2012-05-16T06:00:00.000
PRODUCT_CREATION_TIME     = 2013-01-06T11:43:32.000
PRODUCER_ID               = LRO_DLRE_TEAM
PRODUCER_FULL_NAME        = "DAVID A. PAIGE"
PRODUCER_INSTITUTION_NAME = "UNIVERSITY OF CALIFORNIA, LOS ANGELES"
LRO:LOLA_DEM_VERS           = "1.0"
LRO:DLRE_GEOM_VERSION_ID    = "1.0"
LRO:CALIBRATION_SOFTWARE_VER_ID = "4.1"
LRO:DLRE_JDATE_MIN          = 2456036.459697
LRO:DLRE_JDATE_MAX          = 2456063.762061
LRO:DLRE_CLOCTIME_MIN       = 6.0000
LRO:DLRE_CLOCTIME_MAX       = 18.0000
MINIMUM_WAVELENGTH          = 0.35 <micron>
MAXIMUM_WAVELENGTH          = 400.0 <micron>


DESCRIPTION               = "

Each sample represents the average Julian Date for
all channels, scaled by the value of SCALING_FACTOR.
Conversion from Digital Number (DN) to average
is given by the equation:

TB = (DN * SCALING_FACTOR) + OFFSET

Data is derived from Diviner nadir only data. The effective
field of view for each data point is determined with a 2D
Monte Carlo routine that accounts for the in-track and
cross-track instantaneous field of view of the detectors,
as the detector response and the integration time smearing
results from spacecraft motion in the in-track direction.
Bins are then weighted appropriately where there is detector
overlap. Each map cycle start and stop time is selected to
correspond to 180 and -180 degrees longitude. LRO orbits
progress from 180 degrees longitude to -180 degrees longitude
during that time period resulting in a drift in local time
across each map.

"

OBJECT                    = UNCOMPRESSED_FILE
```

```
FILE_NAME                = "DGDR_JD_AVG_CYL_20120418D_128_JP2.JP2"
RECORD_TYPE              = FIXED_LENGTH
FILE_RECORDS             = 23040
RECORD_BYTES             = 92160
^IMAGE                   = "DGDR_JD_AVG_CYL_20120418D_128_JP2.JP2"


 OBJECT                  = IMAGE
  NAME                   = "JULIAN DATE"
  LINES                  = 23040
  LINE_SAMPLES           = 46080
  SAMPLE_TYPE            = LSB_INTEGER
  SAMPLE_BITS            = 16
  UNIT                   = DAYS
  SCALING_FACTOR         = 0.011296333
  OFFSET                 = 2455818.0
  DERIVED_MINIMUM             = 2456035.5
  DERIVED_MAXIMUM             = 2456064.5
  MISSING_CONSTANT       = -32768
 END_OBJECT              = IMAGE

END_OBJECT               = UNCOMPRESSED_FILE

OBJECT                   = IMAGE_MAP_PROJECTION
 ^DATA_SET_MAP_PROJECTION     = "DSMAP.CAT"
 MAP_PROJECTION_TYPE          = "SIMPLE CYLINDRICAL"
 KEYWORD_LATITUDE_TYPE        = "PLANETOCENTRIC"
 MAP_RESOLUTION               = 128 <pix/degree>
 A_AXIS_RADIUS                = 1737.4 <km>
 B_AXIS_RADIUS                = 1737.4 <km>
 C_AXIS_RADIUS                = 1737.4 <km>
 FIRST_STANDARD_PARALLEL      = 'N/A'
 SECOND_STANDARD_PARALLEL     = 'N/A'
 POSITIVE_LONGITUDE_DIRECTION = "EAST"
 CENTER_LATITUDE              = 0.0 <deg>
 CENTER_LONGITUDE             = 0.0 <deg>
 REFERENCE_LATITUDE           = 'N/A'
 REFERENCE_LONGITUDE          = 'N/A'
 LINE_FIRST_PIXEL             = 1
 LINE_LAST_PIXEL              = 23040
 SAMPLE_FIRST_PIXEL           = 1
 SAMPLE_LAST_PIXEL            = 46080
 MAP_PROJECTION_ROTATION      = 0.0
 MAP_SCALE                    = 236.901175 <m/pix>
 MAXIMUM_LATITUDE             = 90 <deg>
 MINIMUM_LATITUDE             = -90 <deg>
 WESTERNMOST_LONGITUDE        = -180.0 <deg>
 EASTERNMOST_LONGITUDE        = 180.0 <deg>
 LINE_PROJECTION_OFFSET       = 11519.5 <pixel>
 SAMPLE_PROJECTION_OFFSET     = 23039.5 <pixel>
 COORDINATE_SYSTEM_TYPE       = "BODY-FIXED ROTATING"
 COORDINATE_SYSTEM_NAME       = "MEAN EARTH/POLAR AXIS OF DE421"
END_OBJECT                   = IMAGE_MAP_PROJECTION
```

```
END
```

```
PDS_VERSION_ID            = "PDS3"

PRODUCT_VERSION_ID        = "V4.1"
DATA_SET_ID               = "LRO-L-DLRE-5-GDR-V1.0"
PRODUCT_ID                = "DGDR_JD_AVG_CYL_20120502N_128_JP2.JP2"
SOURCE_PRODUCT_ID         = "DGDR_JD_AVG_CYL_20120502N_128_IMG.IMG"
INSTRUMENT_HOST_NAME      = "LUNAR RECONNAISSANCE ORBITER"
INSTRUMENT_HOST_ID        = "LRO"
INSTRUMENT_NAME           = "DIVINER LUNAR RADIOMETER EXPERIMENT"
INSTRUMENT_ID             = "DLRE"
MISSION_PHASE_NAME        = {"NOMINAL MISSION"}
TARGET_NAME               = MOON
START_TIME                = 2012-05-02T11:00:00.000
STOP_TIME                 = 2012-05-29T18:00:00.000
PRODUCT_CREATION_TIME     = 2013-01-07T03:44:41.000
PRODUCER_ID               = LRO_DLRE_TEAM
PRODUCER_FULL_NAME        = "DAVID A. PAIGE"
PRODUCER_INSTITUTION_NAME = "UNIVERSITY OF CALIFORNIA, LOS ANGELES"
LRO:LOLA_DEM_VERS           = "1.0"
LRO:DLRE_GEOM_VERSION_ID    = "1.0"
LRO:CALIBRATION_SOFTWARE_VER_ID = "4.1"
LRO:DLRE_JDATE_MIN          = 2456049.988785
LRO:DLRE_JDATE_MAX          = 2456077.291307
LRO:DLRE_CLOCTIME_MIN       = 18.0000
LRO:DLRE_CLOCTIME_MAX       = 6.0000
MINIMUM_WAVELENGTH          = 0.35 <micron>
MAXIMUM_WAVELENGTH          = 400.0 <micron>


DESCRIPTION               = "

Each sample represents the average Julian Date for
all channels, scaled by the value of SCALING_FACTOR.
Conversion from Digital Number (DN) to average
is given by the equation:

TB = (DN * SCALING_FACTOR) + OFFSET

Data is derived from Diviner nadir only data. The effective
field of view for each data point is determined with a 2D
Monte Carlo routine that accounts for the in-track and
cross-track instantaneous field of view of the detectors,
as the detector response and the integration time smearing
results from spacecraft motion in the in-track direction.
Bins are then weighted appropriately where there is detector
overlap. Each map cycle start and stop time is selected to
correspond to 180 and -180 degrees longitude. LRO orbits
progress from 180 degrees longitude to -180 degrees longitude
during that time period resulting in a drift in local time
across each map.

"

OBJECT                    = UNCOMPRESSED_FILE
```

```
FILE_NAME                = "DGDR_JD_AVG_CYL_20120502N_128_JP2.JP2"
RECORD_TYPE              = FIXED_LENGTH
FILE_RECORDS             = 23040
RECORD_BYTES             = 92160
^IMAGE                   = "DGDR_JD_AVG_CYL_20120502N_128_JP2.JP2"


 OBJECT                  = IMAGE
  NAME                   = "JULIAN DATE"
  LINES                  = 23040
  LINE_SAMPLES           = 46080
  SAMPLE_TYPE            = LSB_INTEGER
  SAMPLE_BITS            = 16
  UNIT                   = DAYS
  SCALING_FACTOR         = 0.011296333
  OFFSET                 = 2455818.0
  DERIVED_MINIMUM             = 2456049
  DERIVED_MAXIMUM             = 2456078.25
  MISSING_CONSTANT       = -32768
 END_OBJECT              = IMAGE

END_OBJECT               = UNCOMPRESSED_FILE

OBJECT                   = IMAGE_MAP_PROJECTION
 ^DATA_SET_MAP_PROJECTION     = "DSMAP.CAT"
 MAP_PROJECTION_TYPE          = "SIMPLE CYLINDRICAL"
 KEYWORD_LATITUDE_TYPE        = "PLANETOCENTRIC"
 MAP_RESOLUTION               = 128 <pix/degree>
 A_AXIS_RADIUS                = 1737.4 <km>
 B_AXIS_RADIUS                = 1737.4 <km>
 C_AXIS_RADIUS                = 1737.4 <km>
 FIRST_STANDARD_PARALLEL      = 'N/A'
 SECOND_STANDARD_PARALLEL     = 'N/A'
 POSITIVE_LONGITUDE_DIRECTION = "EAST"
 CENTER_LATITUDE              = 0.0 <deg>
 CENTER_LONGITUDE             = 0.0 <deg>
 REFERENCE_LATITUDE           = 'N/A'
 REFERENCE_LONGITUDE          = 'N/A'
 LINE_FIRST_PIXEL             = 1
 LINE_LAST_PIXEL              = 23040
 SAMPLE_FIRST_PIXEL           = 1
 SAMPLE_LAST_PIXEL            = 46080
 MAP_PROJECTION_ROTATION      = 0.0
 MAP_SCALE                    = 236.901175 <m/pix>
 MAXIMUM_LATITUDE             = 90 <deg>
 MINIMUM_LATITUDE             = -90 <deg>
 WESTERNMOST_LONGITUDE        = -180.0 <deg>
 EASTERNMOST_LONGITUDE        = 180.0 <deg>
 LINE_PROJECTION_OFFSET       = 11519.5 <pixel>
 SAMPLE_PROJECTION_OFFSET     = 23039.5 <pixel>
 COORDINATE_SYSTEM_TYPE       = "BODY-FIXED ROTATING"
 COORDINATE_SYSTEM_NAME       = "MEAN EARTH/POLAR AXIS OF DE421"
END_OBJECT                   = IMAGE_MAP_PROJECTION
```

```
END
```

```
PDS_VERSION_ID            = "PDS3"

PRODUCT_VERSION_ID        = "V4.1"
DATA_SET_ID               = "LRO-L-DLRE-5-GDR-V1.0"
PRODUCT_ID                = "DGDR_JD_AVG_CYL_20120723D_128_JP2.JP2"
SOURCE_PRODUCT_ID         = "DGDR_JD_AVG_CYL_20120723D_128_IMG.IMG"
INSTRUMENT_HOST_NAME      = "LUNAR RECONNAISSANCE ORBITER"
INSTRUMENT_HOST_ID        = "LRO"
INSTRUMENT_NAME           = "DIVINER LUNAR RADIOMETER EXPERIMENT"
INSTRUMENT_ID             = "DLRE"
MISSION_PHASE_NAME        = {"NOMINAL MISSION"}
TARGET_NAME               = MOON
START_TIME                = 2012-07-23T10:00:00.000
STOP_TIME                 = 2012-08-19T15:00:00.000
PRODUCT_CREATION_TIME     = 2013-01-10T19:55:18.000
PRODUCER_ID               = LRO_DLRE_TEAM
PRODUCER_FULL_NAME        = "DAVID A. PAIGE"
PRODUCER_INSTITUTION_NAME = "UNIVERSITY OF CALIFORNIA, LOS ANGELES"
LRO:LOLA_DEM_VERS           = "1.0"
LRO:DLRE_GEOM_VERSION_ID    = "1.0"
LRO:CALIBRATION_SOFTWARE_VER_ID = "4.1"
LRO:DLRE_JDATE_MIN          = 2456131.955511
LRO:DLRE_JDATE_MAX          = 2456159.163566
LRO:DLRE_CLOCTIME_MIN       = 6.0000
LRO:DLRE_CLOCTIME_MAX       = 18.0000
MINIMUM_WAVELENGTH          = 0.35 <micron>
MAXIMUM_WAVELENGTH          = 400.0 <micron>


DESCRIPTION               = "

Each sample represents the average Julian Date for
all channels, scaled by the value of SCALING_FACTOR.
Conversion from Digital Number (DN) to average
is given by the equation:

TB = (DN * SCALING_FACTOR) + OFFSET

Data is derived from Diviner nadir only data. The effective
field of view for each data point is determined with a 2D
Monte Carlo routine that accounts for the in-track and
cross-track instantaneous field of view of the detectors,
as the detector response and the integration time smearing
results from spacecraft motion in the in-track direction.
Bins are then weighted appropriately where there is detector
overlap. Each map cycle start and stop time is selected to
correspond to 180 and -180 degrees longitude. LRO orbits
progress from 180 degrees longitude to -180 degrees longitude
during that time period resulting in a drift in local time
across each map.

"

OBJECT                    = UNCOMPRESSED_FILE
```

```
FILE_NAME                = "DGDR_JD_AVG_CYL_20120723D_128_JP2.JP2"
RECORD_TYPE              = FIXED_LENGTH
FILE_RECORDS             = 23040
RECORD_BYTES             = 92160
^IMAGE                   = "DGDR_JD_AVG_CYL_20120723D_128_JP2.JP2"


 OBJECT                  = IMAGE
  NAME                   = "JULIAN DATE"
  LINES                  = 23040
  LINE_SAMPLES           = 46080
  SAMPLE_TYPE            = LSB_INTEGER
  SAMPLE_BITS            = 16
  UNIT                   = DAYS
  SCALING_FACTOR         = 0.011296333
  OFFSET                 = 2455818.0
  DERIVED_MINIMUM             = 2456131
  DERIVED_MAXIMUM             = 2456160
  MISSING_CONSTANT       = -32768
 END_OBJECT              = IMAGE

END_OBJECT               = UNCOMPRESSED_FILE

OBJECT                   = IMAGE_MAP_PROJECTION
 ^DATA_SET_MAP_PROJECTION     = "DSMAP.CAT"
 MAP_PROJECTION_TYPE          = "SIMPLE CYLINDRICAL"
 KEYWORD_LATITUDE_TYPE        = "PLANETOCENTRIC"
 MAP_RESOLUTION               = 128 <pix/degree>
 A_AXIS_RADIUS                = 1737.4 <km>
 B_AXIS_RADIUS                = 1737.4 <km>
 C_AXIS_RADIUS                = 1737.4 <km>
 FIRST_STANDARD_PARALLEL      = 'N/A'
 SECOND_STANDARD_PARALLEL     = 'N/A'
 POSITIVE_LONGITUDE_DIRECTION = "EAST"
 CENTER_LATITUDE              = 0.0 <deg>
 CENTER_LONGITUDE             = 0.0 <deg>
 REFERENCE_LATITUDE           = 'N/A'
 REFERENCE_LONGITUDE          = 'N/A'
 LINE_FIRST_PIXEL             = 1
 LINE_LAST_PIXEL              = 23040
 SAMPLE_FIRST_PIXEL           = 1
 SAMPLE_LAST_PIXEL            = 46080
 MAP_PROJECTION_ROTATION      = 0.0
 MAP_SCALE                    = 236.901175 <m/pix>
 MAXIMUM_LATITUDE             = 90 <deg>
 MINIMUM_LATITUDE             = -90 <deg>
 WESTERNMOST_LONGITUDE        = -180.0 <deg>
 EASTERNMOST_LONGITUDE        = 180.0 <deg>
 LINE_PROJECTION_OFFSET       = 11519.5 <pixel>
 SAMPLE_PROJECTION_OFFSET     = 23039.5 <pixel>
 COORDINATE_SYSTEM_TYPE       = "BODY-FIXED ROTATING"
 COORDINATE_SYSTEM_NAME       = "MEAN EARTH/POLAR AXIS OF DE421"
END_OBJECT                   = IMAGE_MAP_PROJECTION
```

```
END
```

```
PDS_VERSION_ID            = "PDS3"

PRODUCT_VERSION_ID        = "V4.1"
DATA_SET_ID               = "LRO-L-DLRE-5-GDR-V1.0"
PRODUCT_ID                = "DGDR_JD_AVG_CYL_20120806N_128_JP2.JP2"
SOURCE_PRODUCT_ID         = "DGDR_JD_AVG_CYL_20120806N_128_IMG.IMG"
INSTRUMENT_HOST_NAME      = "LUNAR RECONNAISSANCE ORBITER"
INSTRUMENT_HOST_ID        = "LRO"
INSTRUMENT_NAME           = "DIVINER LUNAR RADIOMETER EXPERIMENT"
INSTRUMENT_ID             = "DLRE"
MISSION_PHASE_NAME        = {"NOMINAL MISSION"}
TARGET_NAME               = MOON
START_TIME                = 2012-08-06T01:00:00.000
STOP_TIME                 = 2012-09-02T08:00:00.000
PRODUCT_CREATION_TIME     = 2013-01-11T12:42:46.000
PRODUCER_ID               = LRO_DLRE_TEAM
PRODUCER_FULL_NAME        = "DAVID A. PAIGE"
PRODUCER_INSTITUTION_NAME = "UNIVERSITY OF CALIFORNIA, LOS ANGELES"
LRO:LOLA_DEM_VERS           = "1.0"
LRO:DLRE_GEOM_VERSION_ID    = "1.0"
LRO:CALIBRATION_SOFTWARE_VER_ID = "4.1"
LRO:DLRE_JDATE_MIN          = 2456145.557515
LRO:DLRE_JDATE_MAX          = 2456172.847033
LRO:DLRE_CLOCTIME_MIN       = 18.0000
LRO:DLRE_CLOCTIME_MAX       = 6.0000
MINIMUM_WAVELENGTH          = 0.35 <micron>
MAXIMUM_WAVELENGTH          = 400.0 <micron>


DESCRIPTION               = "

Each sample represents the average Julian Date for
all channels, scaled by the value of SCALING_FACTOR.
Conversion from Digital Number (DN) to average
is given by the equation:

TB = (DN * SCALING_FACTOR) + OFFSET

Data is derived from Diviner nadir only data. The effective
field of view for each data point is determined with a 2D
Monte Carlo routine that accounts for the in-track and
cross-track instantaneous field of view of the detectors,
as the detector response and the integration time smearing
results from spacecraft motion in the in-track direction.
Bins are then weighted appropriately where there is detector
overlap. Each map cycle start and stop time is selected to
correspond to 180 and -180 degrees longitude. LRO orbits
progress from 180 degrees longitude to -180 degrees longitude
during that time period resulting in a drift in local time
across each map.

"

OBJECT                    = UNCOMPRESSED_FILE
```

```
FILE_NAME                = "DGDR_JD_AVG_CYL_20120806N_128_JP2.JP2"
RECORD_TYPE              = FIXED_LENGTH
FILE_RECORDS             = 23040
RECORD_BYTES             = 92160
^IMAGE                   = "DGDR_JD_AVG_CYL_20120806N_128_JP2.JP2"


 OBJECT                  = IMAGE
  NAME                   = "JULIAN DATE"
  LINES                  = 23040
  LINE_SAMPLES           = 46080
  SAMPLE_TYPE            = LSB_INTEGER
  SAMPLE_BITS            = 16
  UNIT                   = DAYS
  SCALING_FACTOR         = 0.011296333
  OFFSET                 = 2455818.0
  DERIVED_MINIMUM             = 2456144.5
  DERIVED_MAXIMUM             = 2456173.75
  MISSING_CONSTANT       = -32768
 END_OBJECT              = IMAGE

END_OBJECT               = UNCOMPRESSED_FILE

OBJECT                   = IMAGE_MAP_PROJECTION
 ^DATA_SET_MAP_PROJECTION     = "DSMAP.CAT"
 MAP_PROJECTION_TYPE          = "SIMPLE CYLINDRICAL"
 KEYWORD_LATITUDE_TYPE        = "PLANETOCENTRIC"
 MAP_RESOLUTION               = 128 <pix/degree>
 A_AXIS_RADIUS                = 1737.4 <km>
 B_AXIS_RADIUS                = 1737.4 <km>
 C_AXIS_RADIUS                = 1737.4 <km>
 FIRST_STANDARD_PARALLEL      = 'N/A'
 SECOND_STANDARD_PARALLEL     = 'N/A'
 POSITIVE_LONGITUDE_DIRECTION = "EAST"
 CENTER_LATITUDE              = 0.0 <deg>
 CENTER_LONGITUDE             = 0.0 <deg>
 REFERENCE_LATITUDE           = 'N/A'
 REFERENCE_LONGITUDE          = 'N/A'
 LINE_FIRST_PIXEL             = 1
 LINE_LAST_PIXEL              = 23040
 SAMPLE_FIRST_PIXEL           = 1
 SAMPLE_LAST_PIXEL            = 46080
 MAP_PROJECTION_ROTATION      = 0.0
 MAP_SCALE                    = 236.901175 <m/pix>
 MAXIMUM_LATITUDE             = 90 <deg>
 MINIMUM_LATITUDE             = -90 <deg>
 WESTERNMOST_LONGITUDE        = -180.0 <deg>
 EASTERNMOST_LONGITUDE        = 180.0 <deg>
 LINE_PROJECTION_OFFSET       = 11519.5 <pixel>
 SAMPLE_PROJECTION_OFFSET     = 23039.5 <pixel>
 COORDINATE_SYSTEM_TYPE       = "BODY-FIXED ROTATING"
 COORDINATE_SYSTEM_NAME       = "MEAN EARTH/POLAR AXIS OF DE421"
END_OBJECT                   = IMAGE_MAP_PROJECTION
```

```
END
```

```
PDS_VERSION_ID            = "PDS3"

PRODUCT_VERSION_ID        = "V4.1"
DATA_SET_ID               = "LRO-L-DLRE-5-GDR-V1.0"
PRODUCT_ID                = "DGDR_VB1_AVG_CYL_20120418D_128_JP2.JP2"
SOURCE_PRODUCT_ID         = "DGDR_VB1_AVG_CYL_20120418D_128_IMG.IMG"
INSTRUMENT_HOST_NAME      = "LUNAR RECONNAISSANCE ORBITER"
INSTRUMENT_HOST_ID        = "LRO"
INSTRUMENT_NAME           = "DIVINER LUNAR RADIOMETER EXPERIMENT"
INSTRUMENT_ID             = "DLRE"
MISSION_PHASE_NAME        = {"NOMINAL MISSION"}
TARGET_NAME               = MOON
START_TIME                = 2012-04-18T23:00:00.000
STOP_TIME                 = 2012-05-16T06:00:00.000
PRODUCT_CREATION_TIME     = 2013-01-06T10:13:32.000
PRODUCER_ID               = LRO_DLRE_TEAM
PRODUCER_FULL_NAME        = "DAVID A. PAIGE"
PRODUCER_INSTITUTION_NAME = "UNIVERSITY OF CALIFORNIA, LOS ANGELES"
LRO:LOLA_DEM_VERS           = "1.0"
LRO:DLRE_GEOM_VERSION_ID    = "1.0"
LRO:CALIBRATION_SOFTWARE_VER_ID = "4.1"
LRO:DLRE_JDATE_MIN          = 2456036.459697
LRO:DLRE_JDATE_MAX          = 2456063.762061
LRO:DLRE_CLOCTIME_MIN       = 6.0000
LRO:DLRE_CLOCTIME_MAX       = 18.0000
MINIMUM_WAVELENGTH          = 0.35 <micron>
MAXIMUM_WAVELENGTH          = 2.80 <micron>


DESCRIPTION               = "

Each sample represents the Visual Brightness (VB) for
Channel 1, scaled by the value of SCALING_FACTOR.
Conversion from Digital Number (DN) to average
is given by the equation:

TB = (DN * SCALING_FACTOR) + OFFSET

Data is derived from Diviner nadir only data. The effective
field of view for each data point is determined with a 2D
Monte Carlo routine that accounts for the in-track and
cross-track instantaneous field of view of the detectors,
as the detector response and the integration time smearing
results from spacecraft motion in the in-track direction.
Bins are then weighted appropriately where there is detector
overlap. Each map cycle start and stop time is selected to
correspond to 180 and -180 degrees longitude. LRO orbits
progress from 180 degrees longitude to -180 degrees longitude
during that time period resulting in a drift in local time
across each map.

"

OBJECT                    = UNCOMPRESSED_FILE
```

```
FILE_NAME                = "DGDR_VB1_AVG_CYL_20120418D_128_JP2.JP2"
RECORD_TYPE              = FIXED_LENGTH
FILE_RECORDS             = 23040
RECORD_BYTES             = 92160
^IMAGE                   = "DGDR_VB1_AVG_CYL_20120418D_128_JP2.JP2"


 OBJECT                  = IMAGE
  NAME                   = "VISUAL BRIGHTNESS CHANNEL 1"
  LINES                  = 23040
  LINE_SAMPLES           = 46080
  SAMPLE_TYPE            = LSB_INTEGER
  SAMPLE_BITS            = 16
  UNIT                   = NORMALIZED_RADIANCE
  SCALING_FACTOR         = 0.0001
  OFFSET                 = 0.
  DERIVED_MINIMUM             = -.00035678946971900000
  DERIVED_MAXIMUM             = .25862271118200000000
  MISSING_CONSTANT       = -32768
 END_OBJECT              = IMAGE

END_OBJECT               = UNCOMPRESSED_FILE

OBJECT                   = IMAGE_MAP_PROJECTION
 ^DATA_SET_MAP_PROJECTION     = "DSMAP.CAT"
 MAP_PROJECTION_TYPE          = "SIMPLE CYLINDRICAL"
 KEYWORD_LATITUDE_TYPE        = "PLANETOCENTRIC"
 MAP_RESOLUTION               = 128 <pix/degree>
 A_AXIS_RADIUS                = 1737.4 <km>
 B_AXIS_RADIUS                = 1737.4 <km>
 C_AXIS_RADIUS                = 1737.4 <km>
 FIRST_STANDARD_PARALLEL      = 'N/A'
 SECOND_STANDARD_PARALLEL     = 'N/A'
 POSITIVE_LONGITUDE_DIRECTION = "EAST"
 CENTER_LATITUDE              = 0.0 <deg>
 CENTER_LONGITUDE             = 0.0 <deg>
 REFERENCE_LATITUDE           = 'N/A'
 REFERENCE_LONGITUDE          = 'N/A'
 LINE_FIRST_PIXEL             = 1
 LINE_LAST_PIXEL              = 23040
 SAMPLE_FIRST_PIXEL           = 1
 SAMPLE_LAST_PIXEL            = 46080
 MAP_PROJECTION_ROTATION      = 0.0
 MAP_SCALE                    = 236.901175 <m/pix>
 MAXIMUM_LATITUDE             = 90 <deg>
 MINIMUM_LATITUDE             = -90 <deg>
 WESTERNMOST_LONGITUDE        = -180.0 <deg>
 EASTERNMOST_LONGITUDE        = 180.0 <deg>
 LINE_PROJECTION_OFFSET       = 11519.5 <pixel>
 SAMPLE_PROJECTION_OFFSET     = 23039.5 <pixel>
 COORDINATE_SYSTEM_TYPE       = "BODY-FIXED ROTATING"
 COORDINATE_SYSTEM_NAME       = "MEAN EARTH/POLAR AXIS OF DE421"
END_OBJECT                   = IMAGE_MAP_PROJECTION
```

```
END
```

```
PDS_VERSION_ID            = "PDS3"

PRODUCT_VERSION_ID        = "V4.1"
DATA_SET_ID               = "LRO-L-DLRE-5-GDR-V1.0"
PRODUCT_ID                = "DGDR_VB1_AVG_CYL_20120723D_128_JP2.JP2"
SOURCE_PRODUCT_ID         = "DGDR_VB1_AVG_CYL_20120723D_128_IMG.IMG"
INSTRUMENT_HOST_NAME      = "LUNAR RECONNAISSANCE ORBITER"
INSTRUMENT_HOST_ID        = "LRO"
INSTRUMENT_NAME           = "DIVINER LUNAR RADIOMETER EXPERIMENT"
INSTRUMENT_ID             = "DLRE"
MISSION_PHASE_NAME        = {"NOMINAL MISSION"}
TARGET_NAME               = MOON
START_TIME                = 2012-07-23T10:00:00.000
STOP_TIME                 = 2012-08-19T15:00:00.000
PRODUCT_CREATION_TIME     = 2013-01-10T18:25:18.000
PRODUCER_ID               = LRO_DLRE_TEAM
PRODUCER_FULL_NAME        = "DAVID A. PAIGE"
PRODUCER_INSTITUTION_NAME = "UNIVERSITY OF CALIFORNIA, LOS ANGELES"
LRO:LOLA_DEM_VERS           = "1.0"
LRO:DLRE_GEOM_VERSION_ID    = "1.0"
LRO:CALIBRATION_SOFTWARE_VER_ID = "4.1"
LRO:DLRE_JDATE_MIN          = 2456131.955511
LRO:DLRE_JDATE_MAX          = 2456159.163566
LRO:DLRE_CLOCTIME_MIN       = 6.0000
LRO:DLRE_CLOCTIME_MAX       = 18.0000
MINIMUM_WAVELENGTH          = 0.35 <micron>
MAXIMUM_WAVELENGTH          = 2.80 <micron>


DESCRIPTION               = "

Each sample represents the Visual Brightness (VB) for
Channel 1, scaled by the value of SCALING_FACTOR.
Conversion from Digital Number (DN) to average
is given by the equation:

TB = (DN * SCALING_FACTOR) + OFFSET

Data is derived from Diviner nadir only data. The effective
field of view for each data point is determined with a 2D
Monte Carlo routine that accounts for the in-track and
cross-track instantaneous field of view of the detectors,
as the detector response and the integration time smearing
results from spacecraft motion in the in-track direction.
Bins are then weighted appropriately where there is detector
overlap. Each map cycle start and stop time is selected to
correspond to 180 and -180 degrees longitude. LRO orbits
progress from 180 degrees longitude to -180 degrees longitude
during that time period resulting in a drift in local time
across each map.

"

OBJECT                    = UNCOMPRESSED_FILE
```

```
FILE_NAME                = "DGDR_VB1_AVG_CYL_20120723D_128_JP2.JP2"
RECORD_TYPE              = FIXED_LENGTH
FILE_RECORDS             = 23040
RECORD_BYTES             = 92160
^IMAGE                   = "DGDR_VB1_AVG_CYL_20120723D_128_JP2.JP2"


 OBJECT                  = IMAGE
  NAME                   = "VISUAL BRIGHTNESS CHANNEL 1"
  LINES                  = 23040
  LINE_SAMPLES           = 46080
  SAMPLE_TYPE            = LSB_INTEGER
  SAMPLE_BITS            = 16
  UNIT                   = NORMALIZED_RADIANCE
  SCALING_FACTOR         = 0.0001
  OFFSET                 = 0.
  DERIVED_MINIMUM             = -.05474074935910000000
  DERIVED_MAXIMUM             = .26420046997100000000
  MISSING_CONSTANT       = -32768
 END_OBJECT              = IMAGE

END_OBJECT               = UNCOMPRESSED_FILE

OBJECT                   = IMAGE_MAP_PROJECTION
 ^DATA_SET_MAP_PROJECTION     = "DSMAP.CAT"
 MAP_PROJECTION_TYPE          = "SIMPLE CYLINDRICAL"
 KEYWORD_LATITUDE_TYPE        = "PLANETOCENTRIC"
 MAP_RESOLUTION               = 128 <pix/degree>
 A_AXIS_RADIUS                = 1737.4 <km>
 B_AXIS_RADIUS                = 1737.4 <km>
 C_AXIS_RADIUS                = 1737.4 <km>
 FIRST_STANDARD_PARALLEL      = 'N/A'
 SECOND_STANDARD_PARALLEL     = 'N/A'
 POSITIVE_LONGITUDE_DIRECTION = "EAST"
 CENTER_LATITUDE              = 0.0 <deg>
 CENTER_LONGITUDE             = 0.0 <deg>
 REFERENCE_LATITUDE           = 'N/A'
 REFERENCE_LONGITUDE          = 'N/A'
 LINE_FIRST_PIXEL             = 1
 LINE_LAST_PIXEL              = 23040
 SAMPLE_FIRST_PIXEL           = 1
 SAMPLE_LAST_PIXEL            = 46080
 MAP_PROJECTION_ROTATION      = 0.0
 MAP_SCALE                    = 236.901175 <m/pix>
 MAXIMUM_LATITUDE             = 90 <deg>
 MINIMUM_LATITUDE             = -90 <deg>
 WESTERNMOST_LONGITUDE        = -180.0 <deg>
 EASTERNMOST_LONGITUDE        = 180.0 <deg>
 LINE_PROJECTION_OFFSET       = 11519.5 <pixel>
 SAMPLE_PROJECTION_OFFSET     = 23039.5 <pixel>
 COORDINATE_SYSTEM_TYPE       = "BODY-FIXED ROTATING"
 COORDINATE_SYSTEM_NAME       = "MEAN EARTH/POLAR AXIS OF DE421"
END_OBJECT                   = IMAGE_MAP_PROJECTION
```

```
END
```

```
PDS_VERSION_ID           = "PDS3"

/*** This label describes a compressed image file, its corresponding XML
*/
/*** file, and map projection information.
*/
/*** The files described have the same name as this label but different
*/
/*** extensions. They are:
*/
/***    .JP2 - A compressed image file corresponding to the uncompressed
IMG*/
/***           file, stored with JPEG2000 compression
*/
/***    .XML - An auxiliary text file in XML, provided to aid display of
*/
/***           the JPEG2000 image with certain image processing software
*/
/*** The map projection information includes parameters that are specific
*/
/*** to this image. They are intended to be used with the general map
*/
/*** projection descriptions in the file indicated by the keyword
*/
/*** ^DATA_SET_MAP_PROJECTION. That file is found in the CATALOG
directory  */
/*** of this archive.
*/

/*** GENERAL DATA DESCRIPTION PARAMETERS ***/
PRODUCT_VERSION_ID        = "V2.0"
DATA_SET_ID               = "LRO-L-LOLA-4-GDR-V1.0"
PRODUCT_ID                = "LDEM_128"
INSTRUMENT_HOST_NAME      = "LUNAR RECONNAISSANCE ORBITER"
INSTRUMENT_NAME           = "LUNAR ORBITER LASER ALTIMETER"
INSTRUMENT_ID             = "LOLA"
MISSION_PHASE_NAME        = {"COMMISSIONING","NOMINAL MISSION","SCIENCE
                            MISSION","EXTENDED SCIENCE MISSION"}
TARGET_NAME               = MOON
START_TIME                = 2009-07-13T17:33:17.246
STOP_TIME                 = 2014-06-10T00:10:56
PRODUCT_CREATION_TIME     = 2014-09-15T00:00:00
PRODUCER_ID               = LRO_LOLA_TEAM
PRODUCER_FULL_NAME        = "DAVID E. SMITH"
PRODUCER_INSTITUTION_NAME = "GODDARD SPACE FLIGHT CENTER"
DESCRIPTION               = "This data product is a shape map (radius)
   of the Moon at a resolution of 128 pix/deg by 128 pix/deg,
   based on altimetry data acquired through mission phase LRO_ES_21
   by the LOLA instrument. The preliminary LOLA data are the source for
   this data set. The ground tracks were interpolated using the Generic
   Mapping Tools programs 'surface' and 'grdblend'.  The map is in
   the form of a binary table with one row for each
   0.0078125 degrees of latitude, pixel registered.  Map values
   are relative to a radius of 1737.4 km.
```

```
   This label describes two objects.  The first is a JP2 file of
   the corresponding uncompressed .IMG file.  A jpeg 2000 compression
   is used to render the image.  The second is an auxiliary xml file
   that contains extensible markup language that is interpreted by
   GDAL readers (www.gdal.org).

"

OBJECT                    = COMPRESSED_FILE
FILE_NAME                 = "LDEM_128.JP2"
  RECORD_TYPE             = UNDEFINED
  FILE_RECORDS            = UNK
  ENCODING_TYPE           = "JP2"
  INTERCHANGE_FORMAT      = BINARY
  UNIT                    = METER
  SCALING_FACTOR          = 0.5
  OFFSET                  = 1737400.
  UNCOMPRESSED_FILE_NAME  = "LDEM_128.IMG"
  REQUIRED_STORAGE_BYTES  = "2123366400"
  ^DESCRIPTION            = "JP2INFO.TXT"
END_OBJECT                = COMPRESSED_FILE

OBJECT                    = UNCOMPRESSED_FILE
FILE_NAME                 = "LDEM_128.IMG"
RECORD_TYPE               = FIXED_LENGTH
FILE_RECORDS              = 23040
RECORD_BYTES              = 92160
^IMAGE                    = "LDEM_128.IMG"


  OBJECT                  = IMAGE
    NAME                  = HEIGHT
    DESCRIPTION           = "Each sample represents height relative to a
      reference radius (OFFSET) and is generated using preliminary LOLA
data
      produced by the LOLA team."
    LINES                 = 23040
    LINE_SAMPLES          = 46080
    MAXIMUM               = 21555
    MINIMUM               = -18254
    SAMPLE_TYPE           = LSB_INTEGER
    SAMPLE_BITS           = 16
    UNIT                  = METER
    SCALING_FACTOR        = 0.5
    OFFSET                = 1737400.

/* NOTE:
*/
/* Conversion from Digital Number to HEIGHT, i.e. elevation in meters,
is: */
/* HEIGHT = (DN * SCALING_FACTOR).
*/
```

```
/* The conversion from Digital Number to PLANETARY_RADIUS in meters is:
*/
/* PLANETARY_RADIUS = (DN * SCALING_FACTOR) + OFFSET
*/
/* where OFFSET is the radius of a reference sphere.
*/
/* The planetopotential TOPOGRAPHY is PLANETARY_RADIUS - GEOID_RADIUS,
*/
/* where GEOID_RADIUS is derived from a gravitational equipotential
model. */
/* By convention, the average GEOID_RADIUS at the equator is OFFSET.
*/

  END_OBJECT              = IMAGE
END_OBJECT                = UNCOMPRESSED_FILE

OBJECT                    = AUX_FILE
  FILE_NAME               = "LDEM_128_AUX.XML"
  RECORD_TYPE             = STREAM
  FILE_RECORDS            = UNK
  DESCRIPTION             = "This is an auxiliary file accompanying
     the JPEG2000 file. It contains metadata in XML format that
     is useful for displaying the image using a GDAL supported tool."
END_OBJECT                = AUX_FILE
OBJECT                    = IMAGE_MAP_PROJECTION
 ^DATA_SET_MAP_PROJECTION     = "DSMAP.CAT"
 MAP_PROJECTION_TYPE          = "SIMPLE CYLINDRICAL"
 MAP_RESOLUTION               = 128 <pix/deg>
 A_AXIS_RADIUS                = 1737.4 <km>
 B_AXIS_RADIUS                = 1737.4 <km>
 C_AXIS_RADIUS                = 1737.4 <km>
 FIRST_STANDARD_PARALLEL      = 'N/A'
 SECOND_STANDARD_PARALLEL     = 'N/A'
 POSITIVE_LONGITUDE_DIRECTION = "EAST"
 CENTER_LATITUDE              = 0. <deg>
 CENTER_LONGITUDE             = 0. <deg>
 REFERENCE_LATITUDE           = 'N/A'
 REFERENCE_LONGITUDE          = 'N/A'
 LINE_FIRST_PIXEL             = 1
 LINE_LAST_PIXEL              = 23040
 SAMPLE_FIRST_PIXEL           = 1
 SAMPLE_LAST_PIXEL            = 46080
 MAP_PROJECTION_ROTATION      = 0.0
 MAP_SCALE                    = 0.2369011752 <km/pix>
 MAXIMUM_LATITUDE             = 90 <deg>
 MINIMUM_LATITUDE             = -90 <deg>
 WESTERNMOST_LONGITUDE        = -180 <deg>
 EASTERNMOST_LONGITUDE        = 180 <deg>
 LINE_PROJECTION_OFFSET       = 11519.5 <pix>
 SAMPLE_PROJECTION_OFFSET     = 23039.5 <pix>
 COORDINATE_SYSTEM_TYPE       = "BODY-FIXED ROTATING"
 COORDINATE_SYSTEM_NAME       = "MEAN EARTH/POLAR AXIS OF DE421"
END_OBJECT                    = IMAGE_MAP_PROJECTION
```

```
END
```

Appendix 4: T_{max} to T_{min} Ratio Calculation

This MATLAB code (`tempratio.m`) calculates the T_{max} to T_{min} ratio for the lunar surface. The input is the `outputfile.mat` file created by the `TI2.m` code (see Appendix 2). The code outputs the T_{max} to T_{min} ratio map as an ENVI-compatible file (with no `.hdr` file). The code was written in MATLAB version R2012. To run the code, make sure it is in the same folder as the data file you wish to analyze. The code is available upon e-mail request to rslank9@gmail.com or jhurtado@utep.edu.

```
%Code to calculate temperature ratios

%04162016 RAS

load( 'outputfile.mat' )
% fid = fopen( 'Tmax' , 'r' , 'l' ) ;
% Tmax = fread( fid , [ columns , rows ] , 'float' ) ;
% fclose( fid ) ;
%
% fid = fopen( 'Tmin' , 'r' , 'l' ) ;
% Tmin = fread( fid , [ columns , rows ] , 'float' ) ;
% fclose( fid ) ;
%
% fid = fopen( 'Tday' , 'r' , 'l' ) ;
% Tday = fread( fid , [ columns , rows ] , 'float' ) ;
% fclose( fid ) ;
%
% fid = fopen( 'Tnight' , 'r' , 'l' ) ;
% Tnight = fread( fid , [ columns , rows ] , 'float' ) ;
% fclose( fid ) ;

%Tmax Tmin temperature ratio
Tmaxminratio = Tmax' ./ Tmin' ;

figure( 18 )                % Makes a new figure window.
hold off                 % Allows the figure to be overwritten.
imagesc( Tmaxminratio )         % Plots the image.
colormap( colorcube )     % Sets the colormap.
colorbar
title( ' Tmaxminratio ' )     % Sets the title.
hold on                     % Prevents the figure from being
overwritten.

%EXPORT DATA PRODUCTS AS ENVI-COMPATIBLE FILES
Tmaxminratio = Tmaxminratio' ;
fid = fopen( 'Tmaxminratio' , 'wb' ) ;
fwrite( fid , Tmaxminratio , 'float' ) ;
fclose( fid ) ;

%Tday Tnight temperature ratio
Tdaynight = Tday ./ Tnight ;

figure( 19 )                % Makes a new figure window.
hold off                 % Allows the figure to be overwritten.
imagesc( Tdaynight )      % Plots the image.
colormap( colorcube )     % Sets the colormap.
colorbar
title( ' Tdaynight ' )     % Sets the title.
hold on                     % Prevents the figure from being
overwritten.

%EXPORT DATA PRODUCTS AS ENVI-COMPATIBLE FILES
```

```
Tdaynight = Tdaynight' ;
fid = fopen( 'Tdaynight' , 'wb' ) ;
fwrite( fid , Tdaynight , 'float' ) ;
fclose( fid ) ;
```

Vita

Rachel Ann Slank was born in Trenton, New Jersey. Shortly after, her family moved to Ohio, then moved again to Springdale, Arkansas in 2005. In 2010 Rachel graduated Valedictorian from Har-Ber High School, with advanced honors and was accepted to the University of Arkansas. She was an active member in many school organizations. In addition to many service medals, Ms. Slank was also awarded the title "Distinguished Graduate" among her peers. Rachel graduated in three and a half years with a Bachelor's of Science in Geology and a Bachelor's of Science in Earth Science. In the spring of 2014, Ms. Slank started her graduate program at the University of Texas at El Paso. She combined her love of the Moon, planetary geology, and subsurface cavities in her thesis to focus on finding subsurface cavities using thermal inertia and temperature ratios. Rachel held a research assistant position and three teaching assistant positions, all while maintaining a 4.0 GPA. During 2015, Ms. Slank held an internship at NASA Langley Research Center in Hampton, Virginia. She collected aerosol optical thickness (AOT) measurements using two types of sun photometers. Rachel presented her findings for this research to their entire NASA campus. In the fall of 2015, she took an internship at NASA Langley to purse two projects: Discover Air Quality project, and linking fracking to air pollution. Ms. Slank will attend the University of Arkansas in the fall of 2016, to start her PhD program in Space and Planetary Sciences.

Permanent address: 216 Ohara Lane

Springdale, AR 72762

This thesis was typed by Rachel Ann Slank.